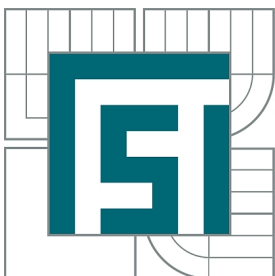


VYSOKÉ UČENÍ TECHNICKÉ V BRNĚ

BRNO UNIVERSITY OF TECHNOLOGY



FAKULTA STROJNÍHO INŽENÝRSTVÍ
ÚSTAV MECHANIKY TĚLES, MECHATRONIKY A
BIOMECHANIKY

FACULTY OF MECHANICAL ENGINEERING
INSTITUTE OF SOLID MECHANICS, MECHATRONICS AND
BIOMECHANICS

OPTIMIZATION OF HIC CRITERION DURING HEAD IMPACTOR HIT INTO THE CAR HOOD

OPTIMALIZACE HIC KRITÉRIA PŘI NÁRAZU IMPAKTOREM HLAVY NA KAPOTU AUTA

DIPLOMOVÁ PRÁCE

MASTER'S THESIS

AUTOR PRÁCE

AUTHOR

Bc. VÍT KYSILKO

VEDOUCÍ PRÁCE

SUPERVISOR

prof. RNDr. Ing. JAN VRBKA, DrSc., dr.
h. c.

BRNO 2013

Vysoké učení technické v Brně, Fakulta strojního inženýrství

Ústav mechaniky těles, mechatroniky a biomechaniky

Akademický rok: 2012/13

ZADÁNÍ DIPLOMOVÉ PRÁCE

student(ka): Bc. Vít Kysilko

který/která studuje v **magisterském studijním programu**

obor: **Inženýrská mechanika a biomechanika (3901T041)**

Ředitel ústavu Vám v souladu se zákonem č.111/1998 o vysokých školách a se Studijním a zkušebním řádem VUT v Brně určuje následující téma diplomové práce:

Optimalizace HIC kritéria při nárazu impaktorem hlavy na kapotu auta

v anglickém jazyce:

Optimization of HIC criterion during head impactor hit into the car hood

Stručná charakteristika problematiky úkolu:

Výpočtové modelování průběhu zpomalení impaktoru hlavy při nárazu na kapotu osobního vozu využitím explicitní varianty metody konečných prvků (MKP). Najít teoretický optimální průběh zpomalení impaktoru hlavy z hlediska velikosti HIC faktoru a minimální dráhy. Následně k tomuto průběhu navrhnout optimální strukturu kapoty (deformační člen).

Detailní zadání a požadavky na vypracování je možno konzultovat s pověřeným pracovníkem koncernu Škoda Auto (zadavatel tohoto diplomového projektu) panem Ing. Holcem.

Cíle diplomové práce:

Výběr teoreticky nejvhodnějšího časového průběhu zpomalení a navržení konstrukčních úprav kapoty a okolních částí, které se dostanou do kontaktu tak, aby se skutečný průběh blížil teoretické fyziologicky přípustné variantě.

Seznam odborné literatury:

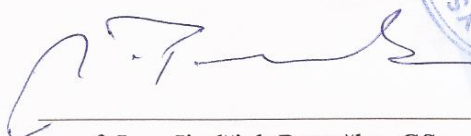
- Brepta, R., Prokopec, M.: Šíření napětových vln a rázy v tělesech. Academia, Praha, 1972
Goldsmith, W.: Impact. The theory and physical behaviour of colliding solids. London, 1960
Cook at all.: Concept and application of finite element analysis. Hamilton Printing Company, 2002.
Firemní podklady společnosti Škoda Auto, a.s.

Vedoucí diplomové práce: prof. RNDr. Ing. Jan Vrbka, DrSc., dr. h. c.

Termín odevzdání diplomové práce je stanoven časovým plánem akademického roku 2012/13.

V Brně, dne 24.9.2012





prof. Ing. Jindřich Petruška, CSc.
Ředitel ústavu



prof. RNDr. Miroslav Doupovec, CSc., dr. h. c.
Děkan

ABSTRACT

Due to still considerable number of death persons during car accidents, the car producers aim is to proper design of car to reduce severity consequence caused by accidents. During collision of head impactor with bonnet of car, the impactor is decelerated and to resultant deceleration curve is applied HIC criterion. HIC shows the rate of possible head injury during collision. Main aim of thesis is to look for most appropriate deceleration curve of child head impactor with collision of Škoda Superb II bonnet from HIC point of view, additionally to propose modification to bonnet structure and surrounding parts to approach of real deceleration curve to analytical physiologically admissible variant. The problem is solved, making use of computational modeling utilizing the explicit variant of Finite Element Method (FEM). In the first part of thesis, the data are analyzed from collision of child head impactor into the bonnet structure, especially data are analyzed of energy absorbed by bonnet. Mentioned data were provided by Škoda Auto a.s. Next part deals with design of analytical deceleration curves by using sinusoidal, rectangular and triangular functions. Further the 2 peak triangular function of deceleration is proposed and modifiable by parameters. Optimization of approximated geometry model of bonnet structure according to previously proposed 2 peak triangular function is done. In next part the original geometry model of bonnet is modified according to optimal deceleration curve.

Keyword: child head impactor, explicit variant of finite element method, optimization of bonnet, HIC criterion, optimization of deceleration curves

ABSTRAKT

Kvůli stále značnému počtu usmrčených chodců při dopravních nehodách se výrobci automobilů snaží pomocí vhodné konstrukce automobilu zmírnit následky způsobené nehodou. Při srážce impaktoru hlavy s kapotou automobilu dochází ke zpomalení impaktoru a na toto zpomalení je aplikováno HIC kritérium. HIC kritérium vyhodnocuje míru možnosti poranění hlavy při srážce. Cílem diplomové práce je výběr nejvhodnějšího časového průběhu zpomalení dětského impaktoru hlavy při srážce s kapotou automobilu Škoda Superb II z hlediska HIC kritéria a návržení konstrukčních úprav kapoty a okolních částí, které se dostanou do kontaktu tak, aby se skutečný průběh blížil teoretické fyziologicky přípustné variantě. Pro výpočtové modelování úlohy byla použita explicitní varianta metody konečných prvků (MKP). V první části práce jsou analyzována data ze simulací úderu impaktoru dětské hlavy na kapotu auta, zvláště pak analýzy částí energie spotřebované kapotou při srážce s impaktorem. Tyto data byly poskytnuté firmou Škoda Auto a.s. Další část se zabývá návrhem křivek zpomalení se sinusovým, čtvercovým a trojúhelníkovým tvarem. Dále je také navržena 2 vrcholová trojúhelníková křivka zpomalení, jež je pomocí parametrů modifikovatelná. Optimalizací aproximovaného modelu geometrie kapoty automobilu při dopadu impaktoru hlavy na navržený model geometrie kapoty je zajištěno podobné shody s dříve optimalizovanou 2 vrcholovou trojúhelníkovou křivkou zpomalení. V další části je použit originální model geometrie kapoty automobilu Škoda Superb II a další optimalizace modelu geometrie kapoty vůči optimálnímu časovému průběhu zpomalení.

Klíčová slova: impaktor dětské hlavy, explicitní varianta metody konečných prvků, optimalizace kapoty, HIC kritérium, optimalizace křivky zpomalení

Citation

KYSILKO, V. *Optimalizace HIC kritéria při nárazu impaktorem hlavy na kapotu auta*. Brno: Vysoké učení technické v Brně, Fakulta strojního inženýrství, 2013. 97 s. Vedoucí diplomové práce prof. RNDr. Ing. Jan Vrbka, DrSc., dr. h. c..

ČESTNÉ PROHLÁŠENÍ

Prohlašuji, že jsem tuto diplomovou práci vypracoval samostatně pod odborným vedením vedoucího diplomové práce za použití uvedené literatury.

V Brně, květen 2013

.....
Bc. Vít Kysilko

Poděkování

Tímto bych chtěl poděkovat vedoucímu diplomové práce prof. RNDr. Ing. Janu Vrbkovi, DrSc., dr.h.c. za cenné rady a připomínky během uskutečnění této práce. Především bych chtěl poděkovat panu Ing. Janu Holcovi a dalším pracovníkům výpočtového oddělení technického vývoje firmy Škoda Auto a.s., kteří mi byli při zpracování práce nápomocni, za velmi cenné rady a připomínky při praktickém vypracování tohoto tématu. Chtěl bych také poděkovat své rodině za podporu a zázemí, kterou mi po celou dobu mého studia vytvářeli.

Contents

1	Introduction	8
2	Problematic situation	9
3	Formulation of problem and objectives of thesis	9
4	Research	10
4.1	The accident rate	10
4.2	Usage of dummy vs. impactors	10
4.3	HIC research	11
4.3.1	The HIC functional	14
5	Description of test	15
5.1	Impactors	17
5.1.1	Certification of headform	17
5.2	Vehicle marking	18
5.3	Determination of impact points and testing procedure	19
5.4	Evaluation	20
6	Analysis of impact	21
6.1	Energy relations	22
6.2	Distribution of internal energy across the bonnet top	26
7	Design of force-trajectory curves	27
7.1	Analytical solution	27
7.2	Basic functions	28
7.2.1	Sinusoidal function	29
7.2.2	Rectangular function	31
7.2.3	Triangular function	33
7.3	Conclusion from basic functions	35
7.4	Parametric model function	36
7.4.1	Model of function	37
7.5	Conclusion of used functions	44
8	Design of approximated bonnet structure	46
8.1	Computational model	46
8.1.1	Geometrical model - first variant 000	46
8.1.2	Modeling of boundary condition	47
8.1.3	Model of contact	49
8.1.4	Model of material	51
8.2	Solution and checking the output file	52
8.2.1	Implicit and explicit FEM algorithm [1]	52
8.2.2	Mass scaling and time step	56
8.3	Post-processing	57

8.4	Variant 001	57
8.5	Variant 002 (<i>SK461_SPC_020_002.pc</i>)	58
8.6	Variant 003	59
8.7	Variant 004	60
8.8	Variant 005	60
8.9	Variant 006	61
8.10	Variant 007	61
8.11	Comparison of variants	62
9	Design of original bonnet structure	63
9.1	Computational model	63
9.1.1	Geometrical model	63
9.1.2	Modeling of boundary condition	64
9.1.3	Model of contact	65
9.1.4	Model of material	65
9.2	Solution and post-processing	65
9.3	Evaluation of FEM model variant <i>SK461_A35</i>	65
9.4	Variant X00 - 002	68
9.5	Variant X01 - 004	68
9.6	Variant X02 - 005	71
9.7	Variant X03 - 006	72
9.8	Variant X04 - 007	73
9.9	Torsional strength	74
9.10	Comparison of design with using original superficial bonnet top	75
10	Analysis of results	76
11	Conclusion	77
12	List of acronyms	85
13	List of symbols	87
Appendix A	Figures	88
Appendix B	HIC analysis script <i>SK461_ALL.m</i>	91
Appendix C	HIC script "HICcalc.m"	96
Appendix D	Triangular parametric function "triangle_acctraj.m"	97

1. Introduction

A trend in automotive industry shows that the aim is not only to increase power of engines or passengers comfort however also they aiming more and more to the persons safety inside or outside of the car.

There is a still a lot of space for improvement in the field of pedestrian safety because during collision of pedestrian with vehicles the pedestrians are worse protected against to occupants of car. Therefore the automobile producers attempt to achieve high safety in pedestrian protection field. For Europe, the independent consortium EuroNCAP gives procedures how to perform partial impact tests. To the tested vehicles, EuroNCAP gives rating from partial test such as occupant safety (adult and child), pedestrian safety and safety assist which represent seat belt reminders (SBR), speed assistance systems (SAS) or electronic stability control (ESC) etc. Each result improvements of tests are reflected in higher score of safety represented by number of stars and it increases the prestige of car.

During collision of pedestrian with car, the various parts of pedestrian body are exposed to impact. Highest probability of pedestrian severe injury is due to impact of the head to the front of car especially bonnet and windscreen. Therefore presented diploma thesis deals with impact of child head substitute called headform with bonnet of car. Within impact the headform is decelerated and onto resultant deceleration curve is applied Head Injury Criterion (HIC) which is measure of the likelihood of head injury arising from an impact. Therefore is necessary to analyze the deceleration curves of headform and to design the bonnet structure exhibiting the best achieved HIC values.

Within EuroNCAP test protocols are proposed physical tests of impactors collision with vehicle. Obviously the test are consuming from time and costs point of view and therefore the computational simulations are offered to use by Finite Element Method utilizing explicit algorithm. The analysis of impact simulation represents main aim of thesis.

To model deceleration curve the portion of energy absorbed by bonnet and time duration of impact are necessary to know. Further application of proposed deceleration curves into the designed bonnet structure which provide the best HIC values is done. The maximal deflection of bonnet structure to 60 mm in vertical direction serves as another restriction where at mentioned position are engine parts which cause hard impact.

Achieved findings is possible to use for further optimization of bonnet structure, where nowadays the active bonnets are used which allow to extension of deformation trajectory for headform.

2. Problematic situation

Pedestrian protection is significant entity from overall safety performance of car. Its main aim is to increase protection of pedestrian during impact to the car. It is necessary to avoid of severe injury of pedestrian and also to reduce possibility of further injury cause by acute subdural haematoma. Nowadays the pedestrian tests proposed by EuroNCAP are modeled by Finite Elements Method which serves as computational simulation of impact. One of partial test are impacts of child headform into the bonnet structure. The impacts are analyzed to obtain view, how the bonnet structure influence the Head Injury Criterion which is measure of the likelihood of head injury arising from an impact.

3. Formulation of problem and objectives of thesis

Problem: The optimization of deceleration curve of headform which arise from impact of headform into a bonnet of car.

Objectives:

- To create computational model of deceleration curves during impact of headform to the bonnet structure of passenger car Škoda Superb II.
- To selection of most proper theoretical deceleration curve
- To create computational model of approximated bonnet structure according to best theoretical deceleration curve from HIC point of view by using Finite Element Method utilizing explicit algorithm
- Then to create computation model of bonnet structure according to previous findings and further optimization of bonnet structure to uniform good results of HIC values across area of bonnet

Restrictions:

- The maximal allowable deformation of bonnet is 60 mm in vertical direction.
- The bonnet structure design has to preserve 5 mm free space between bonnet structure and engine parts (maximal allowable deformation 60 mm)
- The direction of headform remains straight during impact for modeling deceleration curves

4. Research

4.1 The accident rate

In the whole world the number of accidents caused by collision of vehicle and pedestrian is still significant. Therefore the research in this field is necessary. In recent years the pedestrian fatalities decreased by improved technologies however in European Union approximately 7000 pedestrians are annually defeated by severe injuries. In 2011 in Czech Republic approximately 2% of all traffic accidents were caused by pedestrian. However from 707 fatal injuries the 21% pedestrians died. Looking at past years the overall accident rate decrease nevertheless with same portion of pedestrian dies. Descending pedestrian fatalities are seen in urban areas due to preventive precaution of people, especially children. On the other side people use cars more often for short journeys due to their convenience thus it could lead to enlarged number of fatalities.

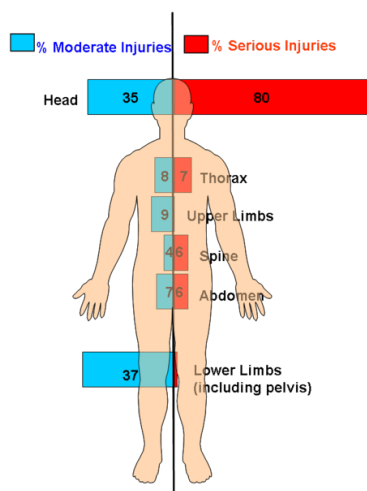


Figure 4.1: Most exposed vulnerable parts of pedestrian by vehicle struck [2]

4.2 Usage of dummy vs. impactors

For objective finding of pedestrian kinematics the several studies were performed using MADYMO pedestrian model. The struck of pedestrian was modeled throughout whole gait at vehicle speeds from 0 to 15 m/s with respect to pedestrian velocity from 0 to 3 m/s. At gait 40% depicted in figure 4.2 and car velocity vector aimed out of paper the head is rotated by 60° out of the paper from direction of pedestrian velocity vector. Also it was found that at certain gait, the head rotation is independent from velocities of vehicle or pedestrian. Likewise the results of calculation shows that at collision the front of head contact with bonnet when struck leg is lagging and the back of head contact with bonnet when struck leg is leading. Also from study implies that the impact of headform rely on velocity of vehicle. [3]

In previous paragraph were used dummy model instead of head impactor. The comparison of post-mortem human surrogates (PMHS) with Polar-II dummy shown some trends in pedestrian collision simulation with small sedan [4]:

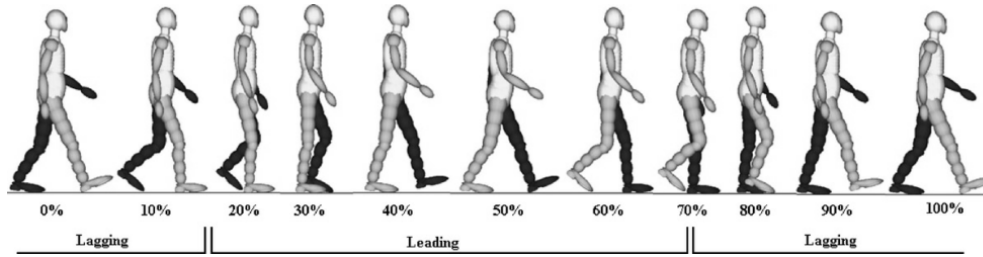


Figure 4.2: Gait cycle stances [3]

- "The wrap-around-distance (shown in figure A.4) for the head strike was 15 – 20% shorter in Polar-II tests on the small sedan against to PMHS tests. This difference was smaller in the SUV tests - around 5 – 10%." [4]
- "In sedan tests, the head velocity profile of Polar-II did not match to the cadaver velocity profiles: The dummy head achieved higher peak speeds but the speed of the head was lower on impact than the cadaver head speeds. In SUV tests, the velocity profiles matched more closely." [4]
- "The velocity of the Polar-II head exhibited a larger vertical component on impact in all tests." [4]
- "In sedan tests, the head of the Polar-II struck the vehicle surface earlier than the PMHS subjects. The average timing of head strike in PMHS tests was 140 ms after first contact, and 126-131 ms in Polar-II tests. In SUV tests, timing was almost identical." [4]

Even though of existing mentioned differences, Kerrigen et al. documented good overall biofidelity of Polar-II dummy with comparison to PMHS [4]. The biofidelity is a scale of agreement dummy and human surrogates represented by PMHS to the pedestrian kinematics, forces, moments and displacements occurred during collision [5].

However several benefits rely from using subsystem test methods such as using impactors which substitute the parts of dummies:

- Facilitating to hit selected impact point on vehicle in advance-
- Within using same configuration of test and position of dummy in collision, the same point on vehicle is impossible to hit repeatedly due to many degrees of freedom in each joint of dummy.
- Due to great mobility of dummy to ensure the same impact speed of each parts to vehicle.
- In collision tests the some impact points could lead to damage of dummies and therefore they are excluded from sum of tests.

4.3 HIC research

As is shown in figure 4.1 the most danger part of body is head due to direct blow face or head into the bonnet which may cause skull fracture accompanied by rising acceleration. The measure of potential severity of injury is Head Injury Criterion (HIC) [6]. The HIC is

fitted to Wayne State Tolerance Curve (WSTC) which was generated regarding to the results from test of dropping cadaver heads onto unyielding, flat surfaces, striking the subject on the forehead. [7]. "In its final form, the WSTC was developed by combining results from a wide variety of pulse shapes, cadavers, animals, human volunteers, clinical research, and injury mechanisms. Skull fracture and/or concussion was used as the failure criterion, except for the long duration human volunteer tests in which there were no apparent injuries." [7]. The WSTC specifies the level at which acceleration or retardation of the head causes concussion and skull fracture and its widely accepted by automotive research [8]. The WSTC curve in log-log coordinate is shown in figure 4.3.

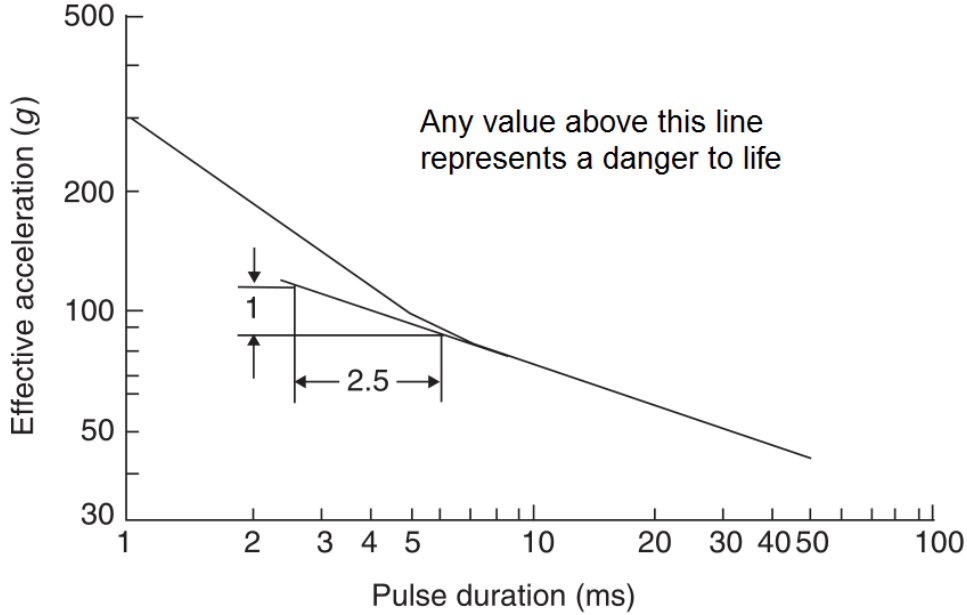


Figure 4.3: Log-Log Wayne State Tolerance Curve [8]

Fitting of WSTC was first introduced by Gadd (1966) which developed Gadd Severity Index (GSI) where value greater than 1000 is life-threatening. It is based on linear approximation of log-log WSTC where the negative slope m is -0.4 . By using the logarithmic equation is calculated weight factor of acceleration. For $T = 1s$ (in which case $\log T = 0$) the corresponding acceleration is $A = 15.85 \cdot g$

$$\log A = m \cdot \log T + \log k \quad (4.1)$$

$$\log 15.85 = -0.4(0) + \log k \quad (4.2)$$

$$15.85 = k \quad (4.3)$$

After putting constant into values of m and k back into eq. (4.1).

$$\log A = -0.4 \cdot \log T + \log 15.85 \quad (4.4)$$

$$\log A = \log T^{-0.4} + \log 15.85 \quad (4.5)$$

$$\log A = \log(15.85T^{-0.4}) \quad (4.6)$$

$$TA^{2.5} = 15.85^{2.5} = 1000 \quad (4.7)$$

"It was based not only on the original Gurdjian data, but also upon additional long pulse duration data by means of the Eiband (1959) tolerance data and other primate sled tests.

The GSI provided a good fit for both the short duration skull fracture data and the longer duration Eiband data out to 100 msec duration.” [8]. The mentioned index is defined as

$$GSI \equiv \int_0^T a^{2.5} dt \leq 1000 \quad (4.8)$$

where a is acceleration in terms of 'g', T total pulse duration in milliseconds. As was mentioned before the value 1000 represents limit which is tolerated without permanent brain damage. The total pulse duration range of $0.25\text{ms} < T < 50\text{ms}$ implies from exponentiation 2.5 which interpolates WSTC as shown in eq. (4.7) at mentioned pulse duration as shown in figure 4.3 [8]. Also acceleration curve should be longer than 3ms due to reason of measurement technique and assumption that shorter durations do not have any effect on the brain [9].

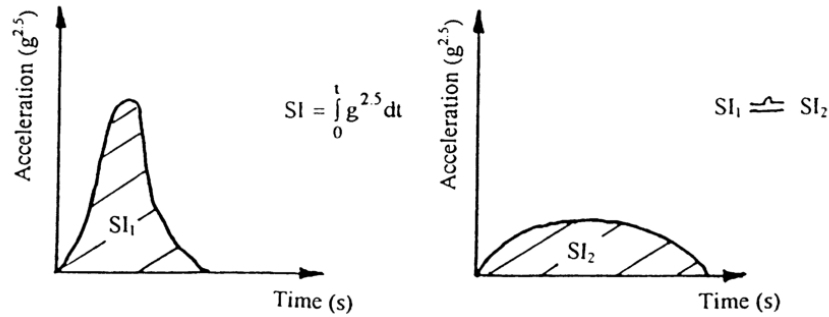


Figure 4.4: Two different waveforms with similar GSI values [10]

Model of Gadd used in figure 4.4 shows the similar values of GSI, however probability of acute subdural haematoma (ASDH) is very different [10]. Gadd developed model to comparison only of average acceleration across different type of cars and accidents and therefore Versace (1971) proposed the HIC which was further modified by National Highway Traffic Safety Administration (NHTSA) and in 1972 replaced older GSI in paper FMVSS No. 208 with following expression: [7, 9]

$$HIC = \max_{t_1, t_2} \left\{ (t_2 - t_1) \left[\frac{\int_{t_1}^{t_2} a dt}{t_2 - t_1} \right]^{2.5} \right\} \quad (4.9)$$

In contrast to GSI the HIC reduce shortcomings of previous criteria and bring possibility to compare of head injury tolerance values irrespective of the waveform shape shown in figure 4.5. ”The HIC considers the more injurious portion of the impact waveform, the peak and close to peak sections (i.e. $t_2 - t_1$, figure 4.5), and excludes the less injurious sections therefore giving a more accurate head injury tolerance level.” [10]

Prasad and Mertz conclude that for value $HIC=1400$ the 50% probability of life-threatening brain injury is associated and $HIC=1000$ cause risk about 20%. It goes out by cadaver head impact test data given by Prasad and Mertz. Mentioned probabilities were proposed to be used with 15ms time pulse duration by Prasad and Mertz...for example HIC of 1000 is caused by an average acceleraion 1g applied for 1000 seconds which clearly is not hazardous for life [11, 12, 13, 14, 10].

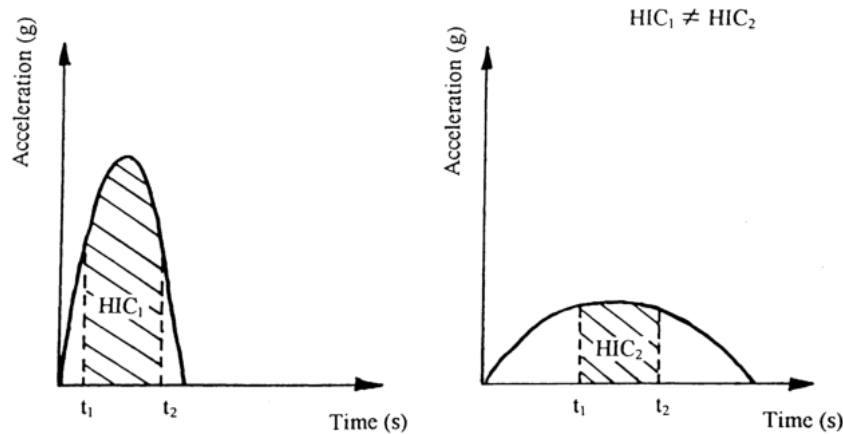


Figure 4.5: Area of waveform utilised for calculating HIC [10]

4.3.1 The HIC functional

During impact test the forces and moments are appearing, however they are hard to measure. Usually load cells used for evaluating force are poorly applicable for impact testing therefore the accelerometers are relatively better to use for impact cases [12]. Bonnet structure should lead to massive reduction of acceleration of the impact and should absorb enough kinetic energy.

Algorithmic consideration

According to eq. (4.9) the function \max_{t_1, t_2} calculate supremum of possible results. As shown in eq. (4.8) the GSI function could be easily integrated to obtain value. However for HIC calculation it is necessary to find where combination of t_1 and t_2 provide maximal value. The 15ms maximal time frame of HIC calculation was proposed by Prasad and Mertz and it is widely used in automotive research to restrict enlarging time frame for HIC calculation into infinity for headform impacts into structure. Mentioned time frame corresponds to usually shorter peak duration of acceleration based on real/simulated acceleration pulses where HIC acquires maximum. The script for calculation of HIC in MATLAB is listed in appendix C [15].

5. Description of test

The car vehicle has to pass several types of tests. The thesis is concerned with tests related to the pedestrian protection. During collision with pedestrian, some body parts are in contact with different parts of car with various physical properties such as stiffness or strength. The dummies initially appeared to be most obvious test tool for assessing a car's pedestrian protection due to have appropriate properties such as joints, etc. However to completely assess whole area of the various type of car in terms of head impact the testing would require a family of dummies due to widespread test area of bonnet and windscreen [16]. Hence the dummy is not practical to use for head impact assessment.

Another reasons to use only impactor instead of whole dummy are to ensure the repeatability of tests, where the impact has to be performed several times into same point on the bonnet, where by using dummies with a lot degrees of freedom it is hard to ensure. Also the crash between dummy and vehicle shall influence the head velocity during impact into the bonnet. For example the velocity of head is reduced if the shoulder contact first with bonnet.

EuroNCAP pedestrian test which use impactors takes into account a possibility of head-form damage, where at edge of bonnet the headform could spin and lead to communication cable damage, therefore points at the edge are excluded from testing.

Therefore the independent body parts represented by impactors bring several advantages such as easiness of using to test whole area likely to strike pedestrians or it could be aimed accurately at selected danger points of car.

The pedestrian protection tests are divided into:

- Impact of lower leg into bumper
- Upper leg impact into edge of lower part of bonnet
- Head impact into bonnet

As far as the vehicle disposes with ground clearance over 500 mm the test of upper leg impact into bumper is performed.

The overall impact zones for each type of test and for different car model is illustrated in figure 5.1.

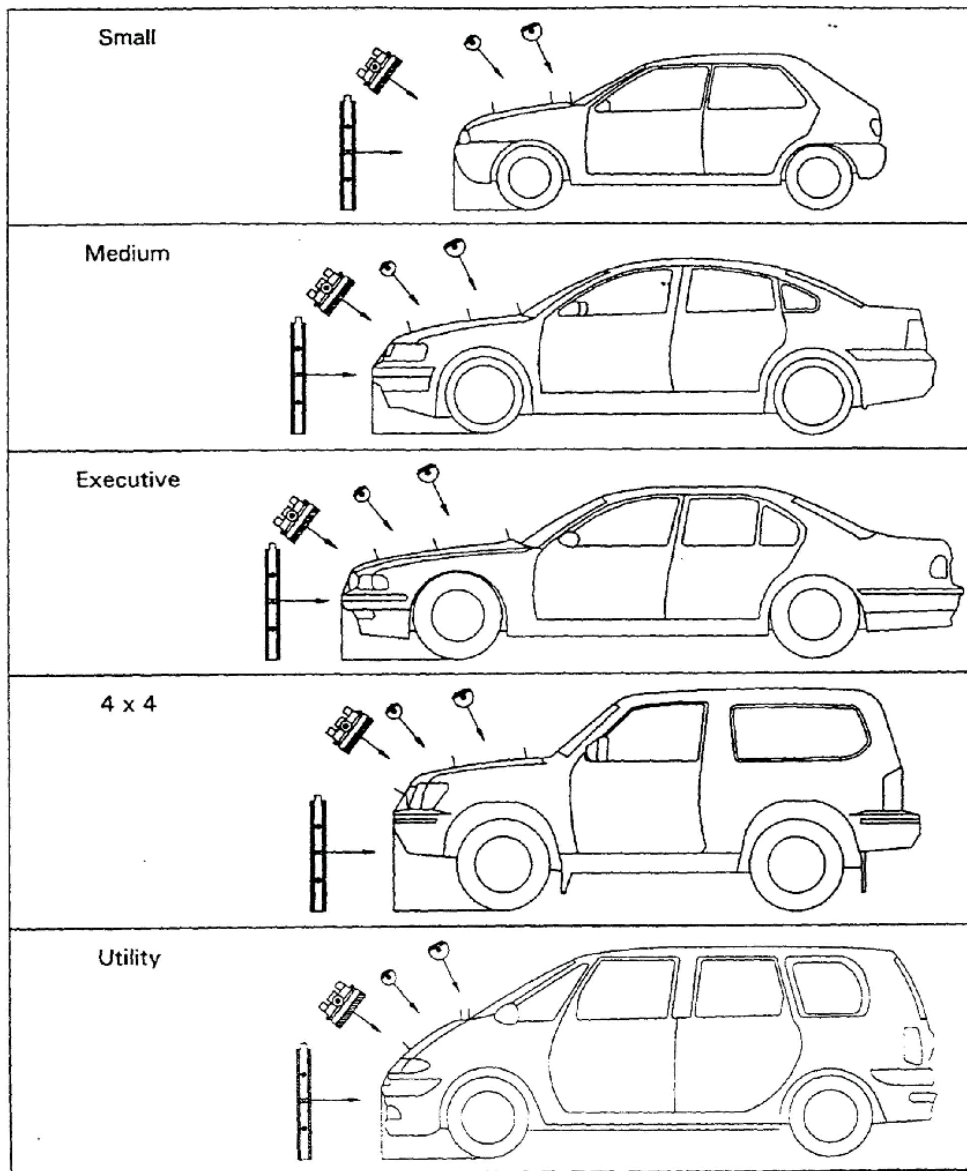


Figure 5.1: Pedestrian impact zones by vehicle category, showing the potential overlap in upper legform impact zone and child headform impact zone for 4x4 off-road and utility vehicles [17]

The assessment of *SK461_A12* project for pedestrian protection is based on test protocol EuroNCAP 4.1 [17].

5.1 Impactors

According to the specification of protocol [17] the two types of headform are used namely adult and child. Mentioned impactors differ only in size and mass however the composition of materials is same. The kinetic energy is calculated from the impact speed of headform tabled in table 5.1.

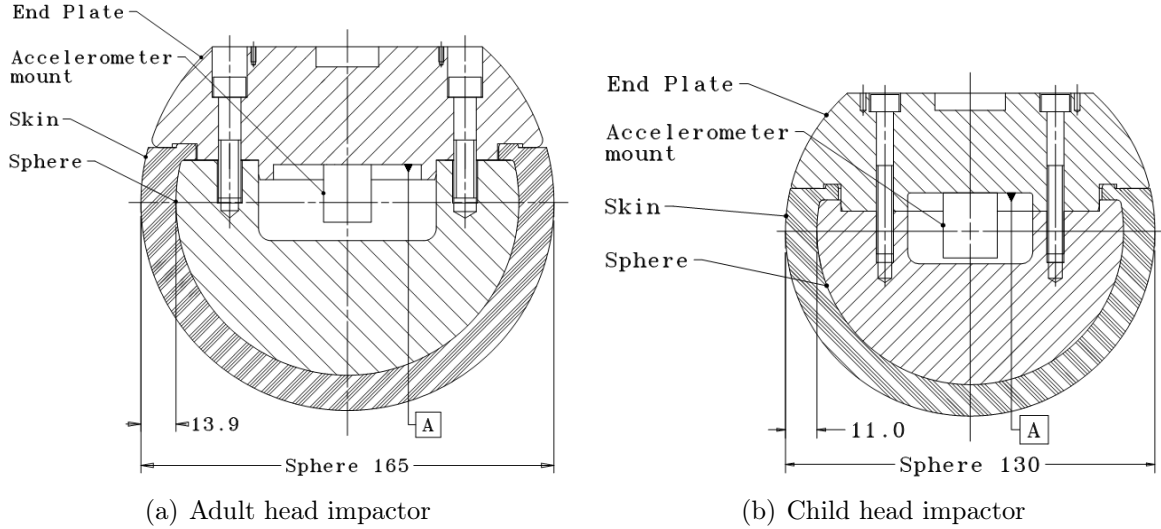


Figure 5.2: Two types of head impactors, dimensions in *mm*

		Adult head impactor (Adult headform)	Child head impactor (Child headform)
Thickness of vinyl skin	[mm]	13.9 ± 0.5	11.0 ± 0.5
Moment of inertia	[kgm^2]	0.0125 ± 0.0010	0.0036 ± 0.0003
Mass	[kg]	3.5	2.5
Speed of impact v	[$\frac{m}{s}$]	11.1 ± 0.2	11.1 ± 0.2
Energy of impact (for $v=11.3 \frac{m}{s}$)	[J]	223.5	159.6

Table 5.1: Technical specification of impactors

The EuroNCAP use certified impactors according to the EEVC WG17 Report where properties are defined [18] and the description of certification procedure is listed in following section.

5.1.1 Certification of headform

The stabilized surrounding temperature should be $20^\circ \pm 2^\circ C$. The child headform is impacted by a linearly guided certification impactor as shown in figure 5.3 and the peak of acceleration resultant curve should not be less than 405 g and not more than 495 g. Because of the accelerometer is measuring in 3 directions therefore by impacting in one direction by certification impactor the resultant acceleration time curve should be only in one direction. For adult headform the peak resultant should be in range of 337.5 g and 412.5 g. [18]

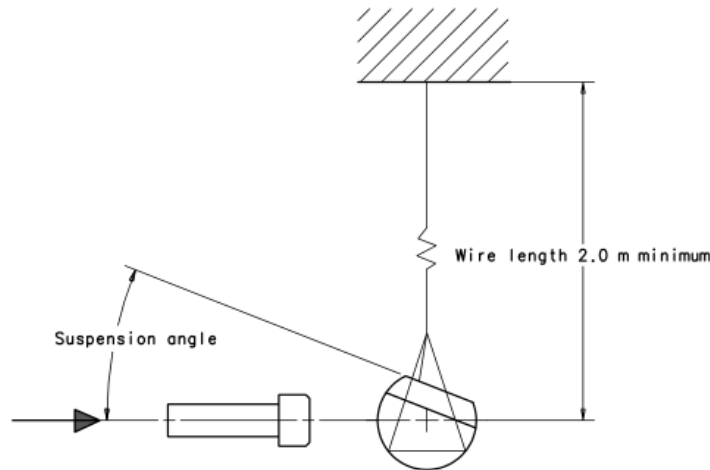


Figure 5.3: Test set-up for dynamic headform impactor certification test [18]

For smoothing of output signal the Channel Filter Class (CFC) 1000 is applied according to ISO 6487:2000. The Channel Amplitude Class (CAC) 500g is used according to ISO 6487:2000. If the peak of acceleration resultant curve during impact exceed CAC value 500g the headform has to be re-certified. Also after 20 impacts and every 12 months regardless of the number of impact they have to be re-certified.

Test procedure

Following steps are cited from EEVC WG17 Report figure 5.3

- "The headform impactor shall be suspended as shown in figure 5.3. The headform impactor shall be suspended with the rear face at an angle between 25° and 90° with the horizontal, as shown in figure 5.3." [17]
- "The certification impactor shall have a mass of 1.0 ± 0.01 kg. This mass includes those propulsion and guidance components which are effectively part of the impactor during impact. The linear guidance system shall be fitted with low friction guides which do not contain any rotating parts. The diameter of the flat impactor face shall be 70 ± 1 mm, while the edge shall be rounded by a 5 ± 0.5 mm radius. The face of the certification impactor shall be made of aluminium, with an outer surface finish of better than 2.0 micrometers." [17]
- "The test shall be performed on three different impact locations on the headform impactor. Previously used and/or damaged skins shall be tested in those specific areas." [17]

In thesis is only considered the child zone testing area of bonnet and therefore only child headform is used with properties and test procedure regarding to the EuroNCAP test protocol [17].

5.2 Vehicle marking

The preparation of vehicle should be done by marking into the bumper and bonnet section. The bumper section definition includes the upper bumper reference line, lower bumper ref-

erence line and the bumper corners shown in figure A.1, figure A.2 and figure A.3 where the details are described in EuroNCAP pedestrian protocol [17]. However main aim of this work is to provide results of headform testing to the bonnet top therefore bonnet marking is described furthermore.

The bonnet top section is bounded by the geometric trace of the 1000mm wrap around line in the front figure A.4, the Bonnet Side Reference Lines figure A.5, and the base of the windscreen. [17].

The zone for testing by child impactor is defined by Wrap Around Lines 1000mm and 1500mm and by Bonnet Side Reference Lines. Over against adult zone definition it includes the 1500mm and 2100mm wrap around lines depicted in figure 5.4. Both zones are divided into sixths where each has 4 subzones marked A-D. The methodology of division into sixths is comprehensively described in the protocol, and is not important for further design analysis. The marking scheme is shown in the figure 5.4.

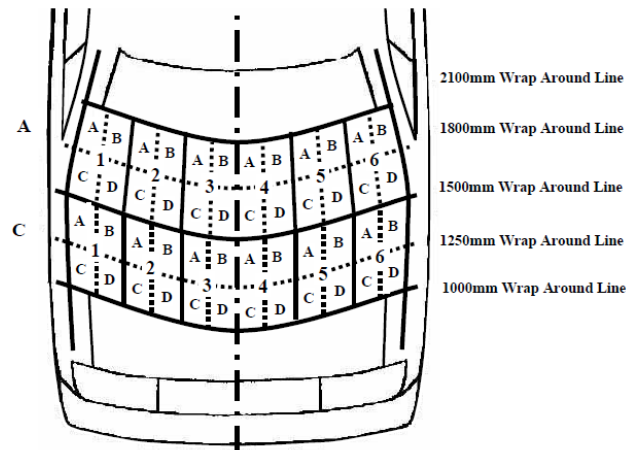


Figure 5.4: Division of the headform test zones [17]

5.3 Determination of impact points and testing procedure

The protocol defines a maximum of 12 EuroNCAP impact points to be tested due to reduce programme size. The choice of impact points rely on visual survey of the engine bay to decide liable locations to cause injury. Then the points are projected between 1000 mm and 1500 mm WAD lines which represents child zone. Also the projected points for child headform shall be a minimum of 65mm inside of Bonnet Side reference line and minimum for 130mm apart of each other. However after evaluation of particular sixth may the manufacturer consider that the single EuroNCAP point does not reflect the overall performance of that area. Therefore is possible to fund one additional test in the remaining test zones inside sixth with fulfilling previously mentioned requirements for projected points. Although the projected points at the edge of bonnet and lower windscreen belong to the adult zone, the points are excluded from testing due to high risk of headform data cable damage caused by fast spin of headform when it impact to the edge between bonnet and windscreen area. [17].

The scoring of assessment is not described due to further another used approach which will serve for comparison between original and designed bonnet structure.

To avoid serious injury of head regarding to EuroNCAP the HIC value should not exceed value of 1000. The testing temperature of surrounding has to be at $20^\circ \pm 2^\circ\text{C}$. Angle of impact into bonnet is $50^\circ \pm 2^\circ$ for child impactor referenced to the Ground Reference Level [17]. The angle of impact is based on dummy kinematics during accident [6]. The technical parameters are given in table 5.1 and the schematic illustration is depicted in figure 6.3.

5.4 Evaluation

As it was mentioned before the assessment of head injury is based on HIC criterion. The criterion is calculated from the resultant curve of acceleration a which is defined as a multiple of 'g' and $t_{1,2}$ which are two time instants (expressed in seconds) defining the time frame of HIC calculation where the HIC value is maximal [17].

However all previous test method and procedures describe the physical testing where impactor hits the bonnet. Therefore for simulation of impacts served the finite element model *SK461_A12* where the *A12* is variant of car model Superb II. generation internally labeled as *SK461*. The FEM model created in ANSA pre-processor consist of front part of car with child impactor shown in figure 6.2 and adapted to be used for headform testing of bonnet. The output data as acceleration, time, velocity etc. were taken from PAM-CRASH solver output for different impact points. The output data from PAM-CRASH solver were provided by FEM model of three-axis accelerometer positioned in the gravity center of head impactor and used as an input data for HIC evaluation by eq. (4.9).

The HIC calculation could be performed in post-processing META software however developed script was used for evaluating HIC criterion in MATLAB software denoted in appendix C due to absence of META software at my university. However to verify the implementation in MATLAB script the μETA post-processor was used in Škoda Auto a.s. company for comparison. The discrepancies did not exceed 1% and thus correct implementation of HIC in MATLAB script is assumed.

6. Analysis of impact

In this chapter the provided data of impacts depicted in figure 6.2 for child impactor are exploited and processed by MATLAB script. The first part of script reflects import procedure where the data are categorized into cells with corresponding name of variable as one can see in *IMPORT part* of script in appendix B. The data contain also magnitude of other components. As an example could be taken a magnitude of velocity MV which includes velocities in X,Y,Z directions and magnitude is expressed by eq. (6.1).

$$MV = \sqrt{XVEL^2 + YVEL^2 + ZVEL^2} \quad (6.1)$$

where XVEL, YVEL, ZVEL represent velocities in each direction.

The second part of script function *HICcalc* listed in appendix C deals with calculation of HIC where the PAM-CRASH output data are modified according to table 6.1.

	Units from PAM-CRASH output	Converted units for MATLAB script
acceleration	$\frac{mm \cdot m}{s^2}$	multiplies of g
displacement	mm	m
time	ms	s

Table 6.1: Table with conversion of units for HIC calculation

Nevertheless the MATLAB software does not include *supremum* function therefore the different approach is needed to be used to calculate HIC eq. (4.9). According to appendix C the script *HICcalc* taken from [15] is a function with as a input of time vector T (in seconds) and acceleration MA (in multiplies of g). The function output is HIC value, time interval $t_2 - t_1$ and time instants t_1 and t_2 which from HIC is calculated. Length of acceleration data vector is used as boundaries for iterative calculation. The 2 *for* cycles are used to obtain the maximal value of HIC across whole acceleration curve along 30 ms time vector T. The velocity is calculated by numerical cumulative trapezoidal integration of acceleration. In second *for* cycle the velocity is divided by time interval $t_2 - t_1$. After the fraction is raise to a power 2.5 and the expression is multiplied by time interval $t_2 - t_1$. This expression h is assigned as new value of *hic* if it is greater than it. The evaluation of criterion lead to correct HIC value and as was mentioned before the script was compared with μETA post-processor. The previous procedure take into account maximal time interval 15 ms and the evaluated maximal HIC value is stored as variable *hic* in MATLAB.

The widespread different mechanical properties across bonnet area cause various value of HIC. By approaching to the bonnet edges it often yield to major head injury represented by HIC value greater than 1000. Therefore the data from different impact points provided by Škoda Auto a.s. and depicted in figure 6.2 serve to overall analysis of bonnet stiffness from HIC point of view and values are divided into three columns i.e. $HIC < 1000$, $1000 < HIC < 1350$ and $HIC > 1350$.

	HIC < 1000
Points of impact	A09, A10, B09, B10, C09, C10, D09, D10, D11
	1000 < HIC < 1350
Points of impact	A11
	HIC > 1350
Points of impact	A12, A13, B11, B12, C11, C12, D12, D13

Table 6.2: HIC criteria for impact points according to figure 6.2

The table 6.2 shows that half of the points are below 1000 of HIC and half above. The following section analyze the impacts in energy perspective.

6.1 Energy relations

The impact into the bonnet is considered as inelastic collision from physical point of view when the part of energy is dissipated into elastic-plastic deformation of bonnet and the rest to kinetic energy of impactor.

During the impact the major portion of energy is absorbed by bonnet deformation (further called as internal energy) and small portion by headform for elastic deformation of headform skin. Because of that the whole kinetic energy is not absorbed by bonnet, the rest of headform kinetic energy cause the movement of headform after impact. The energy absorbed by bonnet could be divided into two components: namely energy absorbed in straight direction and energy absorbed caused by rotational movement of impactor. The fired headform from the ejection device heading to bonnet along straight line (without considering deviation caused by gravitation due to great velocity of headform) and after impact to the bonnet the headform starts to roll because of headform skin is not frictionless. However both of components have direct consequence into resulting HIC value and therefore are taken into account as overall energy absorbed by bonnet.

As was mentioned before the FEM model of 3 direction accelerometer situated in the center of gravity of headform depicted in figure 6.3 serves as point whence the data such as acceleration, velocity, displacement were calculated by PAM-CRASH solver. However for evaluation of HIC is need only of acceleration in global coordinate system directions X-Y-Z, corresponding trajectories for impactor movement and time duration of contact between headform and bonnet. The original file of headform from *SK461* model contain FEM model of accelerometer with local coordinate system for center of gravity point. Therefore was modified to provide results in global coordinate system. However two approaches are available for movement evaluation, described in the following text.

First approach goes out of magnitude of acceleration as it is defined by eq. (6.2).

$$a = \sqrt{a_x^2 + a_y^2 + a_z^2} \quad (6.2)$$

where a is absolute value of acceleration components (i.e. $a_{x,y,z}$ - acceleration in x,y and z direction). Second approach determine the movement by using accelerations in each direction. For both previously mentioned approaches the corresponding impactor movement trajectories are available i.e. magnitude of trajectory $|s|$ and also components $s_{x,y,z}$ as well

as corresponding time duration t . Further by using Newton principle defined by following equations the corresponding forces $F_{x,y,z}$ are obtained.

$$F_x = m_i \cdot a_x \quad (6.3)$$

$$F_y = m_i \cdot a_y \quad (6.4)$$

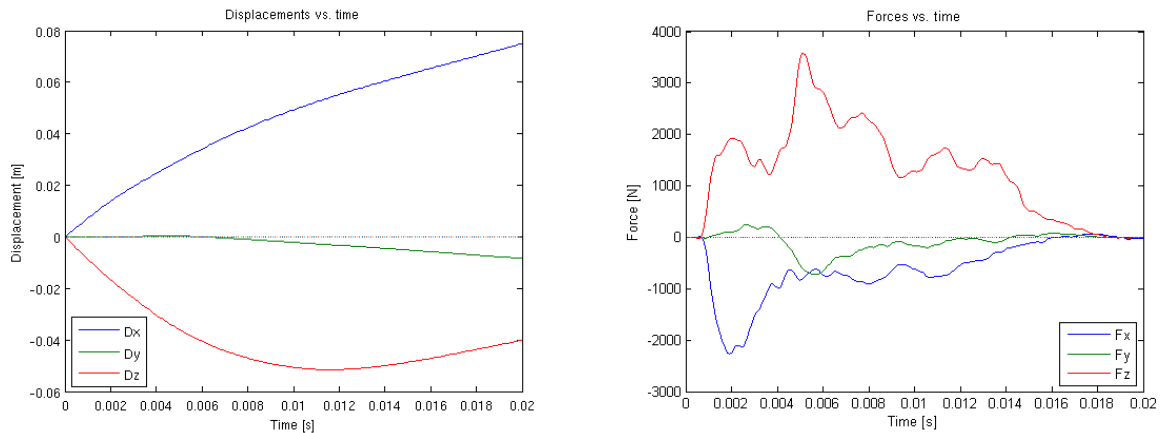
$$F_z = m_i \cdot a_z \quad (6.5)$$

where m_i represents mass of child headform. Hence the force is obtained with corresponding trajectory and the functional dependence of mentioned vectors could be easily plotted. Then the integration of force-trajectory curve leads to the overall internal energy consumed by bonnet.

By using first approach the evaluation lead to the energy of system larger than kinetic energy of impactor before collision with bonnet surface. Therefore this approach dispute to the law of conservation mass and cannot be used. The reason of impropriety depends on force-trajectory curve which is not always positive as shown in figure 6.4. Therefore by using magnitude of deceleration which is always positive due to exponentiation by 2 it lead to incorrect result of energy.

Hence the second approach deals with evaluation of each direction trajectory separately depicted in figure 6.1(a) and deceleration component, therefore by integration of each component it leads to evaluated energy in 3 directions illustrated in figure 6.4. However as known the energy is scalar thus independent on trajectory and therefore the energy from all direction are summed together to obtain total internal energy. The PAM-CRASH data also contain internal and kinetic energy. The internal energy represents energy absorbed by deformation of bonnet top and partially by impactor skin. From the opposite view the kinetic energy represents the movement of impactor, which is residual energy in certain time during collision of impactor with bonnet and also partially represents the kinetic movement of bonnet structure caused by impact.

In PAM-CRASH output files appear contact energy and hourglass energy. The first shows the energy during contact represented by friction and hourglass is support energy which produce zero strain and no stress for single integration point solid, shell elements [19].



(a) Trajectory of impactor in the global coordinate system (b) Force acting to impactor in the global coordinate system

Figure 6.1: Simulation data for A09 point

The point A09 according to figure 6.2 is analyzed as representative and same procedure of obtaining internal energy correspond to other points.

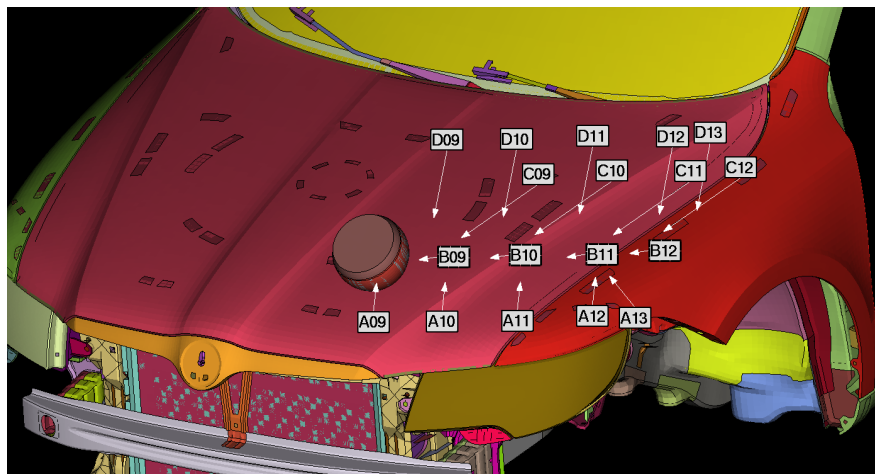


Figure 6.2: Points of impact with corresponding simulation data

As it was mentioned before the acceleration and trajectory vectors corresponds to the global coordinate system. By previous assumption the internal energy could be calculated by simply integration of force-trajectory curves shown in figure 6.4. In figure 6.4(a) the force is all time negative against to positive displacement which means the deceleration of impactor. Therefore the area under curve represents internal energy and results leads to negative energy which is correct. The figure 6.4(b) shows diagram where the impactor first moves with positive displacement and negative force which contributes to internal energy. However when the force is negative with negative displacement the energy is subtracted from internal energy. In figure 6.4(c) the force return back in trajectory position regarding to the trajectory shape Dz depicted in figure 6.1(a).

The test scheme is illustrated in figure 6.3. The shown rotated impactor at deformed bonnet position is due to friction between vinyl skin and bonnet top.

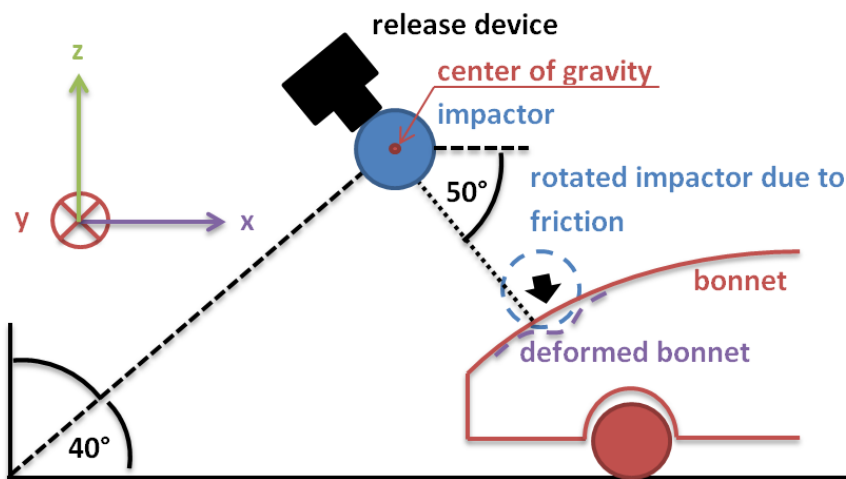
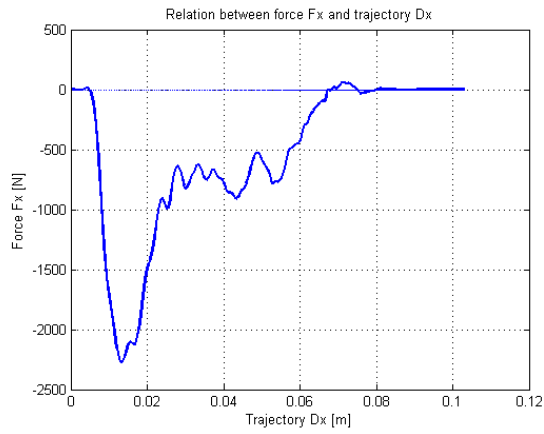
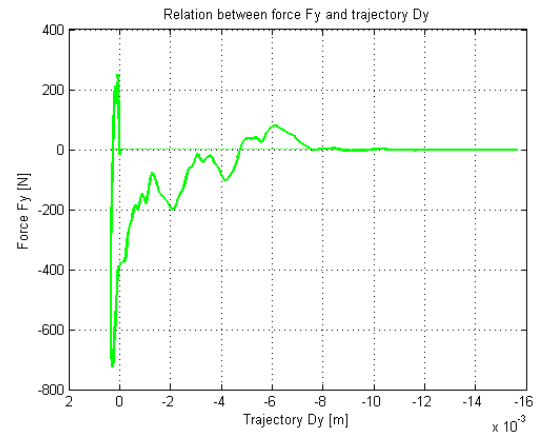


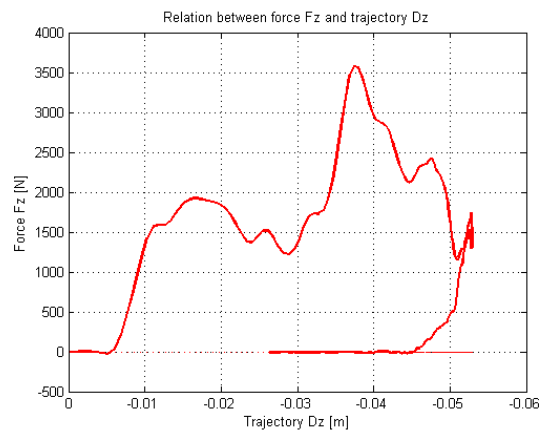
Figure 6.3: The test scheme with rotated impactor due to friction during collision with bonnet



(a) Force-trajectory diagram in x-direction



(b) Force-trajectory diagram in y-direction



(c) Force-trajectory diagram in z-direction

Figure 6.4: Force-trajectory diagrams in 3 directions

6.2 Distribution of internal energy across the bonnet top

The following section evaluate energy for all point of impact for FEM model variant A12 shown in figure 6.2. However all force-trajectory diagrams do not end with zero force at 20ms pulse duration. Therefore considering of these bring inaccuracy to the average of internal energy across the impact points and in table are marked by * and excluded from averaging. In the table 6.3 are tabled values of energy for points with $HIC < 1000$, and $HIC > 1000$.

HIC < 1000		
Point of impact (HIC)	Internal energy [J]	Internal energy by solver [J]
A09	138.5	127.6
A10*	136.2	125.4
B09*	138.1	129.3
B10*	136.3	124.4
C09*	137.0	126.3
C10*	134.1	120.4
D09*	136.2	123.5
D10*	136.1	123.6
D11*	126.2	110.4
Average	138.5	127.6
HIC > 1000		
Point of impact (HIC)	Internal energy [J]	Internal energy by solver [J]
A11	125.7	114.8
A12	116.5	108.1
A13	112.2	102.5
B11	124.2	107.6
B12	116.2	106.4
C11	121.3	107.9
C12	111.1	98.0
D12	119.3	109.9
D13	107.1	91.9
Average	117.1	105.2

Table 6.3: Internal energy

According to table 6.3 the average internal energy corresponds with values obtained from PAM-CRASH solver in 8% of difference. However the internal energy from solver should be increased by contact energy which is average 7J for all points of impact. The contact energy represents energy dissipated by friction between impactor and bonnet top. Then the discrepancy decrease to acceptable value of 3%. Because of in further calculation is considered the minor head injury represented by $HIC < 1000$ the average energy absorbed by bonnet is considered to **138.5 J**.

7. Design of force-trajectory curves

7.1 Analytical solution

Regarding previous chapter the average energy consumed by bonnet structure is $En = 138.5J$ for points where $HIC < 1000$. However one more point of impact was included i.e. E07 located in the middle of bonnet top shown in figure 9.6. The maximal deflection of bonnet top was selected to $Z_t = 60\text{ mm}$ in Z-direction with coordinate system according to figure 6.3. The deflection is selected according to SK461_A12 FEM model where free space between superficial bonnet part and the parts of engine is 60 mm in the center of bonnet. After releasing the impactor moves at 50° to the Ground Reference Level. In FEM model the bonnet surface is inclined approximately by 10° . The figure 7.1 shows schematic drawing.

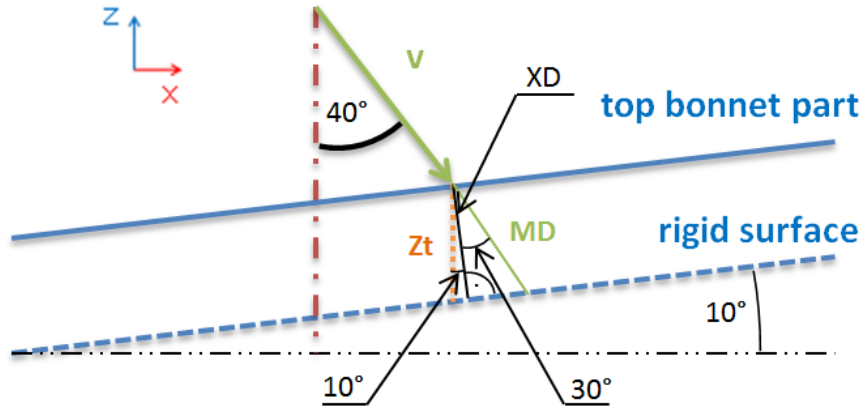


Figure 7.1: Schematic drawing of resultant trajectory

By using trigonometric function one easily obtain the magnitude of displacement from component e.g. in X and Z direction. The Y component is very small in comparison with X and Z direction and therefore is not taken into account for calculation of displacement magnitude. The following eq. results in displacement magnitude MD 7.2:

$$XD = Z_t \cdot \cos(10^\circ) = 60 \cdot \cos(10^\circ) = 59.1\text{mm} \quad (7.1)$$

$$MD = \frac{XD}{\cos(30^\circ)} = \frac{59.1\text{mm}}{\cos(30^\circ)} = 68.2\text{mm} \quad (7.2)$$

However the impact trajectory is not direct and therefore calculated MD trajectory is considered as simplification.

The main aim in the chapter is to design deceleration curve with as small value of HIC as possible with investigating the influence of the trajectory. All further designs are based on principle that draft acceleration curve along time is cumulatively integrated according to the eq. (7.3) to obtain velocity vector v .

$$v = v_0 + \int_{t_1}^{t_2} a dt \quad (7.3)$$

where a is deceleration and time $t_1 = 0$ s and $t_2 =$ length of time interval. The velocity vector had to be adjusted by initial velocity $v_0 = 11.3 \frac{m}{s}$ to obtain zero velocity at the end of draft deceleration. Then to obtain trajectory vector s is used again cumulative integration implemented in MATLAB according to the eq. (7.4).

$$s = \int_{t_1}^{t_2} v dt \quad (7.4)$$

where v is previously calculated velocity vector.

Regarding to dissertation thesis [20] the basic functions are analyzed i.e. sinusoidal, rectangular, triangular function with following parameters:

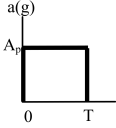
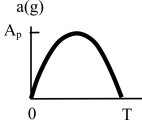
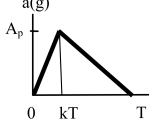
Pulse	Rectangular	Sinusoidal	Triangular
Behaviour			
Deceleration (g)	A_p	$A_p \cdot \sin \frac{\pi}{T} t$	$\frac{A_p t}{k \cdot T}, 0 \leq t \leq kT; \quad \frac{A_p \cdot (T-t)}{(1-k) \cdot T}, kT \leq t \leq T$
Rate of speed $\Delta v [m/s]$	$A_p T g$	$\frac{2}{\pi} A_p T g$	$\frac{1}{2} A_p T g$
Rate of trajectory $\Delta s [m]$	$\frac{1}{2} A_p T^2 g$	$\frac{1}{\pi} A_p T^2 g$	$\frac{1}{6} (1+k) A_p T^2 g$
Time interval for HIC calculation $t_1 [s]$	0	0.1651T	$\frac{3}{7} kT$
Time interval for HIC calculation $t_2 [s]$	T	0.8349T	$\frac{4+3k}{7} T$
HIC	$A_p^{2.5} T$	0.4146 $A_p^{2.5} T$	0.2464 $A_p^{2.5} T$

Table 7.1: Summary of basic relations for idealized pulse shapes [20]

As is obvious from table 7.1 the HIC value of all basic functions depend on maximal magnitude of deceleration A_p and pulse duration T .

The parameter k play significant role for rate of trajectory for triangular function. The trajectory rate for rectangular and sinusoidal function is influenced by magnitude of deceleration A_p and pulse duration T .

Another aspect from [20] is that at time instants t_1, t_2 the deceleration value is same. In the following section the analytical results are verified by designed basic functions.

7.2 Basic functions

The concluded results from table 7.1 are modeled in MATLAB to verify correct implementation of code. As the restriction for design of curves serves the average energy consumed by bonnet $E_n = 138.5 J$ from section 6.2.

7.2.1 Sinusoidal function

In MATLAB script the sinusoidal function is modeled as one peak function with preserving the energy $En = 138.5J$. Created sinus acceleration function with unit magnitude is double integrated to obtain trajectory vector. The acceleration vector multiplied by mass is merged with trajectory vector by time vector and dependency force-trajectory is integrated to obtain energy. The unit magnitude sinus function is multiplied until the integration force-trajectory lead to energy $En = 138.5J$. However for comparison could be used arbitrary value of maximal deceleration. Nevertheless by using pulse duration $T=0.02s$ and $t = \frac{T}{2}$ the deceleration magnitude lead to value $A_p = 84.2g$. After substitution into analytical equations for sinusoidal function the solution lead to the results shown in table 7.2.

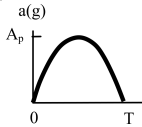
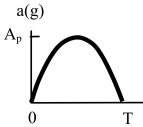
Pulse	Sinusoidal - analytical $T = 0.02$ s, $A_p = 84.2 \cdot g$	Sinusoidal - numerical
Behavior		
Deceleration (g) $[\frac{m}{s^2}]$	$A_p \cdot \sin \frac{\pi}{T} t = 84.2g$	84.2g
Rate of speed $\Delta v [m/s]$	$\frac{2}{\pi} A_p T g = 10.52$	10.52
Rate of trajectory $\Delta s [m]$	$\frac{1}{\pi} A_p T^2 g = 0.1052$	0.1052
Time interval for HIC calculation $t_1 [s]$	$0.1651T = 0.0033$	0.0033
Time interval for HIC calculation $t_2 [s]$	$0.8349T = 0.0017$	0.0017
HIC	$0.4146 A_p^{2.5} T = 539.44$	539.46

Table 7.2: Comparison of analytical and numerical treatment of sinusoidal function

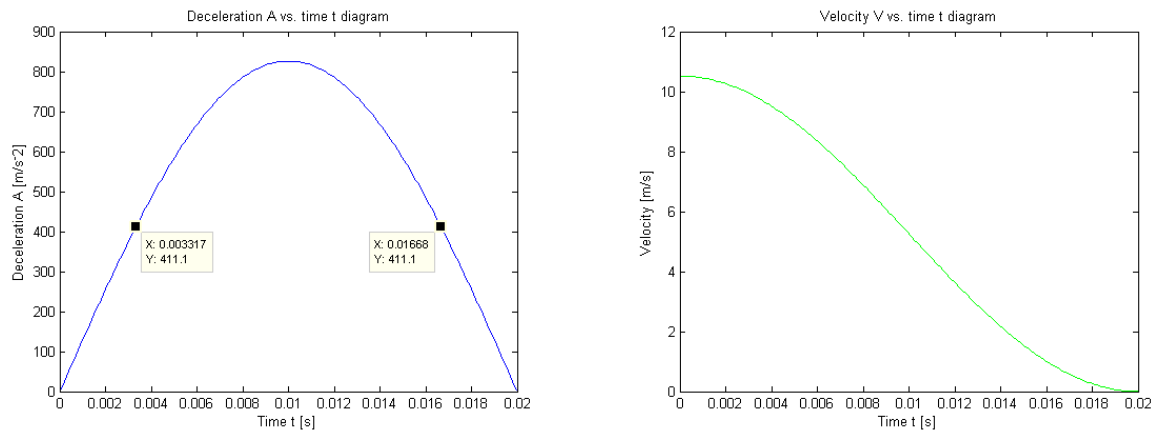
The figures 7.2 show the deceleration, velocity and trajectory function for impulse duration $T = 0.02$ s and results are summarized in table 7.2 for analytical solution which in comparison with numerical solution provide small discrepancy. Thus is assumed correct implementation in the MATLAB script.

Regarding table 7.2 it might be in interest to show the influence of pulse duration to HIC value with corresponding trajectory. The simulation output data contains pulse duration only to 20 ms due to high computational time. However for investigating purposes the pulse duration varies from 5 ms up to 30 ms.

Table 7.3 shows results of HIC values for different pulse duration within preserving internal energy.

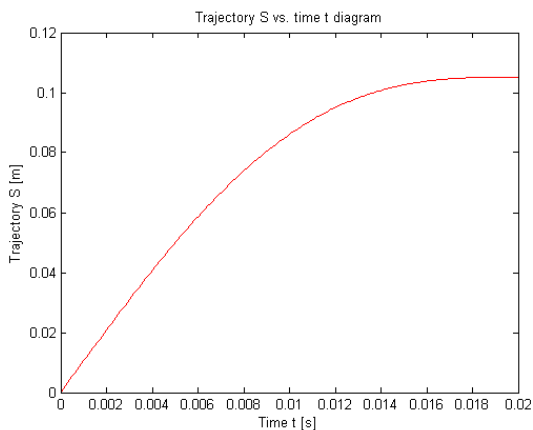
By review of table 7.3 one can notice that the HIC values decrease with increasing trajectory length. In table are highlighted rows i.e. pulse duration and trajectory for HIC value 1000 and 650, pulse duration with HIC value for maximal allowable trajectory $MD = 68.2$ mm. Therefore it could be assumed that pulse duration longer than 13.3 ms lead to HIC values less than 1000 however with trajectory length longer than maximal allowable.

However the sinusoidal function can be modeled as 2 peak in pulse duration to obtain point of view of influence to the HIC value and trajectory with preserving same energy. The



(a) Deceleration vs. time t

(b) Velocity vs. time t



(c) Trajectory vs. time t

Figure 7.2: Sinusoidal function with 1 peak diagrams

Pulse duration T [ms]	Time t_1 [ms]	Time t_2 [ms]	HIC value	Trajectory [mm]
5	0.83	4.17	4322	26.3
10	1.66	8.34	1528	52.6
12.9	2.14	10.76	1041	68.2
13.3	2.21	11.09	1000	70
15	2.49	12.51	832	78.9
17.7	2.94	14.77	650	93
20	3.32	16.68	539	105.2
25	5.03	19.98	381	131.5
30	7.54	22.46	272	157.8

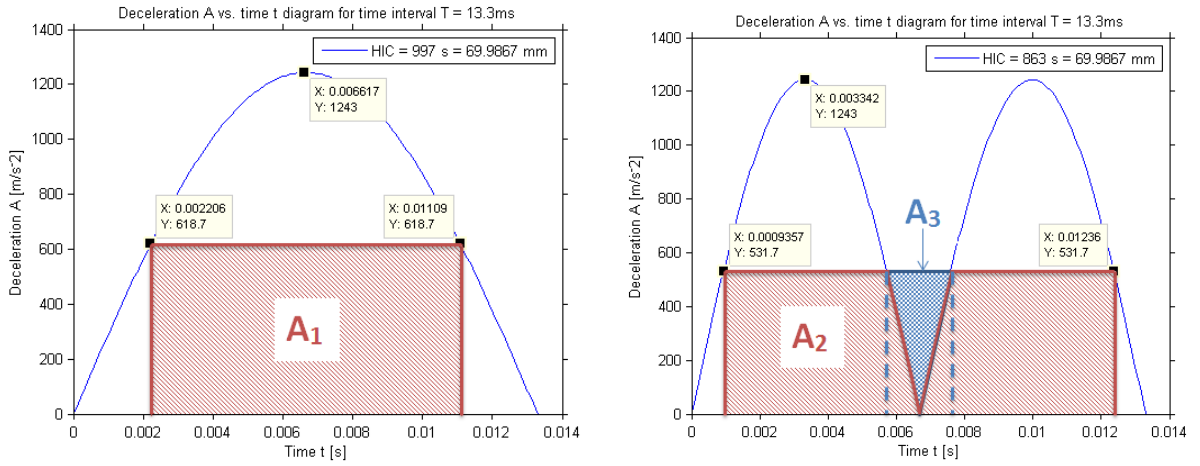
Table 7.3: Sinusoidal function for different pulse duration T whilst preserving energy $E_n=138.5$ J

results are tabled in table 7.4.

As shown in table 7.4, the 2 peak sinus function reduced the HIC value however the trajectory length remain equal to 1 peak function.

pulse duration T [ms]	Time t_1 [ms]	Time t_2 [ms]	HIC value	Trajectory [mm]
5	0.35	4.65	3741	26.3
10	0.70	9.30	1323	52.6
12	0.84	11.16	1000	63.3
12.9	0.91	12.00	901	68.2
15	1.06	13.95	720	78.9
16.1	1.13	14.97	650	84.5
20	2.51	17.49	435	105.2
25	5.03	19.98	223	131.5
30	17.49	27.59	147	157.8

Table 7.4: Sinusoidal function with 2 peaks for different pulse duration whilst preserving internal energy $E_n=138.5 J$



(a) Deceleration A vs. time t for 1 peak function (b) Deceleration A vs. time t for 2 peak function
Figure 7.3: Comparison of 1 peak and 2 peak sinusoidal function

The reason of the HIC value is smaller for 2 peak sinus function could be explained by area considered by HIC criterion. In figure 7.3 the two areas are compared:

$$A_1 = HIC_{acc} \cdot (t_2 - t_1) = 618.7 \cdot (0.01109 - 0.00221) = 5.50 \quad (7.5)$$

$$\begin{aligned} A_2 &= A_{all} - A_3 = HIC_{acc} \cdot (t_2 - t_1) - \frac{1}{2} \cdot HIC_{acc} \cdot (t_{2-tri} - t_{2-tri}) = \\ &= 531.7 \cdot (0.01236 - 0.00094) - \frac{1}{2} \cdot 531.7 \cdot (0.00762 - 0.00568) = 5.56 \quad (7.6) \end{aligned}$$

where HIC_{acc} is acceleration value for corresponding time t_1 and t_2 . Similarly area A_2 is calculated. As one can notice the larger area lead to smaller HIC value.

Therefore the 2 peak design of functions are further considered.

7.2.2 Rectangular function

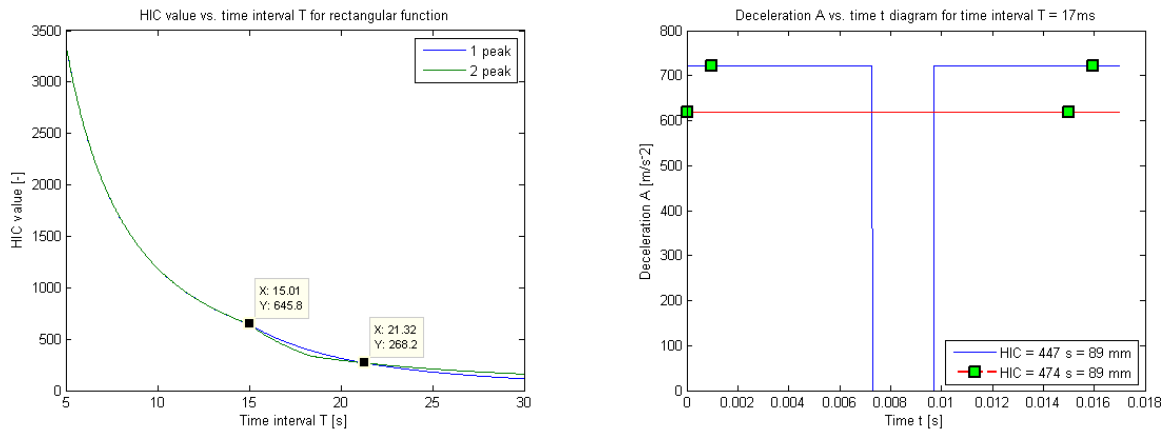
Another possibility to define the deceleration curve leads to use simple rectangular function. Again the restriction of maximal energy is used $E_n = 138.5J$ to perform the design of deceleration curve. The rectangular function could be represented by 2 cases. First simplest

model use constant deceleration value along entire pulse duration. The 2 peak function reflect second used model where at specific time t_s the zero deceleration last until the next time t_e where again arise to original value. All functions are modeled for duration of impact from 5 to 30 ms.

pulse duration T [ms]	1 peak		2 peak	
	HIC value	Trajectory [mm]	HIC value	Trajectory [mm]
5	3372	26.31	3372	26.31
10	1185	52.71	1182	52.71
11.3	1000	59.37	1000	59.37
13	808	68.2	808	68.2
15	650	78.86	650	78.86
17	474	89.50	433	89.50
20	314	105.20	295	105.20
25	180	131.46	211	131.46
30	114	157.50	160	157.50

Table 7.5: Rectangular function for different pulse durations

According to table 7.5 and figure 7.4(a) the one and two peak rectangular function provide same value of HIC due to 15 ms HIC criterion limitation. After 15 ms the HIC value calculated from 2 peak function slightly decrease against to 1 peak function and after 21.3 ms the dependency is vice versa. This is due to fact that 2 peak function had zero value at certain ratio of pulse duration T stated to $t_s = \frac{3}{7}T$ and $t_e = \frac{4}{7}T$ and with increasing the pulse duration T thus increasing zero area which does not contribute to integration of HIC calculation. For better explanation was depicted figure 7.4(b) for 1 and 2 peak function at 17 ms pulse duration. As one can notice the HIC value of 1 peak is higher against to 2 peak because of duration of zero pulse where time frame could only cover 15 ms of whole pulse and the zero pulse is wider than for 15 ms pulse duration. Therefore in range 15ms to 21.3ms the zero pulse contributes to lowering HIC and after 21.3ms to deterioration.

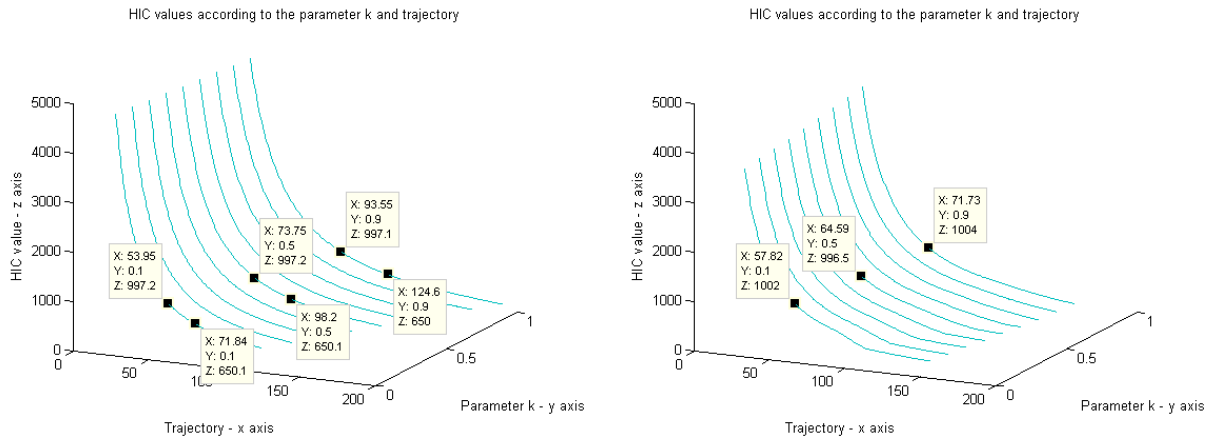


(a) HIC values against to duration of impact T (b) Rectangular function with 2 peaks at 17 ms peak duration

Figure 7.4: Rectangular function diagrams

7.2.3 Triangular function

Last approach from basic group of function by using triangle function with one peak is the most realistic function as deceleration of headform. Due to similar behavior of function in comparison with simulation data the triangular function is further analyzed and used as a starting point for parametric model of functions. Again the deceleration curve is modeled for pulse durations from 5 ms to 30 ms. Regarding table 7.1 the shape of basic triangle function influence the trajectory length due to parameter k which represent the position of peak in pulse duration T . However in expression for evaluation of HIC (triangular section in table 7.1) does not appear parameter k , thus following 3D plot shows dependency of pulse duration with HIC value and trajectory.



(a) Dependency of HIC values according to the parameter k - 1 peak

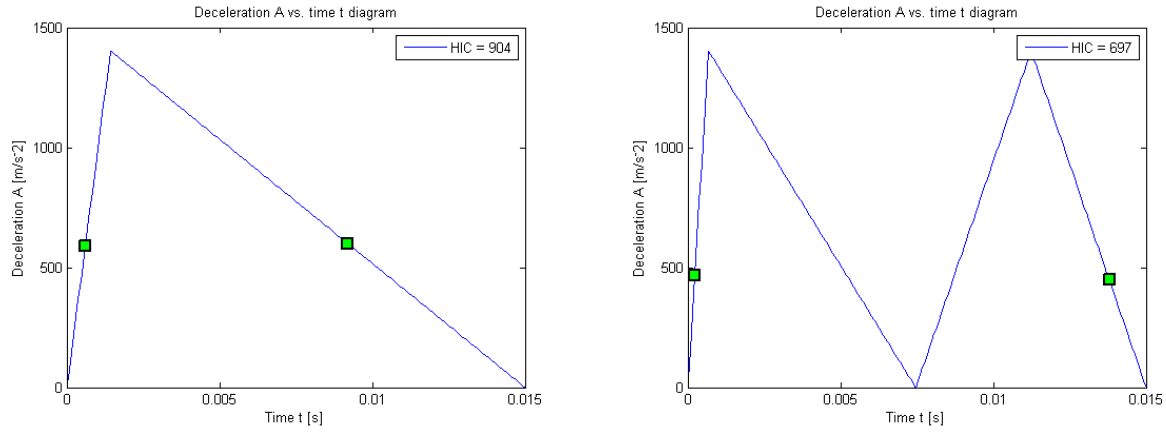
(b) Dependency of HIC values according to the parameter k - 2 peak

Figure 7.5: Comparison of 1 peak and 2 peak triangular function

The figure 7.5 shows dependency of parameter k to trajectory at $HIC = 1000$ and $HIC = 650$ value. By reviewing of 3D plot, for same value of HIC, the trajectory decrease with smaller k parameter. Same principle apply to the 2 peak triangular function shown in figure 7.5(b). The results for 2 peak function are summarized in table 7.6.

Parameter k	HIC=650		HIC=1000	
	Pulse duration T [ms]	Trajectory [mm]	Pulse duration T [ms]	Trajectory [mm]
0.1	15.7	76.9	11.8	57.8
0.2	15.9	79.2	11.9	59.5
0.3	16.0	81.6	12.0	61.2
0.4	16.2	83.7	12.1	62.9
0.5	16.3	85.7	12.2	63.9
0.6	16.5	87.9	12.4	66.3
0.7	16.7	90.6	12.5	68.1
0.8	16.9	93.5	12.7	69.9
0.9	17.0	95.6	12.8	71.7

Table 7.6: 2 peak triangular function with variable parameter $k = 0.1$ for HIC value 650 and 1000



(a) 1 peak triangular function with parameter $k = 0.1$ and pulse duration $T = 15$ ms
 (b) 2 peak triangular function with parameter $k = 0.1$ and pulse duration $T = 15$ ms

Figure 7.6: Comparison of 1 peak and 2 peak triangular function for $T = 15$ ms

The two peak function model is characterized that both peaks has equal time duration from pulse duration T i.e. each peak takes half of T . The first peak position in time is determined by parameter k . The second peak $k_2 = 0.5 \cdot \frac{T}{2}$ is situated in middle of second half of pulse duration T as shown in figure 7.6(b).

As is shown in table 7.6 towards to higher values of parameter k the trajectory increase. Therefore further aim is to design function which rapidly growth and after maximal deceleration point gently decrease to zero. The results for parameter $k = 0.1$ are listed in table 7.7 which corresponds with analytical solution table 7.1.

Pulse duration T [ms]	1 peak		2 peak	
	HIC value	Trajectory [mm]	HIC value	Trajectory [mm]
5	4700	19.2	3626	25.5
10	1654	38.5	1276	49.2
11.8	1297	45.4	1000	57.8
13.9	1000	53.5	780	68.2
15	899	57.5	693	73.8
15.7	845	60.2	650	76.9
17.8	698	68.2	518	87.4
18.7	650	71.8	453	91.7
20	583	77.1	348	98.4
25	417	96.4	211	122.0
30	315	115.2	160	147.1

Table 7.7: Triangular function with parameter $k = 0.1$

However the 1 peak function does not covers problematic of real impact where 2 peaks usually appear. Therefore section 7.4 deals with 2 peak function to approach to more realistic function.

Triangular function with parameter k_2 for second peaks

Another case could be considered that the second peak is also influenced by parameter k_2 where the first peak remain same to the parameter $k = 0.1$. This approach shows additional influence to previous case. The trajectory length is chosen to maximal allowable $MD = 68.2mm$ mentioned in section 7.1 and the influence of parameter k_2 is investigated within again preserving energy $En = 138.5J$.

Parameter $k_2, k = 0.1$	Pulse duration T [ms]	HIC value
0.1	15.1	733
0.2	14.7	749
0.3	14.4	754
0.4	14.2	767
0.5	13.9	781
0.6	13.7	789
0.7	13.4	796
0.8	13.2	814
0.9	13.0	821

Table 7.8: Triangular function with parameter $k = 0.1$ and variable parameter k_2 for trajectory MD=68.2mm

Obviously as it was concluded in section 7.1, the parameter k_2 plays significant role in the trajectory change however the high angular coefficient of second peak which is related to small parameter k_2 is hard to achieve.

7.3 Conclusion from basic functions

The section 7.2 devote to design deceleration curves by using sinusoidal, rectangular or triangular function. According to the previous figures and tables obviously by increasing the duration of impact with preserving energy the HIC values decrease. Because of the HIC value decreases with the length of trajectory the reasonable compromise could be stated to the maximal allowable displacement MD. The table 7.9 shows comparison for all used basic functions. The results are referenced to HIC value 650 and 1000 which are most representing to obtain overall point of view which function provide best results.

By review of table 7.9 one can notice that the best function shape appear triangular with parameter $k = 0.1$. The triangular function provide shortest trajectory from all previous basic functions for HIC=650 and HIC=1000. By considering two peak functions also the triangular function with parameter $k = 0.1$ and $k_2 = 0.1$ provide shortest trajectory against to sinusoidal or rectangular. However the sharp triangular function in the beginning is hard to realize especially at the second peak where the mass of bonnet play significant role.

Higher mass of bonnet represents high moment of inertia against impact of headform and therefore during impact the main portion of kinetic energy is consumed by deflection of bonnet and it cause great slope of deceleration curve in short time interval and bonnet starts to deform. By contrast the mass of bonnet should be as low as possible due to saving of total weight of car.

HIC = 650	Trajectory [mm]	Trajectory [mm]
	1 peak	2 peak
Sinus	93.00	84.50
Rectangle	78.86	78.86
Triangle ($k=0.1, k_2 = 0.5$)	71.84	76.90
Triangle ($k=0.1, k_2 = 0.1$)	71.84	74.31
HIC = 1000	Trajectory [mm]	Trajectory [mm]
	1 peak	2 peak
Sinus	70.00	63.30
Rectangle	59.37	59.37
Triangle ($k=0.1$)	53.50	57.80
Triangle ($k=0.1, k_2 = 0.1$)	53.50	55.85

Table 7.9: Results of trajectories for basic functions for HIC values 650 and 1000

Reason to avoid the rectangular function is that it is problematic to realize because of immediate constant value of deceleration for pulse duration T .

Due to all mentioned reasons the following chapter is devoted to treatment of triangular 2 peak function with adjustable several parameters to obtain the best and most realistic optimized deceleration function.

7.4 Parametric model function

The following section describe the possible designs by using 2 peak triangular function with parameters:

- The ratio RP is multiple of peak magnitude A_p
- The ratio MP is multiple of peak magnitude A_p

After review of several simulation data represented by figure 7.7(a) for impact situated to the middle of bonnet top the time parameters for situation of peaks in the pulse duration was set to: $k_1 = \frac{1}{6}T$, $k_2 = \frac{4}{6}T$, $k_3 = \frac{5}{6}T$ where T is pulse duration. Thus for region of impact points situated in the middle of bonnet top, the T value is assigned to 18ms. Another constant value is the average consumed energy by bonnet previously mentioned to the **En=138.5 J**. Therefore only RP and MP parameters are modified to preserve energy represented by area under force-trajectory curve. The **RP** (ratio peak) parameter depicted in figure 7.7 is ratio of magnitude of first peak to magnitude of second peak in range of **0.1 - 1** where 1 represents same magnitude of both peaks. The **MP** (local minimum) parameter depicted in figure 7.7 is ratio of magnitude of first peak to local minimum between both peaks in range of **0.01 - 0.3** where 0.01 represents almost zero deceleration. However by using range from 0 to certain value for parameters would issue in high computational time. Thus using of deceleration values of peaks from section 7.2.3 serve as starting point for range of parameters which are desired.

Figure 7.7(b) explain all previous mentioned parameter used in further calculations.

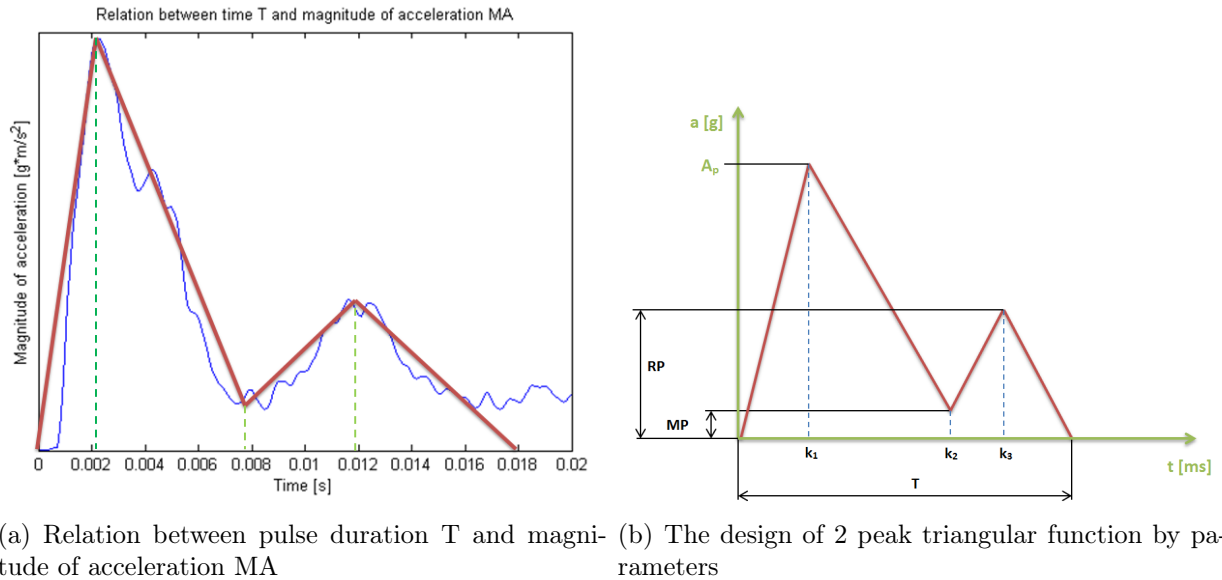
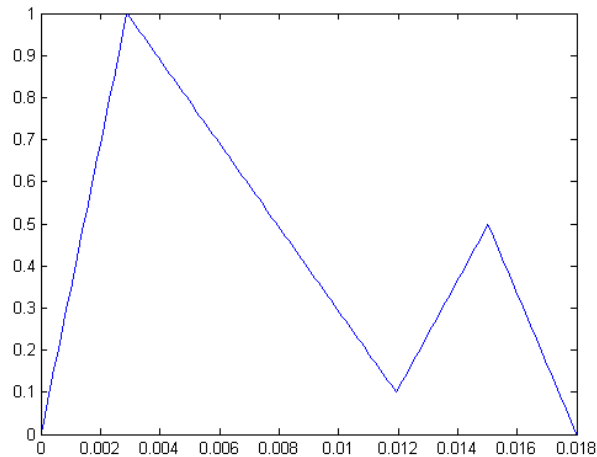


Figure 7.7: The parametric 2 peak triangular function

7.4.1 Model of function

As was mentioned before the pulse duration $T=18\text{ms}$ and internal energy $En = 138.5\text{J}$ has to be preserved. The parameters RP and MP defines magnitude of deceleration peak within pulse duration T . As shown in figure 7.8 in the beginning is modeled two peak triangular function in way that the first magnitude of peak is unit and the rest of function shape depends on parameters RP and MP . In figure 7.8 is shown the $RP=0.5$ where second peak has half magnitude of first peak. The local minimum of curve is 10 times smaller against to first peak magnitude which corresponds to parameter $MP=0.1$.

Figure 7.8: The 2 peak function with unit first peak and shape according to parameters $RP=0.5$ and $MP=0.1$

The design of deceleration curve goes out of internal energy En which has to be preserved. By two times cumulative integration of acceleration function the trajectory curve is obtained.

Therefore one has two curves (acceleration-time, trajectory-time) with same pulse duration T and thus it is possible to merge them together to result one curve i.e. acceleration-trajectory. Mentioned acceleration is multiplied by mass of impactor and it leads to force-trajectory curve. After integration is obtained area which represents the internal energy En . Then the unit acceleration function is multiplied by certain coefficient until the internal energy En is achieved after integration.

Because of two parameters RP and MP the MATLAB script is created to use two *for* iteration cycles where second parameter MP is embedded in first one and parameters are implemented as coefficient range. The script is listed in appendix D.

Obviously the various of RP and MP parameters lead to widespread results of HIC and trajectory. Therefore two methods are used to evaluate parametric function curves i.e. constant HIC level and constant trajectory. The constant HIC level shows parameters which meet the $HIC = 650$ and 1000 . In contrast the constant trajectory method shows parameters which meet the maximal allowable deflection in direction of impact $MD=68.2\text{mm}$. Pulse duration $T = 18\text{ms}$ served as first approach, however in further design is extended to ± 5 ms to show disparity by using different time durations T .

Constant HIC level

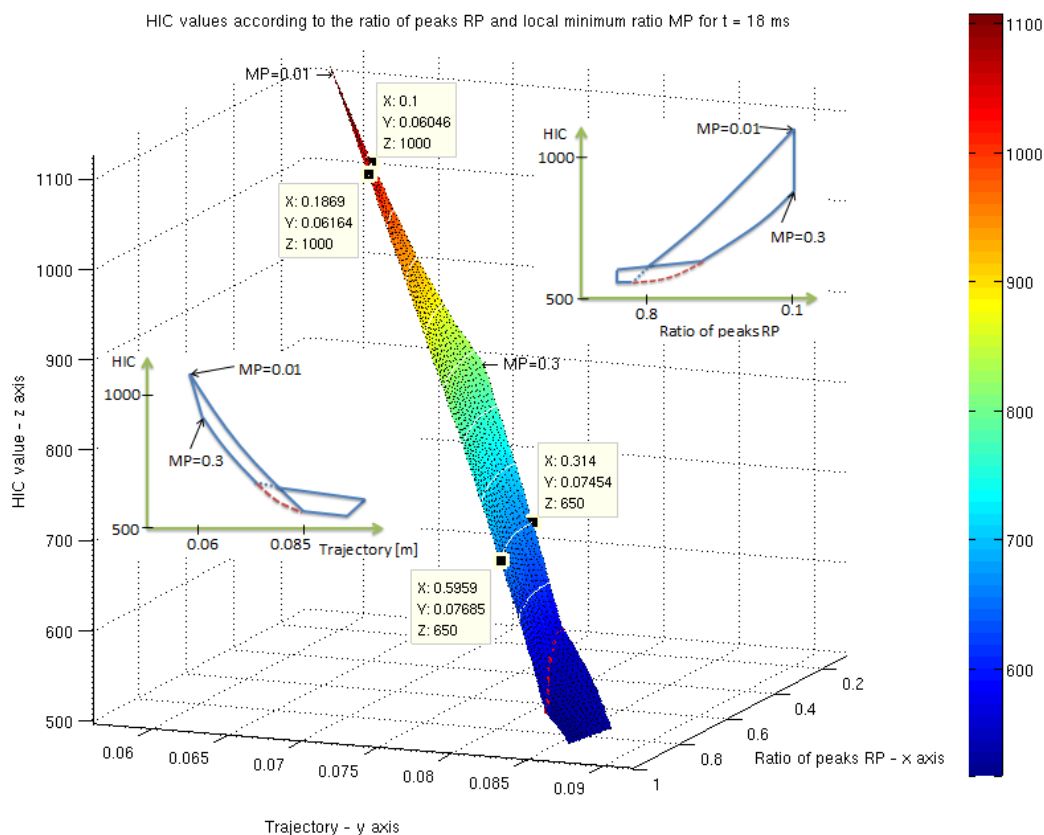


Figure 7.9: Dependency of HIC values according to ratio peak RP and corresponding trajectory

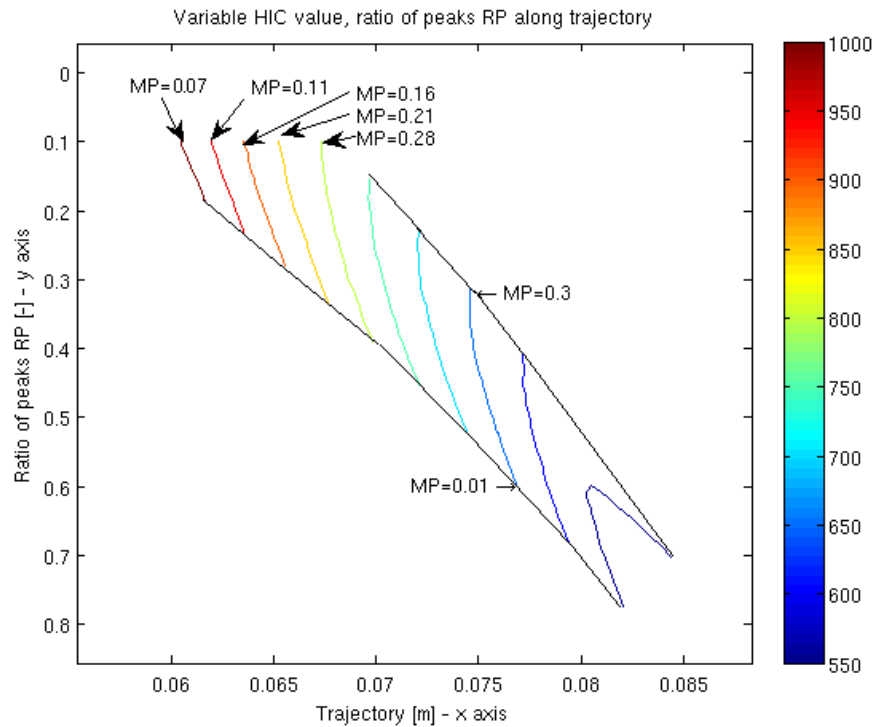
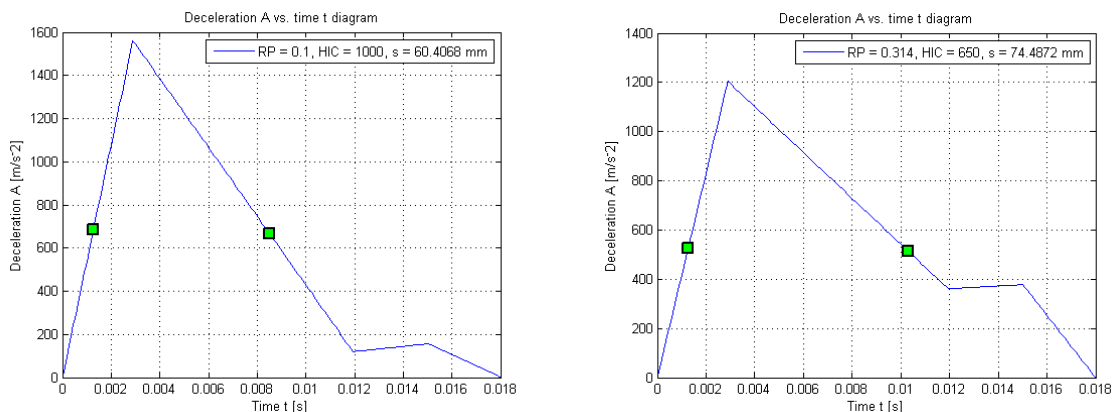


Figure 7.10: Contour plot - dependency of peak ratio RP along trajectory at variable HIC

The figure 7.9 illustrate obtained calculated results for 2 peak parametric function where X axis represents ratio of peaks RP, Y axis represents trajectory and Z axis represents HIC value for pulse duration 18 ms. In the surface plot the white lines represent constant HIC level e.g. in the top of plot the line where data cursors (in beige color) shows at z axis value $HIC = 1000$. Each next downward level defined by white line shows results for HIC tiered by value of 50. Mentioned HIC levels are depicted in figure 7.10 by using contour plot. The y-axis represents RP parameter and depicted line in certain HIC value represents the change of MP parameter. Third line from bottom shows possible combination of MP and RP parameter to obtain $HIC = 650$. The contour lines in figure 7.10 for $HIC=850-1000$ do not end at $MP=0.3$ because of not fulfilling restrictions of internal energy En and also because of set the RP to 0.1.

However each combination has different consequence to resultant trajectory. Therefore to obtain as small trajectory as possible at $HIC 1000$ the $RP=0.1$ and $MP=0.07$ are chosen which lead to trajectory $s=60.5$ mm depicted in figure 7.11(a). Likewise for $HIC 650$ the $RP=0.314$ and $MP=0.3$ are chosen which lead to trajectory $s=74.5$ mm shown in figure 7.11(b). The contour curve at $HIC 550$ shows wrapped shape due to the fact that at $RP=0.7$ and $MP=0.3$ the HIC is calculated from both peaks as shown in figure 7.13(b) and trajectory increase. Also by using $RP=0.775$ and $MP=0.01$ the HIC equal to value 550 however the trajectory is shorter and HIC is calculated from first peak.

The red curve in figure 7.9 divide the surface in two regions where the HIC is calculated from 1 in region above red curve and calculated from 2 peaks. The contour plot of red curve is illustrated in figure 7.12.



(a) The force - time dependency for duration of impact 18 ms with $RP=0.1$ and $MP=0.07$, $HIC=1000$ (b) The force - time dependency for duration of impact 18 ms with $RP=0.314$ and $MP=0.3$, $HIC=650$

Figure 7.11: Parametric triangular function for 18 ms duration of impact

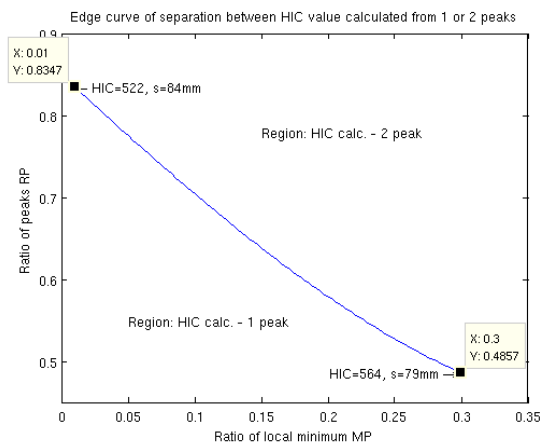
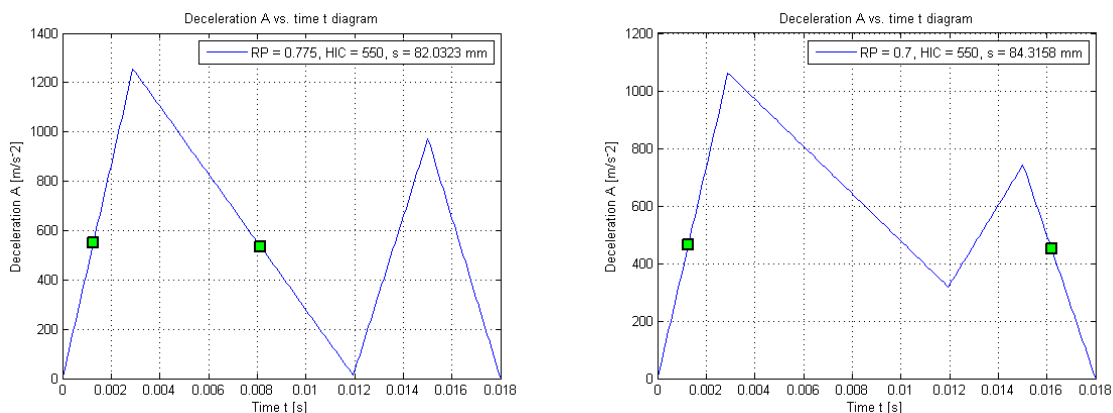


Figure 7.12: Contour plot - dependency of peak ratio RP along ratio of local minimum MP and regions where HIC is calculated from 1 alternatively 2 peaks



(a) The force - time dependency for duration of impact 18 ms with $RP=0.775$ and $MP=0.01$, $HIC=550$ (b) The force - time dependency for duration of impact 18 ms with $RP=0.7$ and $MP=0.3$, $HIC=550$

Figure 7.13: The deceleration - time dependency for duration of impact 18 ms

Constant trajectory level

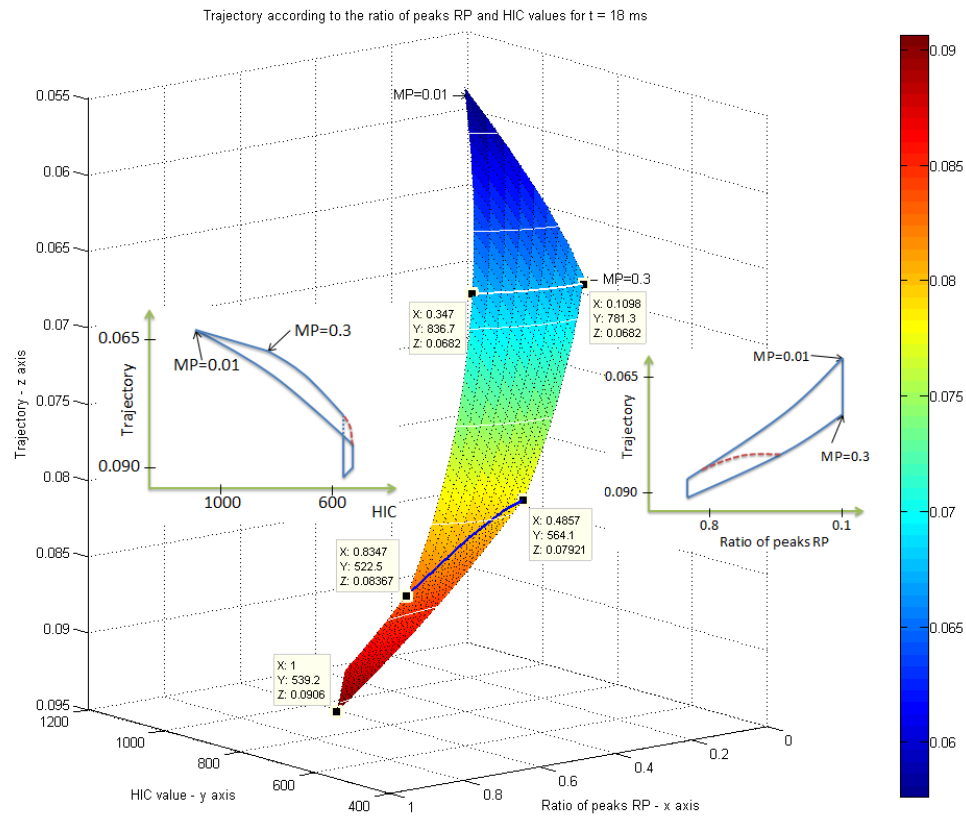


Figure 7.14: Dependency of trajectory according to ratio peak RP and corresponding HIC value

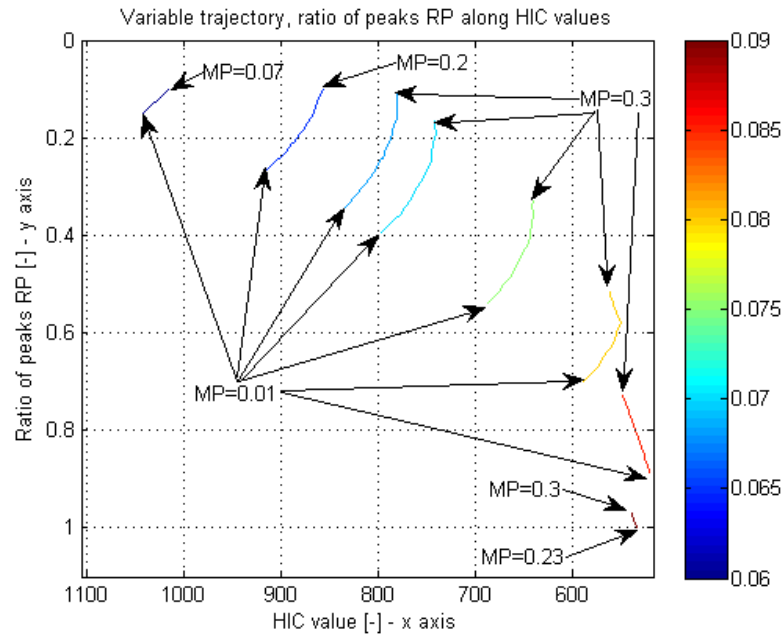
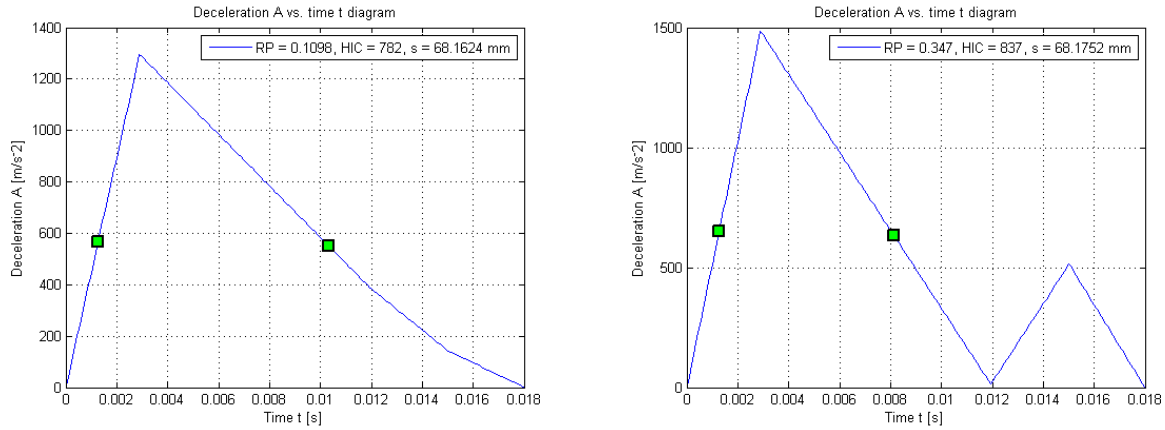


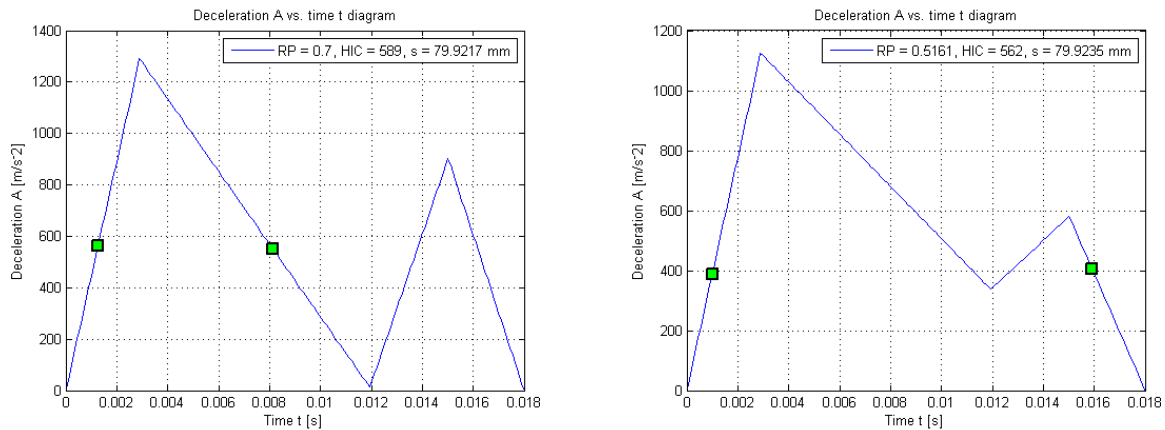
Figure 7.15: Contour plot - dependency of peak ratio RP along HIC value

In the beginning was selected trajectory $MD = 68.2$ mm to show parameters which complies trajectory condition. Two extreme cases are shown in figure 7.16. Parameters are marked in 3D surface plot shown in figure 7.14 and figure 7.15.



(a) The deceleration - time dependency for duration of impact 18 ms with RP=0.1098 and MP=0.3, s=68.2mm
 (b) The deceleration - time dependency for duration of impact 18 ms with RP=0.347 and MP=0.01, s=68.2mm

Figure 7.16: The deceleration - time dependency for duration of impact 18 ms, constant trajectory



(a) The deceleration - time dependency for duration of impact 18 ms with RP=0.7 and MP=0.01, s=80mm
 (b) The deceleration - time dependency for duration of impact 18 ms with RP=0.516 and MP=0.3, s=80mm

Figure 7.17: The deceleration - time dependency for duration of impact 18 ms, constant trajectory

As one can see the smallest value of HIC = 782 for trajectory MD=68.2 lead to function with MP = 0.3 and RP = 0.1098 shown in figure 7.16(a) which could be understood almost as 1 peak triangular function. Otherwise for parameters MP = 0.01 and RP = 0.347 depicted in figure 7.16(b) the HIC value slightly increased however the shape more reflect the realistic deceleration dependency.

The previous design was based on 18ms duration of impact. Therefore in further analysis is chosen 13ms pulse duration and illustrated in figure 7.18.

The shorter pulse duration leads to shorter trajectory length however to higher HIC value. Regarding figure 7.18 for HIC value 1000 the trajectory decreased from 60mm represented in figure 7.11(a) to 55 mm represented in figure 7.18 with parameters RP=0.376 and MP=0.3.

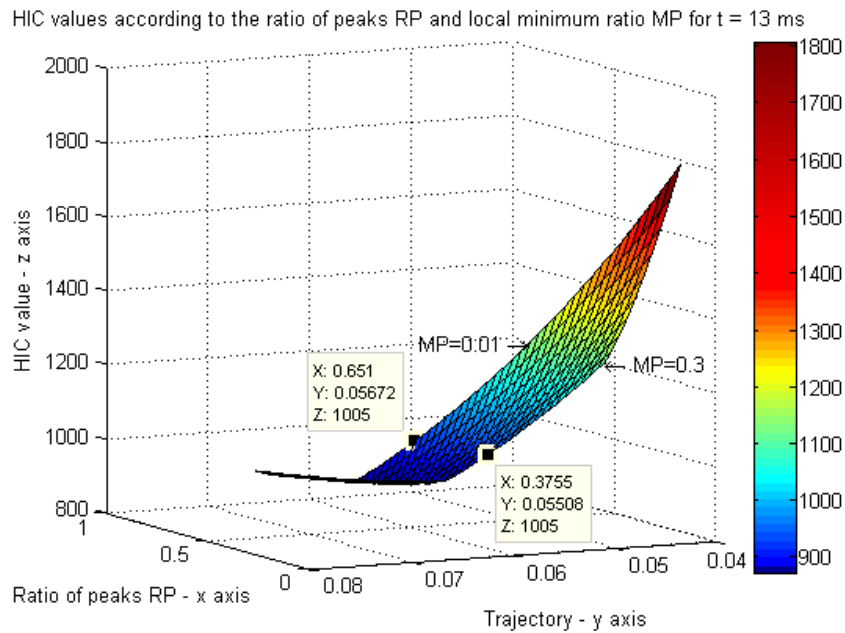


Figure 7.18: Dependency of HIC values according to ratio peak RP and corresponding trajectory

As a third approach was used pulse duration $T=23$ ms.

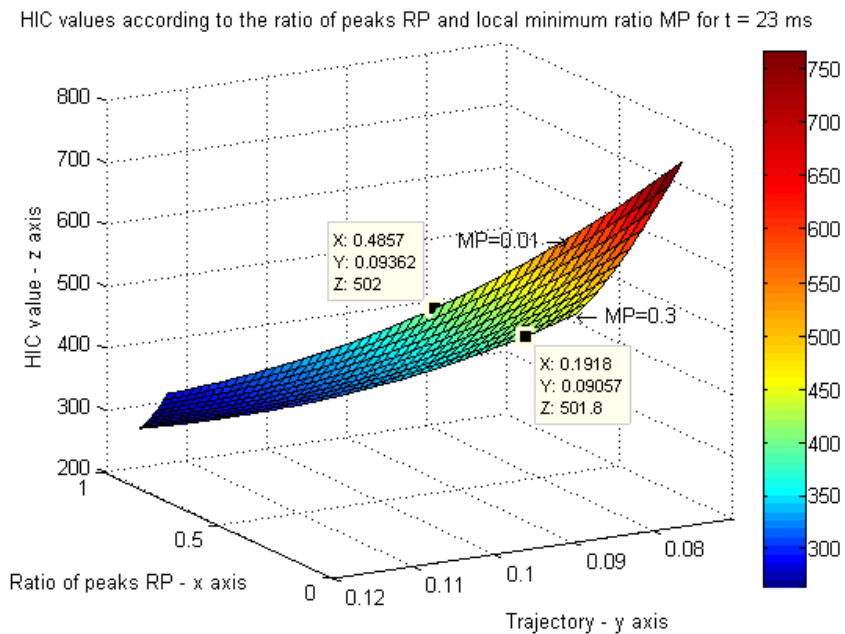


Figure 7.19: Dependency of HIC values according to ratio peak RP, local minimum MP and corresponding trajectory

By increasing pulse duration time to 23 ms obviously the HIC value decreased however the trajectory greatly increased.

7.5 Conclusion of used functions

Basic functions

The section 7.2 was devoted to design the optimal deceleration curves by using sinusoidal, rectangular or triangular function. However the best results of HIC value provide triangular function tabled in table 7.10 due to great slope of first peak and after gentle reduction to zero acceleration. Although sinusoidal function with 1 peak results in higher HIC value than 2 peak function, for triangular curves it is vice versa. The usage of more peak functions is considered as more realistic from impact point of view. The reason of rectangular function good results of HIC is due to fact that function is design as uniform curve along the pulse duration. However mentioned design does not correspond to the real impact to the bonnet.

The comparison in following table is done to proposed trajectory MD=68.2mm (section 7.1) and for HIC=650 and 1000.

Proposed trajectory MD=68.2mm						
	Sinus		Rectangle		Triangle	
	1 peak	2 peak	1 peak	2 peak	1 peak	2 peak
Pulse duration T [ms]	12.9	12.9	13	13	17.8	13.9
HIC	1041	901	808	808	698	780

Table 7.10: Results of pulse duration and HIC values for basic functions within trajectory set to 68.2 mm

HIC=1000						
	Sinus		Rectangle		Triangle	
	1 peak	2 peak	1 peak	2 peak	1 peak	2 peak
Pulse duration T [ms]	13.3	12	11.3	11.3	13.9	11.8
Trajectory [mm]	70	63.3	59.4	59.4	53.5	57.8

Table 7.11: Results of pulse duration and trajectory for basic functions within HIC=1000

HIC=650						
	Sinus		Rectangle		Triangle	
	1 peak	2 peak	1 peak	2 peak	1 peak	2 peak
Pulse duration T [ms]	17.7	16.1	15	15	18.7	15.7
Trajectory [mm]	93	84.5	78.9	78.9	71.8	76.9

Table 7.12: Results of pulse duration and trajectory for basic functions within HIC=650

According to table 7.10 the triangular function provides best results regarding to proposed trajectory MD where the HIC values are lower than by using sinusoidal and rectangular function.

Similar results are obtained within restriction HIC=1000 resp. 650. For triangular function the trajectory length is shorter against to both previous.

Parametric function

After research of shapes impact curves the model of 2 peak parametric function was proposed in detail described in section 7.4 where pulse duration T was set to 18 ms. A possible changeable parameters were ratio of peaks RP and local minimum ratio MP . The RP range from 0.1 to 1 and together with MP from 0.01 to 0.3 have created the 3D plot where trajectory with corresponding HIC are investigated. As was mentioned before the proposed trajectory $MD=68.2\text{mm}$ in this case was not taken into account as mandatory restriction due to effort to shows the dependencies of RP and MP to HIC and trajectory.

For 18 ms pulse duration which is representative and for constant trajectory ($MD=68.2\text{ mm}$) the shape of "1 peak" function provide better HIC value against to distinguishable 2 peak function.

At constant trajectory ($s=80\text{ mm}$) for 18 ms pulse duration the triangular function where the HIC is calculated from both peaks provide obviously better HIC value due to possible longer trajectory to deformation.

In the end the results for 13ms resp. 23ms were shown results in 3D plots. For 13 ms the whole graph moves to higher HIC values with lowering trajectory. Opposite behavior could be observed for 23 ms.

Results shown that the 1 peak function provides better HIC values with respect to trajectory. However as it was mentioned before the 1 peak function in real structures are hard to design which will be shown in following chapter devoted to FEM modeling of bonnet structure to obtain as low HIC as possible.

8. Design of approximated bonnet structure

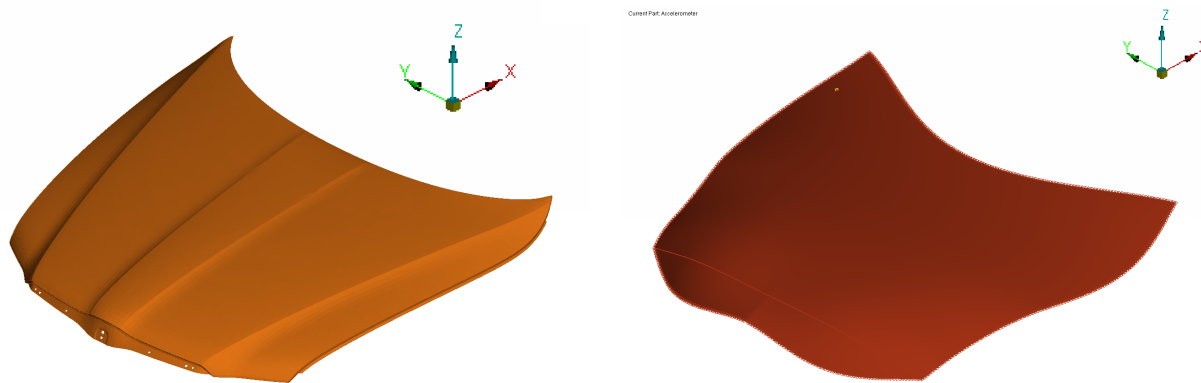
In previous chapter the most ideal-realistic deceleration curve was found. Now we try to design structure of bonnet to follow analytic dependency. The mass of bonnet should be as small as possible. The original bonnet mass is $BM=19.4$ kg therefore all further design it respects as restriction. The model data are stored in `./SK461_SPX_001` directory.

8.1 Computational model

To create a computational model the ANSA preprocessor was used. This software serves as a creator of geometrical model and finite element mesh. Also it allows to create model of boundary conditions, model of material and model of contacts.

8.1.1 Geometrical model - first variant 000

The model of geometry goes out from geometry of superficial part of bonnet (further SupP) depicted in figure 8.1(a). Data file of current variant is `SK461_SPC_020_000.pc`. The model of geometry was created by using edge splines and several points defining the curvature of SupP geometrical model. Then by smoothing edge splines which served as boundaries, the surface was created with respecting approximation points however it does not include superficial skims as shown in figure with SupP. The resultant shape model of geometry of bonnet is shown in figure 8.1(b).



(a) The superficial part of bonnet top from Superb SK461

(b) The approximate model of bonnet top

Figure 8.1: Comparison of superficial to approximated model of bonnet

The first variant contains only the meshed surface by shell elements with thickness of 0.7 mm and its mass around 8.25 kg. The designed model has to have mass approximately equal to the original superficial part of bonnet to ensure approximate strength and stiffness properties which are prime for impact analysis.

Finite element mesh

Due to fact that individual bonnet part are slight sheets and could be considered as thin-wall structure therefore is suitable to use SHELL elements.

The designed bonnet body is meshed by shell elements with thickness 0.7 mm and 5 integration points through thickness positioned in the center of element. Three integration points are sufficient to integrate bending and membrane effects [21]. However due to consideration of material plasticity, the 5 integration points are necessary. The thickness of bonnet surface remains same for all further designs due to keep the original bonnet mass. The mesh generator serves to produce as mapped mesh (with quadratic elements) as possible, however according to curved shape of bonnet it cannot mesh whole bonnet body with quadratic elements and thus somewhere it uses the triangle elements to fill the remain areas. However the triangle elements are not suitable due to increasing stiffness and in extreme they can cause over-stiffing the model, therefore one try to avoid them as much as possible. The quadratic element is 4 node shell element with 6 degrees of freedom in each node i.e. displacement and rotations. Strain at middle surface is obtain from field of displacements and shears from field of rotations. Each node has following deform parameters:

$$(u, v, w, \varphi_x, \varphi_y, \varphi_z)$$

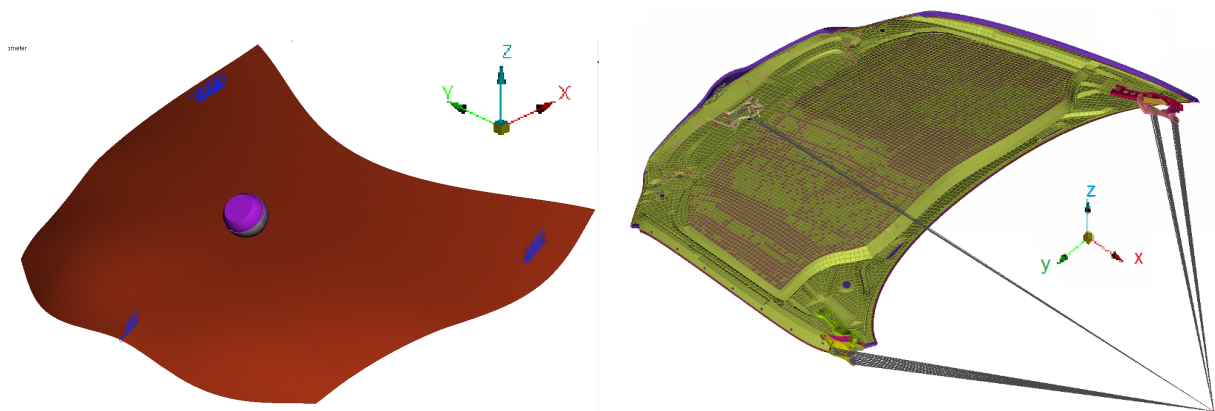
The stress and strains are calculated according to local coordinate system through thickness and by using PAM SHELL 103 with 5 integration points in the middle of elements the stresses are calculated in 5 layers of thicknesses. The triangle elements are similar to quadratic elements however only with 3 node. The internal norm in Škoda Auto a.s. recommends the edge length of elements to be not grater than 10 mm.

In further the foam layer is also used which is meshed by PAM SOLID 45 elements. It is described by 8 nodes with same 6 degrees of freedom at each node as at shell element.

8.1.2 Modeling of boundary condition

Geometrical boundary conditions

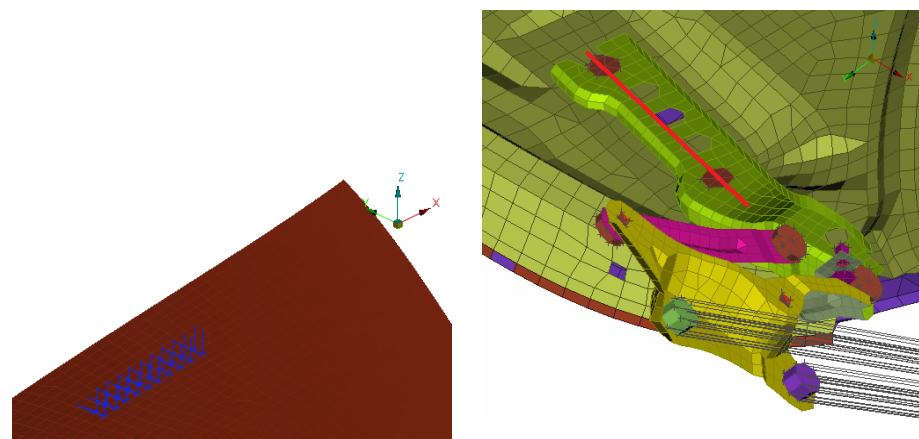
The original model of bonnet is assembled from superficial part figure 8.1(a) and internal part figure 8.2(b). Mentioned parts are glued together at the outer perimeter of both parts. To the internal part left and right hinges are welded depicted in figure 8.3(b) and the front of bonnet is bounded by LINK element which models the front lock of bonnet. Therefore only 3 places and bounded. The ends of hinges and bottom part of front lock are constrained by RIGID body boundary condition which model the connection to the rest of car. However first variant takes into account geometrical model with only approximated superficial bonnet therefore it is necessary to model substitute of hinges. According to previous model of boundary condition on original bonnet, the places where the hinges are welded to the internal structure are shown in figure 8.3(b). The position of red line is transformed to the approximated model of bonnet and corresponding nodes are constrained. The nodes are constrained in two lines due to possible overloading of separate nodes as illustrated in figure 8.3(a). The nodes at left and right hinges are constrained in X,Y and Z direction, only nodes situated in the front of model are constrained in Z and Y direction. Coordinate system is shown in figure 8.3(a). Then is obtained fully constrained model depicted in figure 8.2.



(a) The boundary conditions used for bonnet top (b) The boundary conditions used for original structure of bonnet

Figure 8.2: The boundary conditions used for bonnet top

As one can see in figure 8.3(a) the used boundary condition does not equally corresponds with boundary conditions applied at original bonnet structure where the connection bolts and front hook are constrained by rigid body. However due to lack of modeled hinges for approximated model of bonnet, the mentioned boundary conditions serve as reasonable starting point.

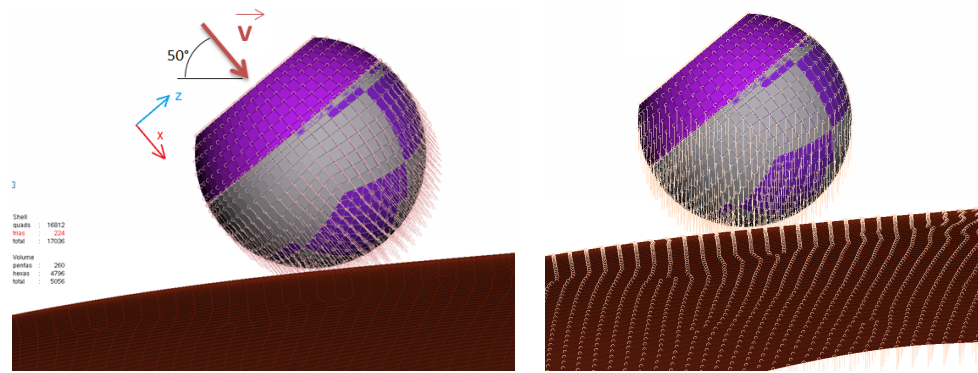


(a) Detail of boundary conditions applied at location of left hinge (b) Detail of boundary conditions applied at left hinge

Figure 8.3: The boundary conditions used for bonnet top - detail

Force boundary conditions

According to figure 8.4 the child impactor is used with internal label *SKxxx_xPC_impactor_110_2008.inc* and situated in the middle of bonnet top as a first approach. The impactor is aligned according to 50° from ground level. Applied initial velocity boundary condition results in movement of impactor in X direction of local coordinate system with velocity $11.3 \frac{m}{s}$ illustrated in figure 8.4(a). The gravitation field acts to the whole model with gravity constant $9.81 \frac{m}{s^2}$ shown in figure 8.4(b).



(a) The initial velocity of impactor

(b) The impactor aligned by 50° from ground level and situated in the middle of surface

Figure 8.4: The initial force conditions used for headform and bonnet structure - initial velocity and gravity field

8.1.3 Model of contact

The model of geometry has several parts which can be in contact. In the first variant only the approximated superficial bonnet and headform are in contact. In the rest of variants the model is more complex however approach of using contact type is identical. The model use two types of contacts recommended for crash simulation i.e. type 33 and type 36. Contact solution is based on penalty method [22]. The definition of contact type 33 is symmetric node-to-segment contact with edge treatment where are treated both surfaces against penetration. The type 33 is Master-Slave contact type, where the slave nodes are checked against penetration to the segments/edges of master side as shown in figure 8.5. Mentioned type use also vice versa approach where the master nodes are treated with slave segments/edges because of symmetric definition of contact. Type 36 is self-impacting contact with edge treatment which need only slave elements where each node/edge of the slave side is checked for penetrations to the segment/edges of same slave side [21].

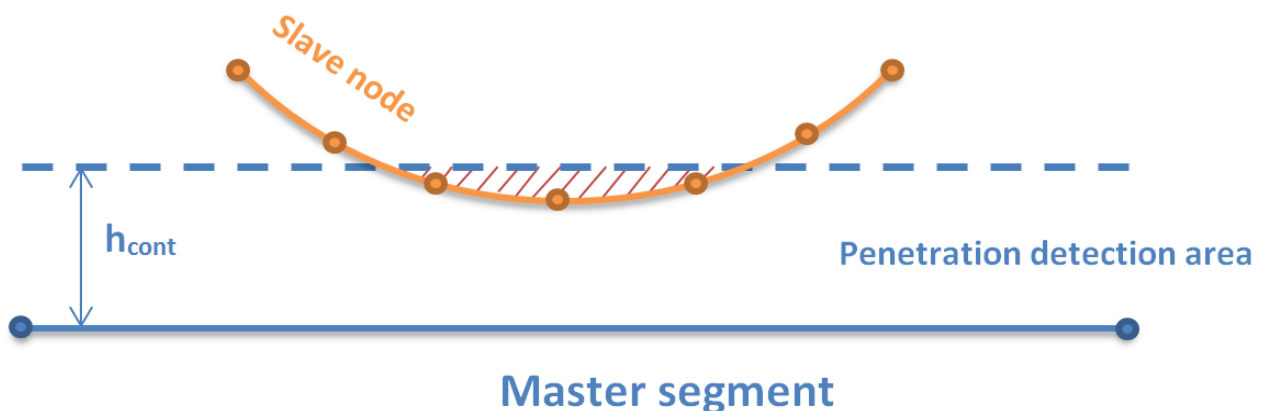


Figure 8.5: Penetration definition for contact type 33

The definition of contact [21] in ANSA corresponds to the following table:

The screenshot shows the 'CNTAC / [CNTAC]' dialog box in ANSA. The 'Name' field is 'CNTAC / seg/seg'. The 'FROZEN_ID' and 'FROZEN_DELETE' fields are both set to 'NO'. The main table contains the following data:

IDCTC	NSS	NMS	NTYPE	T1SL	T2SL	sensor	ISENS	hcont	NACC	NUMBKT	THKEXT	IEDGE	IPCP	SLFACM	FSVNL	IKFOR	PENKIN	CTFRC	TLSTIF	FRICT	IDFRIC	XDMP1	IREMOV	IEROD	ILEAK	IAC32	IOMIT	IFREED	DTHKPLK	SEPSTR	SEPTHK	Comment
9600001	41	40	33	0	0	+		0.5				0		0.1	0	0	0			0.65	0	0.1	0									

The 'Comment' field is empty. The dialog box has 'OK' and 'Cancel' buttons at the bottom.

Figure 8.6: The table with contact properties between skin of impactor and bonnet top

where $IDCTC$ is identification number of contact, NSS is slave set of impactor surface elements, NMS is master set of bonnet surface elements. The $T1SL$ and $T2SL = 0$ therefore the sliding interference remains active until end of run. The h_{cont} is the contact thickness defined by distance away from a contact face where the physical contact is established showed in figure 8.5.

$SLFACM$ - penalty factor remains at 0.1 due to recommendation in [21]. $SLFACM < 0.1$ can cause perforation and otherwise greater value lead to severe stability problems.

$FSVNL$ reflect force scaling factor for a penetration equal to the contact thickness. Regarding to $FSVNL = 0$ the contact force rise linearly along the contact thickness. The $IKFOR = 0$ not activate calculation of kinematic force. $PENKIN$ is unused dimensionless scale factor due to not taking into account the kinematic force calculation.

The $IREMOV = 0$ neglect the removal of initial penetration from the sliding interface. The headform is situated close to the bonnet structure. During positioning of headform to the bonnet is possible to reach the contact thickness where the nodes would be in contact, therefore in the beginning of solution are moved out from contact thickness h_{cont} . In the output file contains information about number of iteration to remove initial penetration. Due to not using the removal initial penetration is necessary to after solution review the output file to number of iteration. If the nodes of impactor were in penetration area, then the impactor is moved out from bonnet. The $ILEAK = 0$ disable obstruction of vent and leakage areas. If the nodes and segments simultaneously defined as slaves in the TIED INTERFACE with parameter $IAC32 = 1$ these affected nodes are not excluded from contact type 33. The

FRICT represents standard Coulomb friction model where $\mu_c = FRICT$. By internal norm for contact between child impactor and steel bonnet is friction coefficient set to 0.65, for friction between steel material to 0.1 and to friction between steel material and foam material to 0.3. The *IDFRIC* = 0 neglect any advanced friction model ID [23]. The *XDMP1* represents stiffness proportional nodal damping added to the normal contact penalty spring forces between slave nodes and the master segments of this interface [21].

8.1.4 Model of material

Model of material used for shell elements

The material type used for original bonnet parts could not be used for educational purposes, therefore my supervisor provide me steel material with similar properties internally labeled as *zste220i_CVUT_st_SHE_plc_sko*. The model of material corresponds to elastic-plastic isotropic thin shell material with enhanced plasticity algorithm that includes transverse shear effect. It exactly satisfies Hill's criterion and precisely updates the element thickness during plastic deformation. [21]. The elastic behavior is defined by [24]:

- elastic modulus E
- shear modulus $G = \frac{E}{2(1+\mu)}$
- Poisson's ratio μ
- thickness t_e (due to large displacement/deformation geometric nonlinearity)

The plastic hardening is inputted as multi linear curve definition shown in figure 8.7. In ANSA is necessary to input strain without units and corresponding stress in GPa.

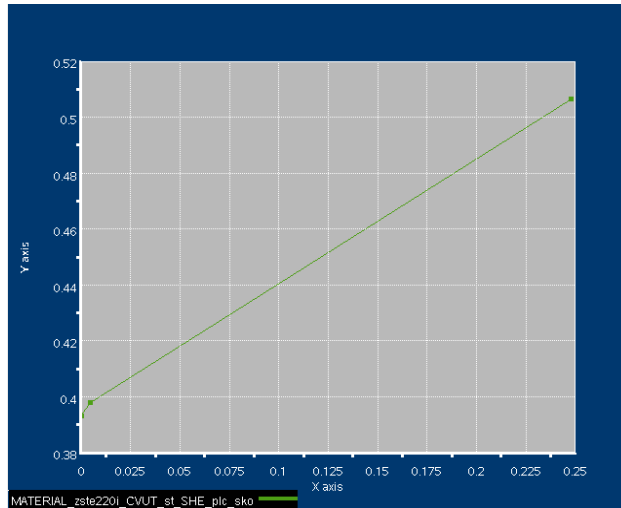


Figure 8.7: The model of material *zste220i* defined by coordinates - plastic hardening

In the figure 8.7 is shown only plastic behavior of material. The modulus of elasticity is $E = 210000$ MPa and Poisson's ratio $\mu = 0.3$. The yield strain $\varepsilon_y = 0.001872$ is used for calculation of Yield stress $\sigma_y = 393.3$ MPa by Hook equation. Therefore after merging both characteristic the model of material is defined in table 8.1 where after definition of last point, the extrapolation of strain-stress curve is horizontal.

Strain ε [-]	Stress σ [MPa]
$\varepsilon_y = 0.001872$	$\sigma_y = 393.3$
$\varepsilon_{p1} = 0.006584$	$\sigma_{p1} = 397.9$
$\varepsilon_{p2} = 0.249872$	$\sigma_{p2} = 506.5$
$\varepsilon_{p3} > 0.249872$	$\sigma_{p3} = 506.5$

Table 8.1: Model of material - elastic-plastic behavior

Model of material used for solid elements

In further variants is also used foam material. Material type 45 corresponds to highly compressible nonlinear elastic foam with strain-rate dependency. Due to VW policy the material data could not be published, however in tension and compression is material behavior linear and after strain $\varepsilon = 0.9$ the stress greatly increase.

8.2 Solution and checking the output file

In previous chapters were defined partial computational model of geometry, boundary condition, material and contact. Each of model was created in ANSA preprocessor however for solution the setup of PAM-CRASH solver is necessary. As geometric non-linearity type is used large displacement / large deformation. The PAM-CRASH solver use implicit or explicit algorithm. The differences are described below:

8.2.1 Implicit and explicit FEM algorithm [1]

The term implicit or explicit algorithm relates to mode of time integration of movement equation. To fully understand the difference between both variant is proper to show approach of equation compilation by mentioned algorithms.

Implicit algorithm

Let us consider solution of unsteady dynamic problem, described by movement equation eq. (8.1). Suppose that is known solution in time instant $t_0, t_1, t_2, \dots, t_n$ and main aim is to determine all unknown variable in time instant t_{n+1} . Actual time step is $\Delta t = t_{n+1} - t_n$

$$\mathbf{M} \cdot \ddot{\mathbf{U}} + \mathbf{K} \cdot \mathbf{U} = \mathbf{F}(t) \quad (8.1)$$

where eq. (8.1) is movement equation (without damping). Movement equation in time instant t_{n+1} is

$$\mathbf{M} \cdot \ddot{\mathbf{U}}_{n+1} + \mathbf{K} \cdot \mathbf{U}_{n+1} = \mathbf{F}_{n+1} \quad (8.2)$$

First is need to express required velocities and accelerations from differential formulas

$$\dot{\mathbf{U}}_{n+1} = (\mathbf{U}_{n+1} - \mathbf{U}_n) / \Delta t \quad (8.3)$$

$$\ddot{\mathbf{U}}_{n+1} = (\dot{\mathbf{U}}_{n+1} - \dot{\mathbf{U}}_n) / \Delta t \quad (8.4)$$

By using previous expressions one could evaluate acceleration $\ddot{\mathbf{U}}_{n+1}$ through displacements

$$\ddot{\mathbf{U}}_{n+1} = (\mathbf{U}_{n+1} - 2\mathbf{U}_n + \mathbf{U}_{n-1})/\Delta t^2 \quad (8.5)$$

and substitute to eq. (8.1). After treatment one obtain set of equation for determination unknown displacements in time instant t_{n+1}

$$(\mathbf{K} + \mathbf{M}/\Delta t^2)\mathbf{U}_{n+1} = \mathbf{F}_{n+1} + \mathbf{M}(2\mathbf{U}_n - \mathbf{U}_{n-1}/\Delta t^2) \quad (8.6)$$

If one marks dynamic stiffness matrix following matrix

$$\hat{\mathbf{K}} = \mathbf{K} + \mathbf{M}/\Delta t^2 \quad (8.7)$$

and dynamic load matrix following matrix

$$\hat{\mathbf{F}} = \mathbf{F}_{n+1} + \mathbf{M}(2\mathbf{U}_n - \mathbf{U}_{n-1})/\Delta t^2 \quad (8.8)$$

then displacements in time instant t_{n+1} are obtained by solving set of equation formally similar to static problem

$$\hat{\mathbf{K}} \cdot \mathbf{U}_{n+1} = \hat{\mathbf{F}} \quad (8.9)$$

Characteristics of implicit algorithm

- Displacements in time instant t_{n+1} one obtain from movement equation in same time instant
- If inertia forces are insignificant then from set of equation 8.9 is possible to not consider mass matrix \mathbf{M} and evaluation transfer to evaluation of static problem. To evaluate each time step is must be calculated eq. (8.9) repeatedly.
- Implicit algorithm is *unconditionally stable* which means stable solution regardless to time step Δt . For unstable behavior is typical total collapse of solution during evaluation of firsts time steps.

The longest time step are tried to be used if implicit algorithm is used. Long steps require usage of tensor of large deformations to description kinematics of movement and lead to necessity to iterate during each steps like that to enough-accurate fulfill movement equation 8.6 in each time step. It is usually done by increment-iteration algorithm modified Newton-Raphsons method.

Explicit algorithm

Similarly to previous section the main aim is to solve movement equation eq. (8.1) to approximate acceleration however now is used central difference method:

$$\ddot{\mathbf{U}} = (\mathbf{U}_{n+1} - 2\mathbf{U}_n + \mathbf{U}_{n-1})/\Delta t^2 \quad (8.10)$$

by substitution of acceleration to movement equation in time instant t_n

$$\mathbf{M} \cdot \ddot{\mathbf{U}}_n + \mathbf{K} \cdot \mathbf{U}_n = \mathbf{F}_n \quad (8.11)$$

after modification for displacements in time instant t_{n+1}

$$(\mathbf{M}/\Delta t^2)\mathbf{U}_{n+1} = \mathbf{F}_n - \mathbf{K} \cdot \mathbf{U}_n + \mathbf{M}(2\mathbf{U}_n - \mathbf{U}_{n-1})/\Delta t^2 \quad (8.12)$$

Basic characteristic features explicit algorithm are stated in same order as are at implicit algorithm - this lead to better illustration of differences between both algorithms.

Characteristics of explicit algorithm

- Displacements in time instant t_{n+1} one obtain from movement equation 8.11, defined for previous time instant t_n , thence term - explicit.
- If one neglect mass matrix the algorithm becomes unusable, is not possible to solve static problems.
- The fundamental advantage of explicit formulation shows if is used diagonal mass matrix \mathbf{M} . In that case the set of equations 8.12 decay into separate independent equations. From each one is possible directly express unknown variable on element level without necessity of compilation global stiffness and mass matrices. One time step of explicit algorithm is by several order faster to solve against to corresponding time step of implicit algorithm. Moreover within increasing the complexity of problem increase the number of operation of explicit solver only linearly to number of unknown variables, while by using of implicit solver the quadratic dependence on width of cue matrix system. That is major limitation for spatial problem with complex topology mesh.
- Major limitation of explicit formulation is in other side the conditioned stability of algorithm. Stable results are obtained only by using sufficient small time step

$$\Delta t \leq \Delta t_{cr} \quad (8.13)$$

where critical length of time step Δt_{cr} depends on density of mesh and on velocity c sound speed (stress waves) in evaluated structure

$$\Delta_{cr} = L/c \quad (8.14)$$

$$c = \sqrt{\frac{E}{\rho}} \quad (8.15)$$

In aforementioned equations the L represents characteristic dimension of smallest element in mesh, E is Young modulus and ρ is density of material. The critical time step could be defined as transit period stress wave by smallest element of mesh. For typical sizes of elements in common analyzes and with velocity of stress waves in steel material $c \approx 5000m/s$ is usual time step very short, in order up to $10^{-5} - 10^{-7}$ s. It is 100-1000 times less than typical time step of implicit algorithm. By using explicit algorithm it therefore analyzed time interval discretized to far more shorter time steps, which solution is much faster than by using implicit algorithm.

As input file to solver serves the *.pc file which contains several parameters:

ANALYSIS - explicit

Characteristic	Explicit	Implicit
Convenient for class of problems	fast dynamic transient problems with distinctly nonlinear behavior, impact loading, large spatial problems with complicated topology of mesh	static and "slow" dynamic problems with gentle nonlinearities of plasticity type, plane and topologically simple spatial mesh
Software character	simple source code, internal memory	more sophisticated programs, communication with external memory
Time step	short	long (100-1000 times longer)
Matrix inversion	no	yes
Balanced iteration within step	no	yes
Kinematic description of movement within step	small rotations	large rotations
Memory requirements	small	large

Table 8.2: Comparison of explicit and implicit characteristics

STOPRUN ENERGY XX - if total energy E_{TOT} increases by XX percent or more, the execution is stopped. Total energy is defined according to eq. (8.16) [21].

$$E_{TOT} = E_{INT}^{Struct} + E_{INT}^{SIT} + E_{KIN}^{Struct} - W_{EXT} \quad (8.16)$$

$$E_{INT}^{SIT} = E_{INT}^{SIS} + E_{INT}^{SIF} \quad (8.17)$$

where

- E_{TOT} is the total energy present at any time in the system
- E_{INT}^{Struct} is the internal energy, stored and absorbed by the material of the structure, plus the absorbed hourglass mode energy
- E_{INT}^{SIS} is the elastic energy stored by Sliding Interface contact Spring
- E_{INT}^{SIF} is the energy dissipated by Sliding Interface contact Friction
- E_{KIN}^{Struct} is the kinetic energy of structure
- W_{EXT} is the work done by externally applied forces (including acceleration field, pressure, velocity boundary conditions.)

SHELLCHECK - NO

SOLIDCHECK - NO

SHELLCHECK and SOLIDCHECK serves as a check of quality of used shell and solid elements. Due to preprocessors norm in ANSA the distorted shell and solid elements are avoided during creation of geometrical model therefore in solution setup is checking disabled.

DATACHECK - YES, it checks consistency of the data in the input file e.g. kinematic compatibilities.

MERGE GAP - X.XX is the tolerance where the nodes of adjacent unconnected elements are taken to be merged.

UNIT MM KG MS KELVIN - units used in model.

TIME 30 ms - the termination time of solution

CTRL - output parameters, which are default and only essential value is **THPOUTPUT**

INTRERVAL set to 0.1ms and therefore data of acceleration, velocity curves etc. are with 30Hz discretization frequency.

TCRTL - Time step control

INITIAL 0 - by user imposed initial time step, if 0 time steps are computed by the program

INIT_MASS_SCALE - mass scaling criterion time step, explained in section 8.2.2.

NODAL - YES - activate nodal time step scheme.

DYNA_MASS_SCALE - dynamic mass scaling time step, explained in section 8.2.2.

STIFFNESS_SCALE XX1 XX2 - XX1 value is the minimum solution time step, XX2 is the minimum factor $\alpha_{min} = \Delta t_e / XX1$.

SHELL_TIMESTEP SMALL BEND - is strongly recommended if more options for time step controls are used. SMALL stringent time step criterion is used. For BEND the shell

time step is $\Delta t_{shell} = k \cdot \min \left\{ \frac{L}{c}; \min \left\{ 1; \frac{L}{3^{1/2} \cdot t_e} \right\} \right\}$

CTRL - Element control

RATEFILTER XX - "Strain Rate Filtering damps high frequency vibrations and avoid erroneous predictions of stresses that may occur when using common strain rate laws together with elastic-plastic materials" [21]

STRAINRATE YES - activated strain rate, stress-strain curves are dependent on strain rate which define the behavior of material.

After solving by *.pc file one can review the output of PAM-CRASH solver. It contains several important informations. Errors, warning, and infos sorted by importance shows the problems occurred in solving process. Only one warning appeared at acceleration field of impactor where the slave nodes have been removed and therefore problem was fixed.

8.2.2 Mass scaling and time step

The element time step is calculated according to eq. $\Delta t_{elem} = l_c \sqrt{\frac{\rho}{E}}$ where l_c is characteristic length, ρ mass density of element, E elastic modulus [25]. If the element time step calculated regarding to initial check of mesh size is smaller than defined by Initial Mass Scale = XXms, the time step is adjusted by density of elements to obtain Initial Mass Scale XXms time step. Obviously shorter time step lead to convergence calculation however with high computational time. Therefore is applied scale factor 0.9 to preserve conservative calculation with highest time step as possible.

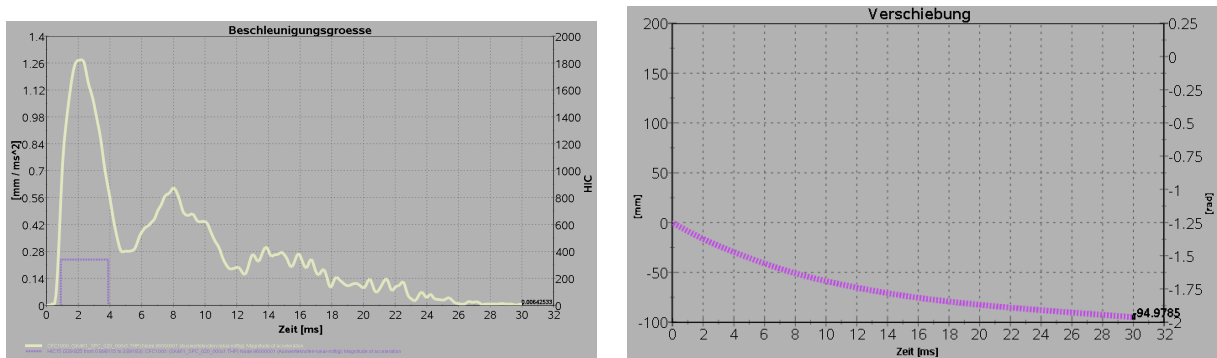
During calculation where the structure is deformed mentioned time step is further tried to be preserved by Stiffness scale control. Corresponding time step to deformed structure

$\Delta t_{elem} = l_c \sqrt{\frac{\rho}{E}}$ is adjusted by parameter E which is possible to minimal reduction to 0.1 time to original E . Stiffness scale control protect against excessive reduction of stable solution time step Δt_s due to large mesh distortion [21]. Another approach is to change dynamic mass scaling function where the mass density is modified. However both parameters could not be arbitrarily modified. One side of problem where the stiffness is too small controlled by coefficient $0.1 * E$ and the density mass could be checked in PAMCRASH output solver by Mass Scaling Scaling information where for example 100g added mass to the whole car structure is in tolerance however 15 kg is unacceptable.

As an output are generated *.DSY and *.THP files which first one contain an animation of impact and geometry of model and the second contains all time history post processor entities such as curves of displacement, acceleration etc.

8.3 Post-processing

The default post-processor for PAM-CRASH solver is Virtual Environment. However at Škoda Auto a.s. μETA post processor by BETA Systems is used with extension of several scripts developed by Škoda Auto a.s. By using them the results are opened and represented in 3 tabs. First serve to shown of animated 3D model impact. The most interesting tab contains deceleration curve along the time with calculated HIC values shown in figure 8.8(a). First variant of geometrical model shows that the displacement in Z direction which represent maximal deflection of bonnet, achieved maximal value of 95 mm illustrated in figure 8.8(b). Although the **HIC** value of **340** appears very small, regarding to the large deflection it is obvious. According to section 7.1 the maximal deflection of bonnet remain at $Z_t = 60mm$ therefore further improvements of bonnet design are calculated.



(a) The magnitude of acceleration (left y-axis) with (b) The Z displacement of impactor for the first HIC value (right y-axis) for the first model of bonnet model of bonnet top

Figure 8.8: The solved first design of bonnet top

8.4 Variant 001

Data file of current variant is *SK461_SPC_020_001.pc*. According to the section 8.1 the computational model is similar except minor changes. The section 7.4 deals with analytical

deceleration curves with two peaks and therefore by creating shifted rigid surface is possible to approach to 2 peak analytical model of deceleration pulse.

The geometrical model of variant 001 include same shape of approximated superficial bonnet part, however the model is extended by copied and shifted bonnet surface by 60 mm in Z direction as depicted in figure 8.9(a).

The model of boundary condition is extended for all DOF applied to shifted bonnet part which simulate tough engine parts where the headform after deformation of superficial bonnet part could hit. Due to applied constraint the acceleration field is not applied to rigid surface.

The model of contacts is extended to contact between superficial and rigid surface due to necessity of not perforation and penetrations of element entities to each other. Therefore the contact type 33 with friction coefficient 0.1 were used again due to contact between metal materials.

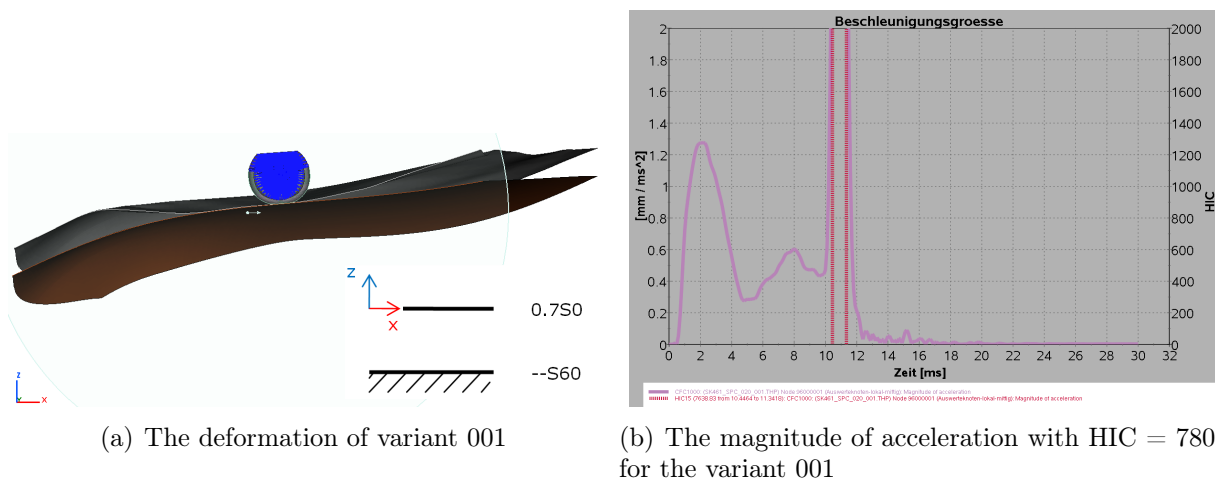


Figure 8.9: The results of variant 001

According to figure 8.9 the **HIC** value increased to **7800** due to immediately stopped movement in Z direction of headform which hit to the bottom surface. The structure of variant 001 is schematically depicted in figure 8.9(a) where the syntax is based on following rules. The first number represent of layer thickness, letters represent type of element (S-shell, SL-solid) and last number represents position of layer in Z direction from first layer where Z coordination is zero.

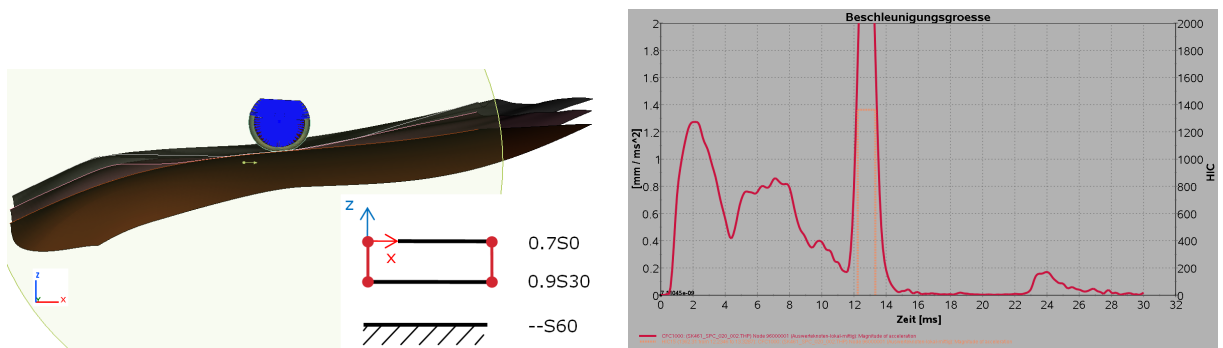
As one can notice in figure 8.9(b) the first peak magnitude is quite small and during first peak is impactor slowed down. The HIC criterion should be calculated from region of first peak as it was concluded in section 7.4 and therefore the second peak should be as small as possible to ensure that.

8.5 Variant 002 (*SK461_SPC_020_002.pc*)

Data file of current variant is *SK461_SPC_020_002.pc*. The previous variant shows great second peak which results to unacceptable HIC value. Therefore was necessary to improve the geometrical model. Another shell bonnet part is set between top and rigid surface nevertheless with the thickness which corresponds to maximal allowable mass of bonnet structure $BM=19.4$ kg defined in chapter 8.

As a first approach is added middle shell surface between top and rigid shell part in -30 mm in Z direction from top shell surface. According to figure 8.10(b) the **HIC** value decreased to **1362** due to smaller second peak which still results in unacceptable HIC. With considering middle shell surface with thickness 0.9 mm the mass of structure increased to 18.7 kg which fulfill requirements.

The model of boundary conditions takes into account the connection between middle surface and top surface, where at the edges of both surfaces are corresponding nodes constrained by type 1 of rigid body shown as red lines with dots in the schematic sub-figure in figure 8.10(a). Rigid bodies are elements of infinite stiffness. The type 1 is stiff rigid body where the moments are transmitted from both connected nodes. The boundary conditions at the edges correspond to the original bonnet where the edges are glued together and therefore whole bonnet structure behave as one part.



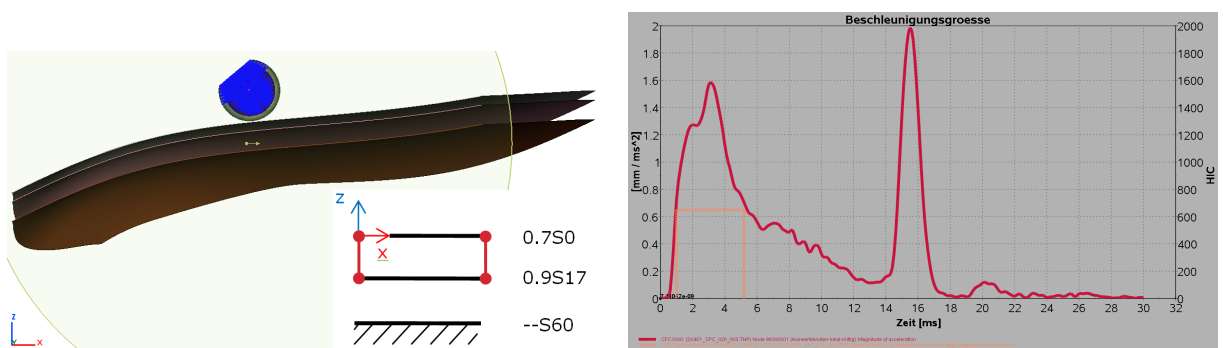
(a) The deformation of variant 002

(b) The magnitude of acceleration with HIC = 1245 for the variant 002

Figure 8.10: The results of variant 002

8.6 Variant 003

Data file of current variant is *SK461_SPC_020_003.pc*. The difference to variant 002 is only in the position of middle surface between top and bottom face. The best achieved results of HIC are shown in figure 8.11 with **HIC=650**.



(a) The deformation of variant 003

(b) The magnitude of acceleration with HIC = 650 for the variant 003

Figure 8.11: The results of variant 003

8.7 Variant 004

Data file of current variant is *SK461_SPC_020_004.pc*. Although was mentioned before that the further movement of impactor does not influence the HIC value, for verification the rigid surface is in this variant neglected. The maximal deformation of bonnet in Z direction increased to 71 mm. The magnitude of acceleration is illustrated in figure 8.12 where the red curve represents variant 003 and purple represents current variant.

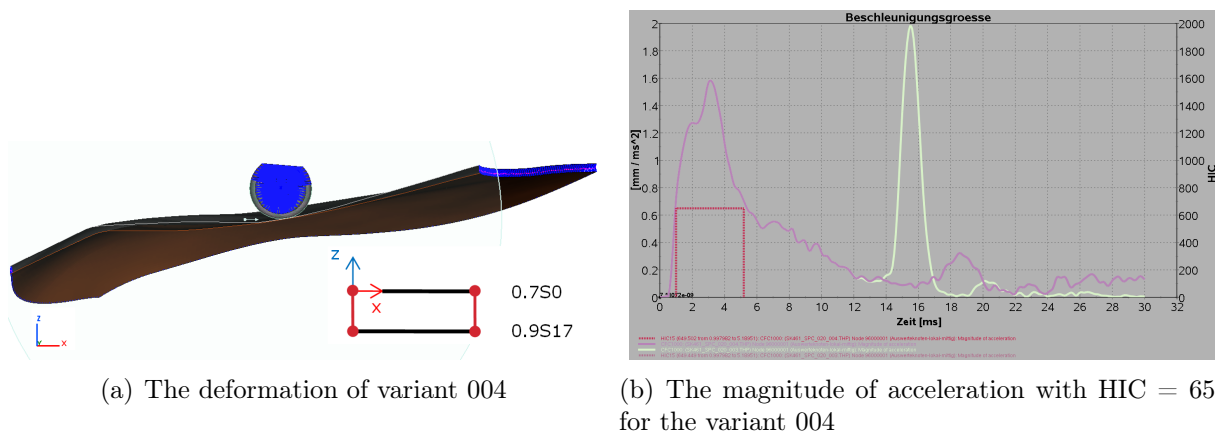


Figure 8.12: The results of variant 004

All previous variants take into account the maximal allowable mass of bonnet and maximal deflection restrictions except last one, where is shown indifference to calculated HIC value to variant 003. Because of HIC criterion is calculated in region of first peak any further impact to engine parts after 60 mm deflection does not influence HIC value.

8.8 Variant 005

Data file of current variant is *SK461_SPC_020_005.pc*. The following variants takes into account again rigid surface situated in the -60 mm from top surface. To preserve smaller second peak magnitude, the geometrical model includes foam layer from solid material PAM-SOLID 45 where model of material is described in section 8.1.4. The foam layer is also connected at the edges to the top and middle surface of bonnet structure by rigid bodies. The edge nodes of top surface are constrained with the edge nodes of top face of foam layer and at same time with the edge nodes of bottom surface as shown in schematic part of figure 8.13(a). The 3 node rigid body element was used according to schematic part of figure 8.13(a).

As in previous variant again is here introduced only configuration of geometrical model where the position in Z direction and thickness of foam layer provide best achieved HIC value. The **HIC** value decreased to **630**.

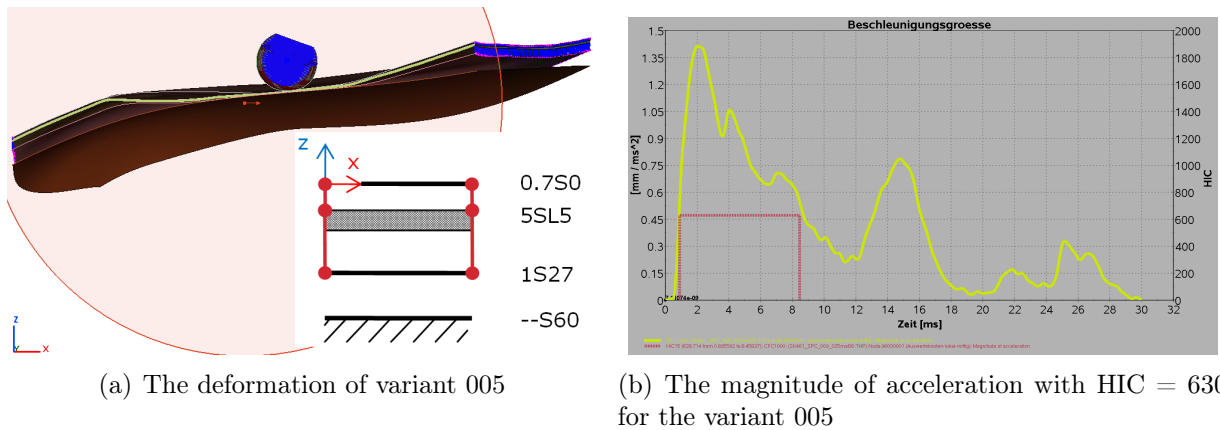


Figure 8.13: The results of variant 005

In comparison with variant 003 the HIC value slightly decreased with smaller magnitude of second peak. Therefore the variant with foam layer provide better results of HIC however it results in more complicated geometrical model.

8.9 Variant 006

Data file of current variant is *SK461_SPC_020_006.pc*. Actual variant differ only in removed rigid body surface at 60 mm to show the independence of HIC value on further deflection of bonnet where the impactor can hit to engine parts.

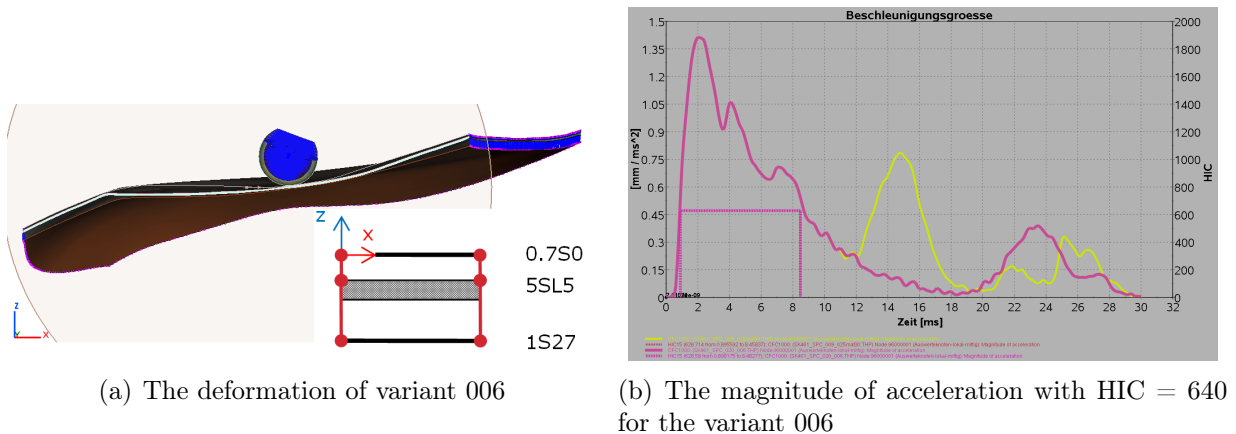


Figure 8.14: The results of variant 006

8.10 Variant 007

Data file of current variant is *SK461_SPC_020_007.pc*. The last variant of designed bonnet structure merge all previous variants into one. In previous variant the foam is set to 5 mm under the bonnet top. In reality is hard to manufacture the structure with foam material is certain position between steel faces due to insufficient stiffness which preserve form of foam layer. Therefore actual variant geometrical model is modified to foam layer attached to the middle surface. Also is possible to attach the foam layer to the top bonnet surface however

the bonnet structure would not be possible to manufacture. In manufacturing process the top and middle bonnet part are glued at the edges and then inserted to the high temperature furnace where the glue is hardened. If would be foam layer present during hardening it would be damaged. Therefore after hardening process the foam layer is attached to the middle surface. The actual variant depicted in figure 8.15(a) lead to $HIC = 644$ with mass 18.9 kg of bonnet structure.

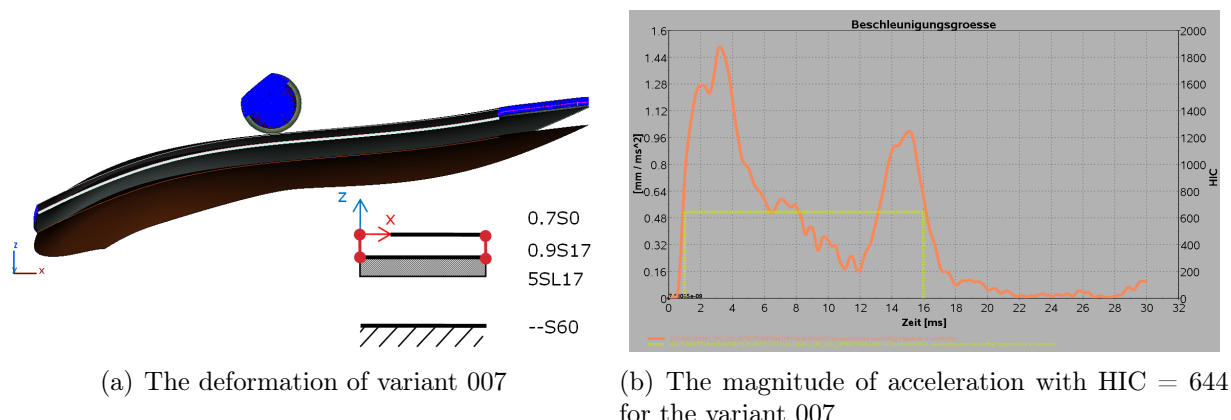


Figure 8.15: The results of variant 007

8.11 Comparison of variants

According to the previously designed variants is obvious the procedure to achieve as small HIC value as possible within preserving mass and deflection restrictions. The each further variant decreased HIC value by using more complex structure. The last variant shows slightly higher HIC value against to variant 005 (variant 006 is not considered because of neglecting rigid body surface). Nevertheless the foam layer is necessary to attach to the metal structure due to manufacturing reasons as was mentioned before. The rigid body surfaces was always positioned from origin of coordinate system by -60 mm in Z direction.

However in real geometrical model of car the engine parts are not uniformly distributed in 60 mm from the surface of superficial bonnet part. Therefore the rigid surface simulates the worst possible case for impact simulations and for evaluation of HIC.

9. Design of original bonnet structure

The acquired knowledge from previous chapter now are used for computational model of original bonnet structure with modification of internal part of bonnet. The model data are stored in `./SK461_SPX_002` directory. As design restriction is 5 mm space between bonnet structure and rigid surface where it is positioned in 60 mm in Z direction.

9.1 Computational model

As a original computational model served internally labeled FEM model variant `SK461_A12` depicted in figure 6.2. The model was modified to use only bonnet part without rest of front of car.

9.1.1 Geometrical model

The geometrical model of `SK461_A12` was reduced to bonnet structure depicted in figure 9.1(a).

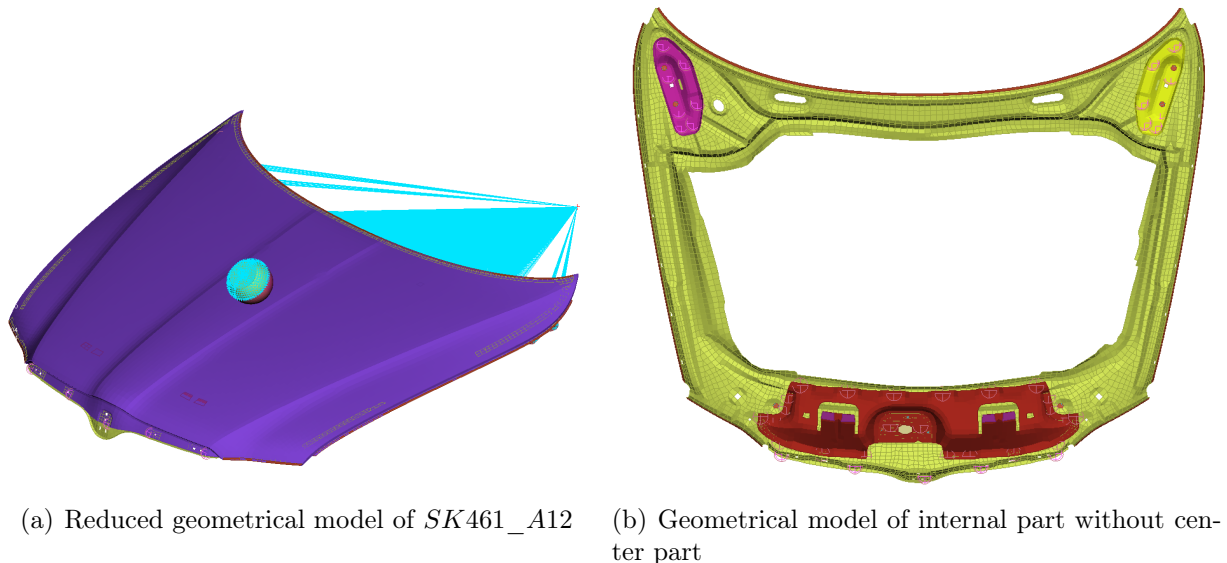


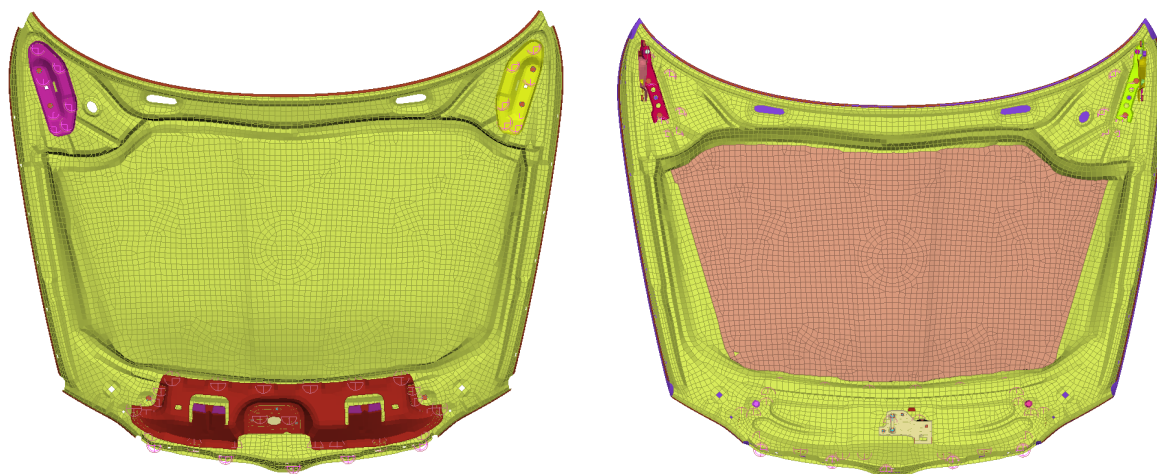
Figure 9.1: FEM model `SK461_A12`

The figure 9.1(b) shows the internal structure (with missing center structure) which is connected with superficial bonnet part depicted in violet color in figure 9.1(a).

The internal structure contains also support parts for hinges (yellow and pink) and support part for front lock (red), hinges and bonnet rubber stops. The hinges are connected by PLINK constrains which serves as welding points. Also the superficial part with internal part is connected in the front of bonnet by PLINKs where the logo of Škoda is situated.

The missing center structure of internal bonnet part is replaced by structure from superficial part. The shape of missing structure is projected to the superficial bonnet part and it was copied and offset to the internal bonnet part. By preprocessing and connecting the offset part to the internal structure the geometrical model is illustrated in figure 9.2(a).

The foam layer were also used in thickness of 5 mm and attached from back side of internal part shown in figure 9.2(b) according to the manufacturing reasons described before. The dimensions of foam layer correspond to the dimensions of shifted cut of superficial part.



(a) Modified geometrical model of internal part -top view (b) Modified geometrical model of internal part - rear view

Figure 9.2: FEM model *SK461_A12*

Finite element mesh

The procedure is same as was described in section 8.1.1.

9.1.2 Modeling of boundary condition

Geometrical boundary conditions

The original geometrical model was constrained according to figure 9.3 and figure 8.3(b).



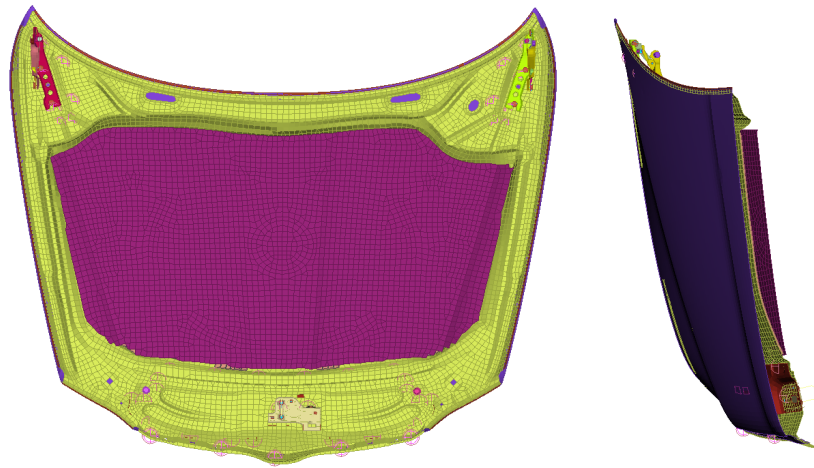
Figure 9.3: Rigid body condition to the bonnet rubber stops and front lock

The difference in model of boundary conditions against to FEM model *SK461_A12* is, that the sides and rear part of bonnet are not supported by car structure, therefore the FEM model variant *SK461_A12* was recalculated to not consider the rest of car as model of boundary condition.

Due to lack of car structure, again was used of shell element surface shown in figure 9.4 which was positioned in -60mm in Z direction and which was constrained by rigid bodies. The shape of rigid surface goes out from shape of offset central structure.

Force boundary conditions

The force boundary conditions are same as were used in section 8.1.2.



(a) The rigid surface positioned in -60mm simulating engine parts - top view

(b) The rigid surface positioned in -60mm simulating engine parts - side view

Figure 9.4: Rigid surface

9.1.3 Model of contact

Again equal model is used as in section 8.1.3.

9.1.4 Model of material

According to section 8.1.4 the model of material are used same except to different numerical values of stress-strain curves. The values of original used materials could not be published due to VW policy, however publishable materials used in section 8.1.4 provide similar behavior of material.

9.2 Solution and post-processing

The modified variants were solved with same setup of PAM-CRASH solver and post-processed in META software as in section 8.2 and section 8.3.

9.3 Evaluation of FEM model variant *SK461_A35*

Whole computational model was prepared according to FEM model variant *SK461_A12*, however during working on thesis the variant *SK461_A35* perform better results of HIC. Therefore as a geometrical model was used variant *SK461_A35* with same other models according to the computational model 8.1 (material, boundary conditions, contact etc.)

The variants differ only (from *SK461_A12*) in foam material mounted to rear side of internal structure and thus the variant model more corresponds to my geometrical model proposals where is also used foam layer. Another geometrical modification to *SK461_A35* added rigid surface positioned in -60 mm in Z direction. From original *A35* variant also

the geometrical boundary conditions differ due to lack of front car structure. Therefore the evaluation of HIC result do not correspond to real car structure where also the engine parts are not in uniform distance from superficial part of bonnet.

The foam layer in the A35 variant would interfere with the rigid surface and therefore the geometry was modified according to figure 9.5. In further evaluation A35 variant, the impact point positioned to the structure where is missing rigid surface will provide better value of HIC due to longer trajectory of impactor during collision and will be excluded from evaluation of overall performance.

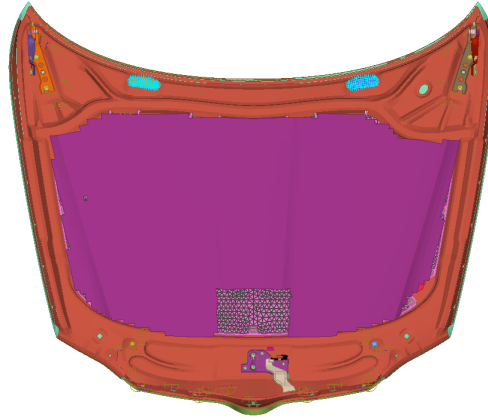


Figure 9.5: The modified rigid surface - back view

As evaluation criterion served the quantitative comparison called **OVERALL PERFORMANCE - OR**. According to the test protocol [26] the evaluation of head injuries goes out from following color boundaries listed in table 9.1

Group	HIC value range	Points
Green	≤ 650	1
Yellow	650-1000	0.75
Orange	1000-1350	0.5
Brown	1350-1700	0.25
Red	≥ 1700	0

Table 9.1: HIC value range for evaluation according to test protocol [26]

Whole bonnet top structure is then evaluated according to test protocol, where as output serve number of points from child zone of headform testing. However mentioned scale is too rough for showing difference between own design variants and therefore the refinement of scale is listed in table 9.2.

Group	HIC value range	Points	Coefficient c_{group}
Green	≤ 650	1	1
Yellow	650-750	0.75	0.75
Orange	750-850	0.5	0.5
Brown	850-950	0.25	0.25
Red	≥ 950	0	0

Table 9.2: Modified HIC value range for evaluation

Evaluation of each variant is done by point achievement and also according following equation of OVERALL PERFORMANCE:

$$OR = \frac{c_1 \cdot NOP_1 + c_2 \cdot NOP_2 + c_3 \cdot NOP_3 + c_4 \cdot NOP_4 + c_5 \cdot NOP_5}{NOP_{total}} \quad (9.1)$$

where $c_{1,2,3,4,5}$ are coefficients representing each group and $NOP_{1,2,3,4,5}$ are number of points belong to corresponding HIC value range. NOP_{total} is number all test points.

The HIC values of original bonnet top from series A35 are used as original results of bonnet structure which serves for further design as results to be compared with. As was mentioned before due to VW policy the value of HIC could not be published therefore further design shows only percentage of improvement.

The method is based on value range and is obvious to non-possibility of achievement 100% of overall performance.

Group	Number of impact points within range $NOP_{1,2,3,4,5}$	Total achieved points
Green	0	$0 \cdot 1 = 0$
Yellow	3	$3 \cdot 0.75 = 1.5$
Orange	12	$12 \cdot 0.5 = 6$
Brown	16	$16 \cdot 0.25 = 4$
Red	26	$26 \cdot 0 = 0$
Total	57	11.5
Overall performance OP = 20%		

Table 9.3: Overall performance for A35 variant

Following figure shows original HIC values of series variant A35 with overall rating to 20%.

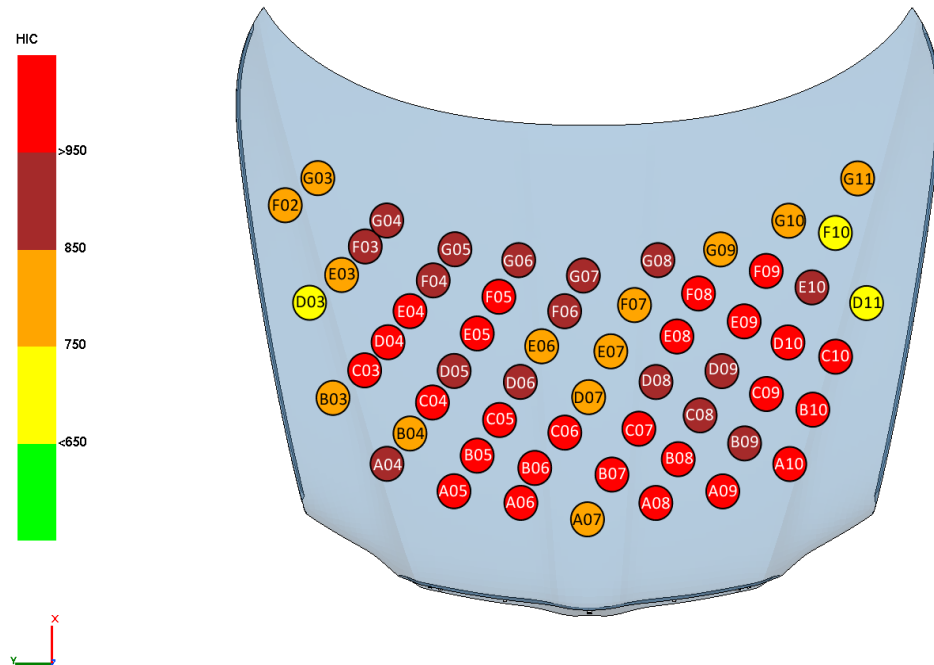


Figure 9.6: HIC overall performance for series A35 FEM model with rigid surface at -60 mm and missing front car structure - OP = 22%

9.4 Variant X00 - 002

Data file of current variant is *SK461_SPC_002_000.pc*. Following sections describe the design approaches of internal structure. The geometrical model design procedure is described in section 9.1.1. The first variant X00 is designed according to the similar shape of deceleration curve shape in variant 007 section 8.10 from previous chapter where the foam layer is attached to the bottom surface of internal structure which corresponding to the bonnet structure of 007 variant. As was mentioned, the center part of superficial bonnet structure is copied and offset. For this variant to -6 mm in Z direction. The offset element surface was connected to the internal part and at the places of connection the mesh was improved by ANSA tools for creation of mesh. The modified internal structure is illustrated in figure 9.7 with first approach of morphing mesh.

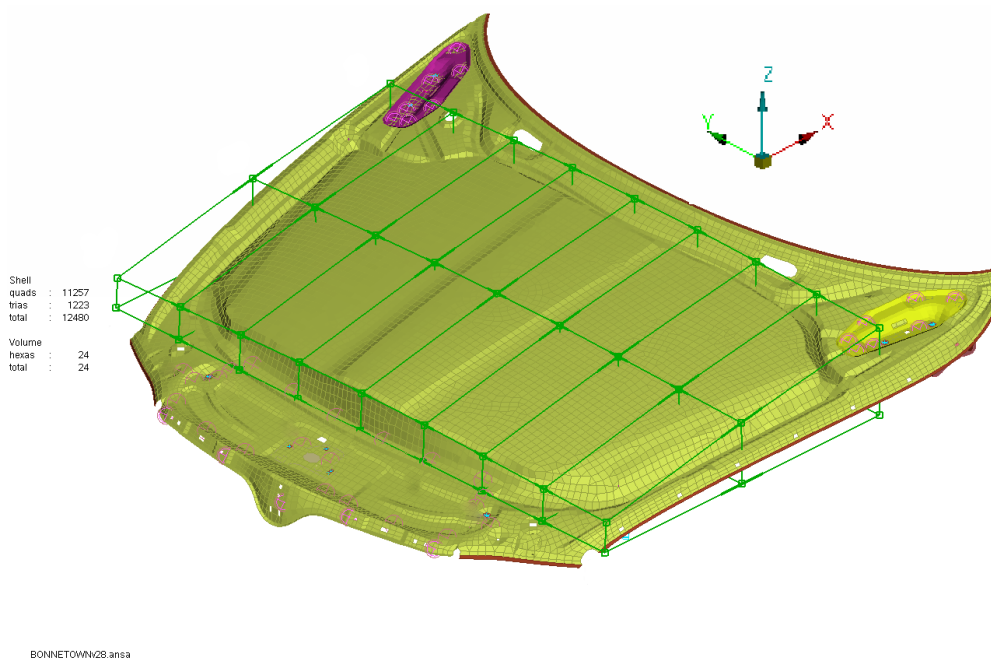


Figure 9.7: The internal structure by offsetting part of superficial bonnet top with rough morphing grid - variant X01

Current variant shows similar result regarding to variant 007 of HIC value where the headform impact direct into the center of bonnet.

The main aim is to investigate best deceleration of impactor by design proper bonnet structure however also obtaining well results is desired across the whole area of bonnet. Therefore further improvement of designs are tested on whole area of bonnet and further variants show overall performance with modification of morphing points.

9.5 Variant X01 - 004

Data file of current variant is *SK461_SPC_004_000.pc*. The X01 variant uses finer morphing grid and center part final shape of internal bonnet structure is shown in figure 9.8. The morphing grid serves as a tool for modification of geometry for editing distance between superficial part and internal structure. As one can notice the grid cover almost whole bonnet.

However the center of structure was only content of morphing grid in ANSA preprocessor. Each box has 8 vertices where for surrounding lines are applied tangent conditions. The modification in Z direction lead to move of elements close to the position of modified vertex and therefore due to tangent restriction the surface is smooth.

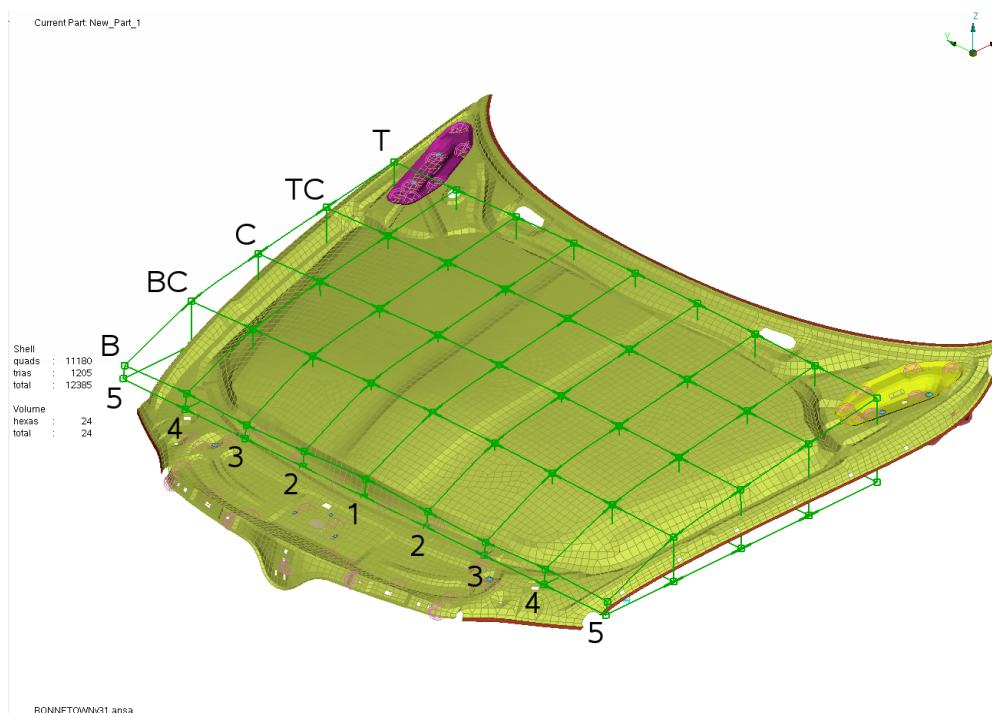


Figure 9.8: The internal structure by offsetting part of superficial bonnet top - variant X01

As it is shown in figure the morphing grid is labeled according to position e.g. T - top, TC - top-center, C - center, BC - bottom-center, B - bottom. The number shows position along transverse position and due to symmetry the points with same number are modified together. Therefore each variant will use table with modification to variant X00 which serves as base variant.

The variant X01 differ from X00 variant by modification of following points:

longitudinal position	transverse position	Z value [mm]
B	1	-30
B	2	-35

Table 9.4: Variant X01

The variant X01 provide by application of overall performance rating the $OP = 52\%$ and HIC values distribution is shown in figure 9.9.

According to the variant A35 one can notice of overall improvement of HIC values regarding especially to points located in the middle of bonnet. However by approaching to the edges of bonnet in current variant, the bonnet provide worse results. This is obvious due to different internal structure stiffness across the bonnet. The cut view of bonnet in the middle of width is depicted in figure 9.10. The impact point in the middle of bonnet top is quite far from boundary edges therefore the internal structure in the middle is more flexible and

Group	Number of impact points within range $NOP_{1,2,3,4,5}$	Total achieved points
Green	9	$9 \cdot 1 = 9$
Yellow	14	$3 \cdot 0.75 = 10.5$
Orange	14	$14 \cdot 0.5 = 7$
Brown	15	$15 \cdot 0.25 = 3.75$
Red	6	$6 \cdot 0 = 0$
Total	58	30.25
Overall performance OP = 52%		

Table 9.5: Overall performance for X01 variant

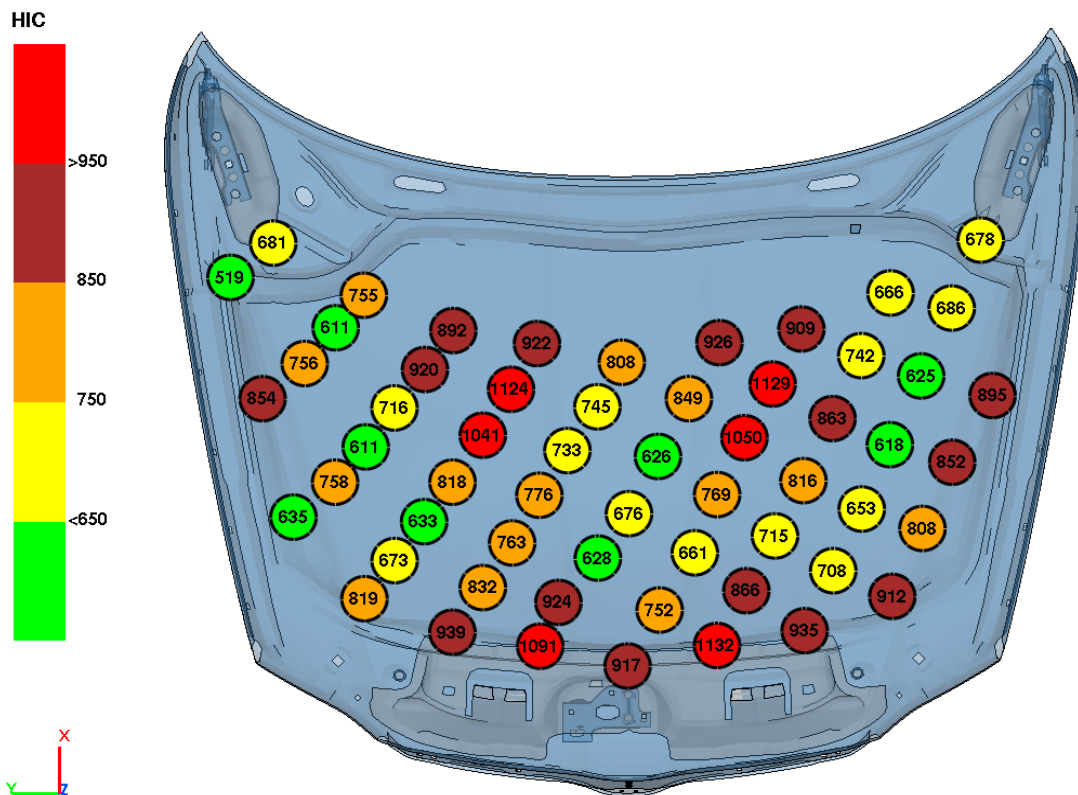


Figure 9.9: HIC overall performance for variant X01 - OP = 52%

therefore the impactor is slowed down gently. Otherwise at the bonnet edges the structure is more stiff and impactor motion last shorter time which it leads to higher deceleration value.

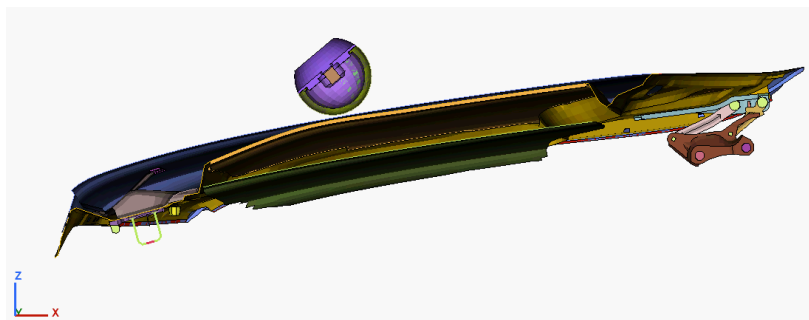


Figure 9.10: Cut view for impact point D07 of variant X01

9.6 Variant X02 - 005

Data file of current variant is *SK461_SPC_005_000.pc*. Following variant differ from previous by moving tabled morphing points in Z direction.

longitudinal direction	transverse direction	Z value [mm]
B	2, 3	-20
BC	1	-5
BC	3	+5
ALL	1	-5
ALL	2, 3	-10

Table 9.6: Variant 005

The variant X02-005 provide overall performance $OP=58\%$.

Group	Number of impact points within range $NOPI_{1,2,3,4,5}$	Total achieved points
Green	4	$4 \cdot 1 = 4$
Yellow	27	$27 \cdot 0.75 = 20.25$
Orange	17	$17 \cdot 0.5 = 8.5$
Brown	4	$4 \cdot 0.25 = 1$
Red	5	$5 \cdot 0 = 0$
Total	58	33.75
Overall performance $OP = 58\%$		

Table 9.7: Overall performance for X02 variant

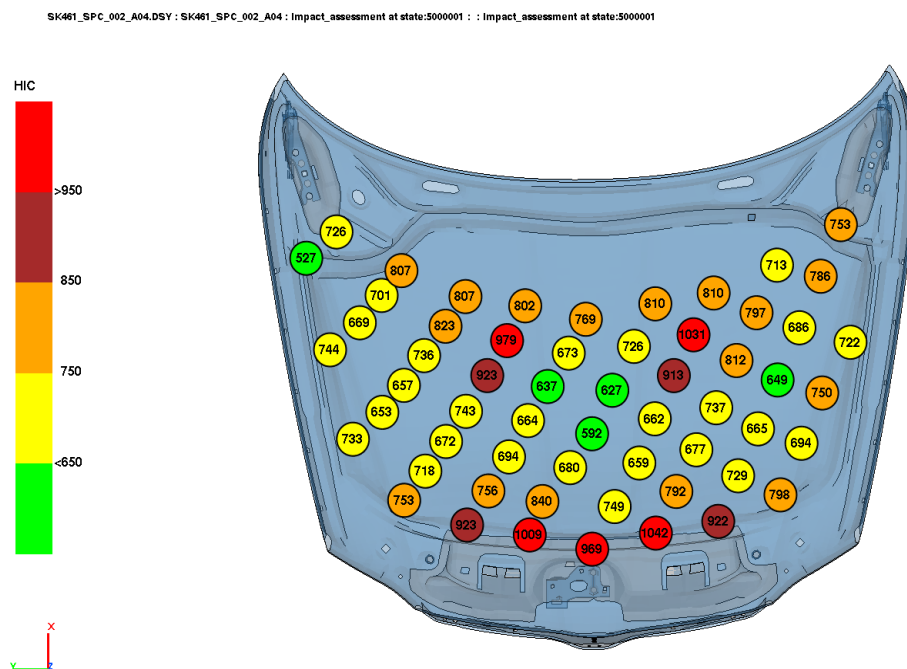


Figure 9.11: HIC overall performance for variant X02 - $OP = 58\%$

9.7 Variant X03 - 006

Data file of current variant is *SK461_SPC_006_000.pc*. By moving almost every morphing point far from superficial bonnet, the results are better. The design still reflect the condition of 5 mm space between bonnet structure and rigid surface. Table 9.8 lists modifications of bonnet structure:

longitudinal direction	transverse direction	Z value [mm]
ALL except B	ALL	-5

Table 9.8: Variant 006

Group	Number of impact points within range $NOP_{1,2,3,4,5}$	Total achieved points
Green	12	$12 \cdot 1 = 12$
Yellow	27	$27 \cdot 0.75 = 20.25$
Orange	12	$12 \cdot 0.5 = 6$
Brown	4	$4 \cdot 0.25 = 1$
Red	3	$3 \cdot 0 = 0$
Total	58	39.25
Overall performance OP = 67%		

Table 9.9: Overall performance for X03 variant

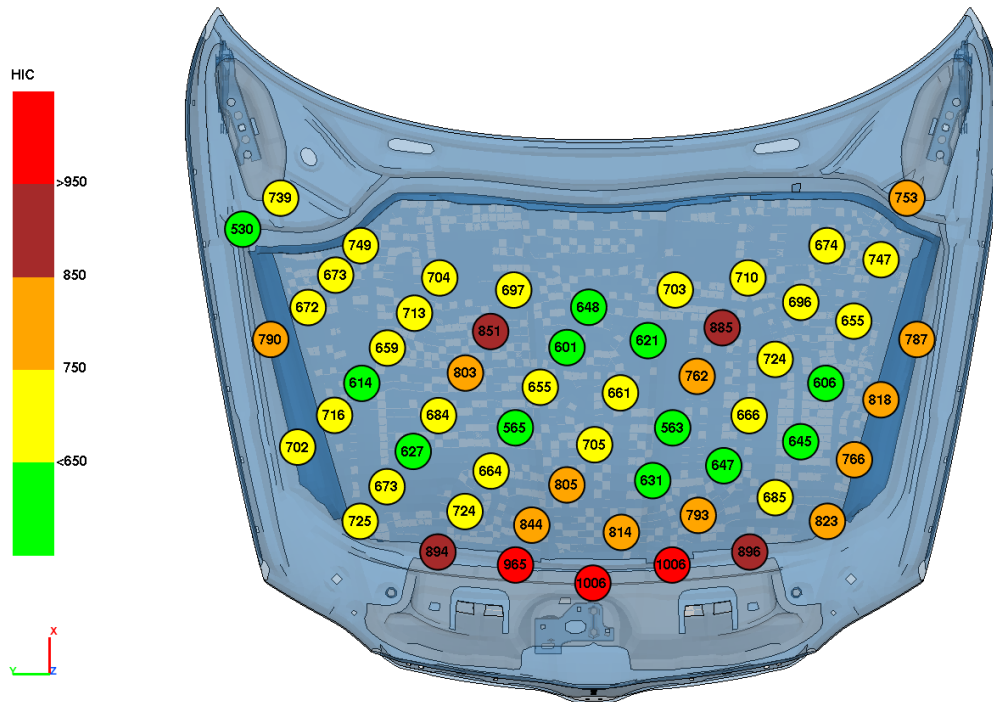


Figure 9.12: HIC overall performance for variant X03 - OP = 67%

Results obtained from simulation shows in overall performance OP=67%.

9.8 Variant X04 - 007

Data file of current variant is *SK461_SPC_007_000.pc*. Variant X04 provide better results by again application of point moving by values listed in table 9.8 where overall performance increased to $OP=72\%$. Also was tried to improve the current variant by moving several morphing points however without recognizable improvement. Therefore is concluded that present variant is the best from all previous analyzed designs. For the middle point E07 is depicted the deceleration curve in figure A.8(a), energy relations in figure A.8(b) and force curves in figure A.8(c).

Group	Number of impact points within range $NO P_{1,2,3,4,5}$	Total achieved points
Green	22	$22 \cdot 1 = 22$
Yellow	19	$19 \cdot 0.75 = 14.25$
Orange	8	$8 \cdot 0.5 = 4$
Brown	7	$7 \cdot 0.25 = 1.75$
Red	2	$2 \cdot 0 = 0$
Total	58	42

Overall performance OP = 72%

Table 9.10: Overall performance for X04 variant

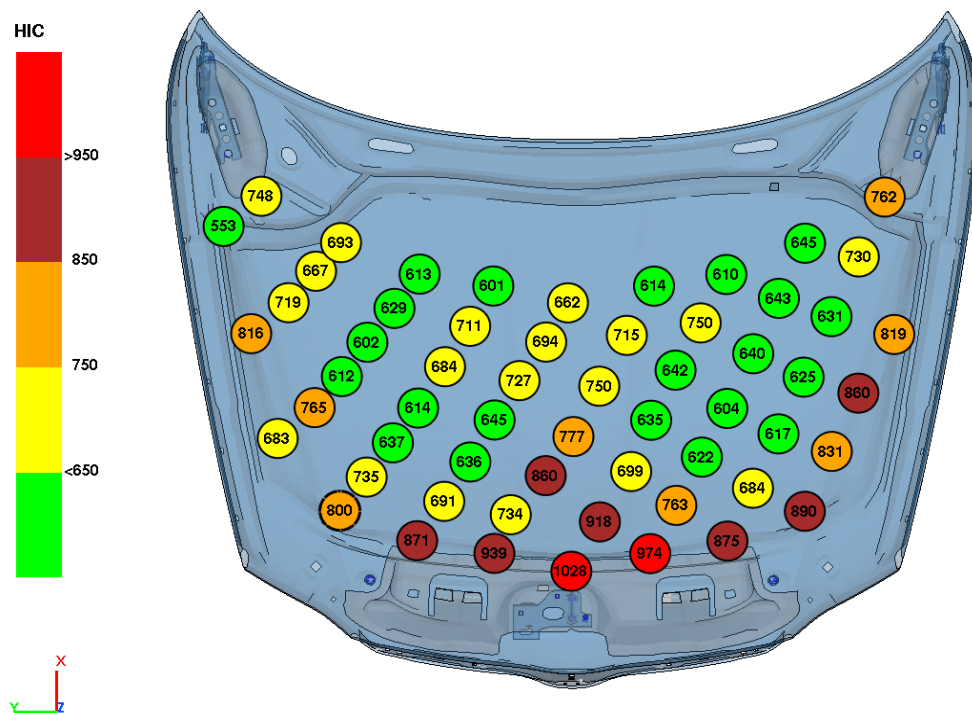


Figure 9.13: HIC overall performance for variant X04 - $OP = 72\%$

9.9 Torsional strength

Although the bonnet structure was designed to provide the best performance from HIC point of view, it has to fulfill also the mass restriction and torsional strength.

First two restriction are taken into account in the all previous sections, however after modification of last variant, the check of bonnet stiffness is necessary by performing the torsional strength calculation.

The bonnet structure is clamped at hinges and in the end of one rubber stopper. The rubber stopper is made of elastic material and therefore after applying clamped boundary condition to the stopper is still possible the movement is position A. Instead of the second rubber stopper is applied force at certain value. The force value and dimensions due to VW policy could not be presented. Scheme of torsional strength test is shown in figure 9.14.

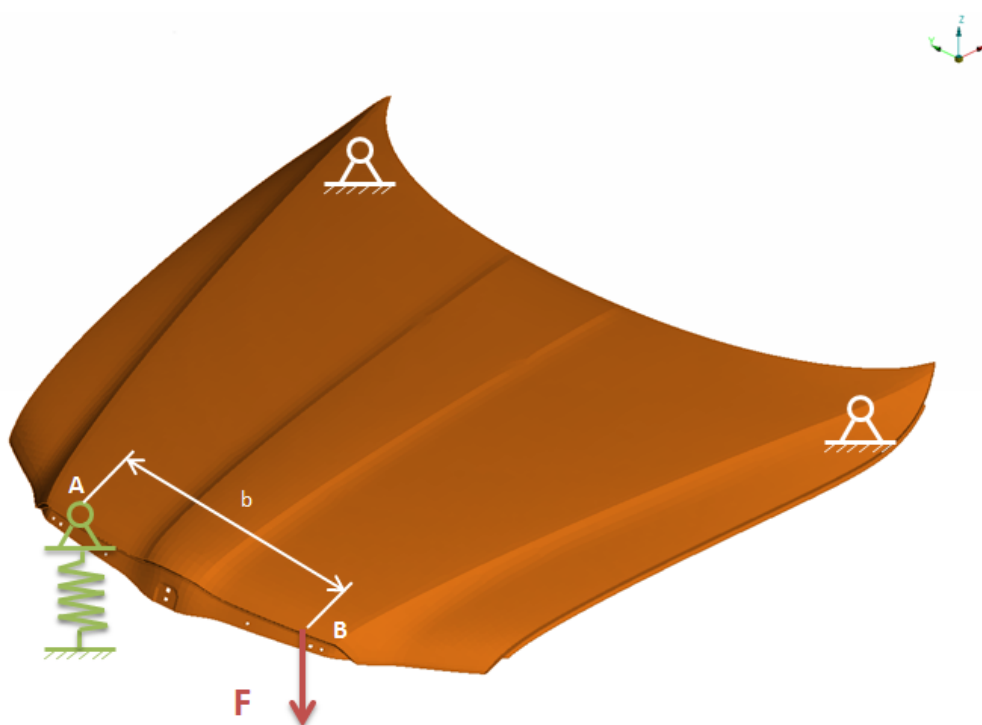


Figure 9.14: The torsional strength test

According to the regulation EP81601.21 the torsional strength is calculated by following eq.

$$c_T = \frac{F \cdot b}{\varphi_{ist} \cdot 1000} \left[\frac{Nm}{grad} \right] \quad (9.2)$$

where F is applied force, b is distance between force and clamped boundary condition. The φ_{ist} angle of torsion defined as

$$\varphi_{ist} = \arcsin \frac{|s_A| + |s_B|}{b} \quad (9.3)$$

where s_A , s_B is deflection at both structural points A or B.

The deflection of bonnet at positions A and B are measured on the superficial part of bonnet.

The computational model was modified to the static analysis where was used implicit solver. Therefore some of geometrical boundary condition was modified to application with implicit solver. The weld elements represented by PLINK were replaced by MTOCO elements. After creating correct model of force boundary condition where the force was applied the calculation shows results of torsional strength lower than original bonnet around 13% however with similar deflection. Therefore requirements of torsional strenght c_T and deflection were fulfilled.

9.10 Comparison of design with using original superficial bonnet top

By modifying bonnet structure the design was gained as good as possible. In the beginning was shown rating criterion which was applied to each variant. The original bonnet structure represented by FEM model A35 served for comparison to each variant by overall performance factor OR . Following table 9.11 shows results of all previous mentioned variants.

Variant	Achieved points	Overall performance [%]
A35	11.5	20
X01	30.25	52
X02	33.75	58
X03	39.25	67
X04	42	72

Table 9.11: Overall rating for different variants

Variant X04 perform best overall performance OR with 72%. As was mentioned before the overall rating could not lead to 100% cause of rating criterion. The each variant fulfill the restriction of 5 mm free space between bonnet structure and rigid surface which is situated in 60 mm from superficial part of bonnet.

10. Analysis of results

For the proposed deceleration curves, the energy absorbed by bonnet and maximal deflection of bonnet were used as restriction. The evaluation of basic function shown that the results obtained by triangular function against to rectangular and sinusoidal provide best HIC values and shortest trajectory in feasible point of view. The trajectory is dependent on slope of first triangular peak where the greater slope lead to shorter trajectory. Therefore as most ideal deceleration curve is one peak triangular function with great slope of increasing part of peak. It could be achieved by active bonnet where the energy would be absorbed by moving and then by deformation of bonnet. The HIC value only depends on magnitude of acceleration and pulse duration.

Further the 2 peak triangular function was used as type of deceleration curve because of hard realization one peak function. Again the absorbed energy served as restriction. The evaluation against HIC level shows that above HIC=600 the one certain parametric configuration of 2 peak triangular function provide shortest trajectory. By decreasing the level of HIC the trajectory increased. For HIC around 600 and below, the 2 parametric configurations of triangular function provide same value of HIC however with different trajectory. It is caused by HIC calculation from first respective both peaks. Obviously again the possible longer trajectory would lead to dramatic reduction of HIC values.

The design of approximated bonnet structure served to application of proposed deceleration curves. The headform was situated in the middle of bonnet structure. The center position is far from geometrical boundary condition and therefore at center the bonnet structure is most flexible. By proper design of bonnet the proposed deceleration curve was obtained which lead into small HIC value as was possible to achieve. The foam material significantly improved bonnet structure from HIC point of view simultaneously with respecting of the bonnet mass restriction.

The analysis from approximated bonnet structure was applied into more realistic bonnet structure. Again the foam material was used for performance improvement. The original bonnet structure A35 provide worse results from HIC point of view against to last proposed variant, where the results were evaluated from whole child zone of bonnet. By appropriate modification of internal bonnet structure could be achieved more uniform low HIC values.

The further better optimization of bonnet structure is by using active bonnet, where before of impact the bonnet is ejected more distant from engine parts. Therefore two mandatory effects could be suppressed. It would be possible extend trajectory during impact and also by first deflection followed by deformation of bonnet will cause the great slope of first peak.

11. Conclusion

The thesis aimed to present optimization of deceleration curve of headform impact into car bonnet of Škoda Superb II to provide best HIC values as possible.

- The research study shown that 21% of fatal injuries affect the pedestrian. Study dealt with usage of dummies and impactors which serves as replacement of dummies parts for pedestrian testing. From research goes out several advantages of impactors using due to more accurate testing of chosen points against usage of dummies. Further the research dealt with evaluation criteria for deceleration curve of decelerated impactor by collision with bonnet. The Head Injury Criterion (HIC) is widely used and accepted from 1970's by automotive industry and goes out from extensive research of head injuries tolerance represented by Wayne State Tolerance Curve (WSTC).
- The evaluation of impact analysis was performed by own written script in MATLAB software and also by META post-processor software which served as verification tool, where the provided data from Škoda Auto a.s. served as an input for evaluation. As a headform was used child impactor. The simulated impacts to the child zone of bonnet by explicit computational model were evaluated from energy point of view. For the impact simulations where the HIC was smaller than 1000 the average energy consumed by bonnet of $En = 138.5J$ was obtained. This energy served as restriction to the design variants of bonnet structure.
- In section 7.1 the analytical solution was performed. For geometrical model *SK461_A12* variant was set the rigid surface to distance in -60 mm in Z direction from superficial bonnet surface. The rigid surface substitute the engine parts. However the substitution is conservative because of not uniform distance between bonnet and engine parts. The impact into bonnet by child headform is done aligned by 50° from Ground Reference Level and the bonnet is tilted by 10° therefore maximal direct translation of impactor was calculated to $MD = 68.2$ mm. However real movement of impactor is not direct therefore the MD trajectory served as simplification. As a first approach to design deceleration curves were used sinusoidal, rectangular and triangular functions. Mentioned functions were used to model 1 or 2 peak deceleration curve. The HIC evaluation is only dependent on magnitude of deceleration and pulse duration T. The resultant trajectory depends on the magnitude of deceleration and pulse duration T except for triangular function where in addition on parameter which determines the first slope of peak. The greater slope causes shorter trajectory. From HIC point of view the triangle function provide smallest values with respecting the trajectory $MD=68.2$ mm. The HIC for the 1 peak triangular function is smaller than for 2 peak, however in real bonnet structure the 1 peak deceleration curve is hard to ensure. After review of all obtain deceleration curve from Škoda Auto a.s., the parametric deceleration curve was proposed with pulse duration $T = 18$ ms. As restriction parameter again served average absorbed energy of bonnet $En = 138.5J$. The parameters RP (ratio of peaks) and MP (local minimum peak) served for modification of function. The 3D plots shown the dependency of both parameters to HIC and trajectory. For each level of HIC was shown possible set of parameters where always the maximum of MP and minimum of RP led to shortest

trajectory. Only one difference was only at HIC level 550, where the contour curve has turning point in the middle and for same trajectory are possible two sets of parameters.

- Chapter 8 dealt with design of approximated bonnet structure for application of previous analysis where the best analytical deceleration curve was obtained. Therefore the computational model of bonnet structure was created where by modification of bonnet structure the best deceleration 2 peak curve was obtained. The rigid surface positioned in -60mm represented uniform area of engine parts which is responsible to existence of distinct second peak in deceleration curve. For structure was used boundary conditions which corresponds to the original computational model created by Škoda Auto a.s. The last variant used a foam layer of material attached from under bonnet structure. The finite element mesh consist of SHELL elements with 5 integration points through thickness for sheet parts of bonnet. The SOLID elements was used for meshing foam layer. To the approximated bonnet structure was applied boundary conditions in hinges and front lock. The FEM model of child impactor (headform) consist of FEM model of 3 axis accelerometer which served as point for evaluation of acceleration, velocity and displacement data. The velocity of 11.3 m/s was applied to the headform. The whole model was set in gravity field. During impact the headform is in contact with bonnet structure, therefore was created model of contact which use penalty method. As a model of material for shell elements served multi linear isotropic elastic-plastic material with enhanced plasticity algorithm. The elastic behavior was described by elastic modulus E , shear modulus G , Poisson's ratio μ and thickness t_e . For plastic region served the sets of stress-strain values tabled in section 8.1.4. For solid elements was also used multi linear material. Calculation was performed by PAM-CRASH solver which used explicit algorithm, where the large displacement and strain were used as type of geometric nonlinearity. The time step was calculated according to characteristic length of elements used in mesh and during deformation of structure the time step is modified. The best variant 007 of approximated bonnet structure appeared to be structure with foam material.
- The chapter 9 was devoted to the design of bonnet structure and its modification from HIC point of view. The computational model was almost identical to the model described in chapter 8. It differs only by geometrical model where the FEM model *SK461_A35* served as original bonnet structure. The geometry of superficial part was not modified. Center structure of internal part of bonnet was substituted by offset surface where the shape corresponds to superficial shape of bonnet. The shifted surface was connected to the internal part and at regions of connection the mesh size was restored. From the bottom of internal part the foam layer of 5 mm thickness was attached. Again from superficial part was the surface of center part shifted in -60 mm in Z direction which served as rigid surface simulating engine parts. The internal structure was modified by grid of morphing points in ANSA preprocessor which served for geometrical modification of bonnet structure. The several variants was done to approach the best distribution of HIC value across bonnet structure. For evaluation was used modified *SK461_A35* geometrical model where the rigid surface was set to -60 mm in Z direction. The front part of car was neglected therefore the car support parts which served as another boundary conditions along the perimeter of bonnet surface were not considered. The rigid surface does not completely correspond to engine parts, where the space between bonnet and engine parts are not uniform. The modified variant

SK461_A35 could not be compared with real Škoda Superb II car. It served as first results for evaluation of bonnet design improvement. The last variant X04 according to the modified scale was provide 42 points (overall performance 72%) against modified variant *SK461_A35* - 11.5pts. (overall performance 20%). The simulation of torsional strength was done with fulfilling requirements of VW regulation.

According to previous items is concluded, that aims of the diploma thesis are satisfied.

Bibliography

- [1] J. Petruška. Mkp v inženýrských výpočtech. 2012.
- [2] Wikipedia. Pedestrian safety through vehicle design — wikipedia, the free encyclopedia, 2013. [Online; accessed 20-March-2013].
- [3] J.R. Elliott, C.K. Simms, and D.P. Wood. Pedestrian head translation, rotation and impact velocity: The influence of vehicle speed, pedestrian speed and pedestrian gait. Accident Analysis & Prevention, 45(0):342 – 353, 2012.
- [4] Robert William Gerard Anderson, AJ McLean, Giulio Ponte, and L Streeter. Pedestrian reconstruction using multibody madymo simulation and the polar-ii dummy: a comparison of head kinematics. In Proc. 20th International Technical Conference on the Enhanced Safety of Vehicles, Paper, pages 07–0273, 2007.
- [5] N Yoganandan, FA Pintar, TA Gennarelli, MR Maltese, and RH Eppinger. Biofidelity evaluation of recent side impact dummies. In PROCEEDINGS OF THE INTERNATIONAL IRCOBI CONFERENCE, 2002.
- [6] Abayomi Otubushin and John Green. An analytical assessment of pedestrian head impact protection. In Proc. of the 16th International Technical Conference on the Enhanced Safety of Vehicles (ESV), paper, volume 7, pages 98–S10, 1998.
- [7] M. Kleinberger and United States. National Highway Traffic Safety Administration. Development of Improved Injury Criteria for the Assessment of Advanced Automotive Restraint Systems. National Highway Traffic Safety Administration, 1998.
- [8] Guoxing Lu and Tongxi Yu. Energy absorption of structures and materials. Woodhead Publishing, 2003.
- [9] Hans-Wolfgang Henn. Crash tests and the head injury criterion. Teaching mathematics and its applications, 17(4):162–170, 1998.
- [10] C.Z Cory, M.D Jones, D.S James, S Leadbeatter, and L.D.M Nokes. The potential and limitations of utilising head impact injury models to assess the likelihood of significant head injury in infants after a fall. Forensic Science International, 123(2-3):89–106, 2001.
- [11] Euro NCAP. Assessment protocol-pedestrian protection. Assessment Protocol Version, 5, 2009.
- [12] John Hutchinson, Mark J Kaiser, and Hamid M Lankarani. The head injury criterion (hic) functional. Applied mathematics and computation, 96(1):1–16, 1998.
- [13] P. Prasad and H. Mertz. The position of the united states delegation to the iso working group 6 on the use of hic in the automotive environment. SAE Technical Paper 851246, (doi:10.4271/851246), 1985.
- [14] Prasad P. Mertz, H. and G. Nusholtz. Head injury risk assessment for forehead impacts. SAE Technical Paper 960099, (doi:10.4271/960099), 1996.

- [15] Roger Stafford. Thread Subject: Calculating SI and HIC. http://www.mathworks.com/matlabcentral/newsreader/view_thread/289372, 2010. [Online; accessed 19-July-2011].
- [16] Graham JL Lawrence. The next steps for pedestrian protection test methods. In Experimental Safety Vehicles Conference, 2005.
- [17] Euro NCAP. Assessment protocol-pedestrian protection. Assessment Protocol Version, 4.1, 2004.
- [18] European Enhanced Vehicle safety Committee et al. Improved test methods to evaluate pedestrian protection afforded by passenger cars. EEVC Working Group, 17, 1998.
- [19] LS-DYNA Support. Hourglass. <http://www.dynasupport.com/howtos/element/hourglass>, 2013. [Online; accessed 19-April-2013].
- [20] Jiří Svoboda. Pasivní bezpečnost chodců. PhD thesis, České vysoké učení technické v Praze, fakulta strojní, Praha, Česká republika, June 2009.
- [21] ESI-GROUP. Virtual performance solution 2010 solver notes manual. www.esi-group.com, -, 2010.
- [22] Werner Goldsmith. Impact, the theory and physical behavior of colliding solids. 1964.
- [23] ESI-GROUP. Virtual performance solution 2010 explicit solver reference manual. www.esi-group.com, -, 2010.
- [24] Robert D Cook et al. Concepts and applications of finite element. John Wiley & Sons, 2007.
- [25] Rudolf Brepta and Miroslav Prokopec. Šíření napěťových vln a rázy v tělesech. Academia, 1972.
- [26] Euro NCAP. Assessment protocol-pedestrian protection. Assessment Protocol Version, 6, 2012.

List of Figures

4.1	Most exposed vulnerable parts of pedestrian by vehicle struck [2]	10
4.2	Gait cycle stances [3]	11
4.3	Log-Log Wayne State Tolerance Curve [8]	12
4.4	Two different waveforms with similar GSI values [10]	13
4.5	Area of waveform utilised for calculating HIC [10]	14
5.1	Pedestrian impact zones by vehicle category, showing the potential overlap in upper legform impact zone and child headform impact zone for 4x4 off-road and utility vehicles [17]	16
5.2	Two types of head impactors, dimensions in <i>mm</i>	17
5.3	Test set-up for dynamic headform impactor certification test [18]	18
5.4	Division of the headform test zones [17]	19
6.1	Simulation data for A09 point	23
6.2	Points of impact with corresponding simulation data	24
6.3	The test scheme with rotated impactor due to friction during collision with bonnet	24
6.4	Force-trajectory diagrams in 3 directions	25
7.1	Schematic drawing of resultant trajectory	27
7.2	Sinusoidal function with 1 peak diagrams	30
7.3	Comparison of 1 peak and 2 peak sinusoidal function	31
7.4	Rectangular function diagrams	32
7.5	Comparison of 1 peak and 2 peak triangular function	33
7.6	Comparison of 1 peak and 2 peak triangular function for $T = 15\text{ms}$	34
7.7	The parametric 2 peak triangular function	37
7.8	The 2 peak function with unit first peak and shape according to parameters $RP=0.5$ and $MP=0.1$	37
7.9	Dependency of HIC values according to ratio peak RP and corresponding trajectory	38
7.10	Contour plot - dependency of peak ratio RP along trajectory at variable HIC	39
7.11	Parametric triangular function for 18 ms duration of impact	40
7.12	Contour plot - dependency of peak ratio RP along ratio of local minimum MP and regions where HIC is calculated from 1 alternatively 2 peaks	40
7.13	The deceleration - time dependency for duration of impact 18 ms	40
7.14	Dependency of trajectory according to ratio peak RP and corresponding HIC value	41
7.15	Contour plot - dependency of peak ratio RP along HIC value	41
7.16	The deceleration - time dependency for duration of impact 18 ms, constant trajectory	42
7.17	The deceleration - time dependency for duration of impact 18 ms, constant trajectory	42
7.18	Dependency of HIC values according to ratio peak RP and corresponding trajectory	43

7.19	Dependency of HIC values according to ratio peak RP, local minimum MP and corresponding trajectory	43
8.1	Comparison of superficial to approximated model of bonnet	46
8.2	The boundary conditions used for bonnet top	48
8.3	The boundary conditions used for bonnet top - detail	48
8.4	The initial force conditions used for headform and bonnet structure - initial velocity and gravity field	49
8.5	Penetration definition for contact type 33	49
8.6	The table with contact properties between skin of impactor and bonnet top .	50
8.7	The model of material zste220i defined by coordinates - plastic hardening . .	51
8.8	The solved first design of bonnet top	57
8.9	The results of variant 001	58
8.10	The results of variant 002	59
8.11	The results of variant 003	59
8.12	The results of variant 004	60
8.13	The results of variant 005	61
8.14	The results of variant 006	61
8.15	The results of variant 007	62
9.1	FEM model <i>SK461_A12</i>	63
9.2	FEM model <i>SK461_A12</i>	64
9.3	Rigid body condition to the bonnet rubber stops and front lock	64
9.4	Rigid surface	65
9.5	The modified rigid surface - back view	66
9.6	HIC overall performance for series A35 FEM model with rigid surface at -60 mm and missing front car structure - OP = 22%	67
9.7	The internal structure by offsetting part of superficial bonnet top with rough morphing grid - variant X01	68
9.8	The internal structure by offsetting part of superficial bonnet top - variant X01	69
9.9	HIC overall performance for variant X01 - OP = 52%	70
9.10	Cut view for impact point D07 of variant X01	70
9.11	HIC overall performance for variant X02 - OP = 58%	71
9.12	HIC overall performance for variant X03 - OP = 67%	72
9.13	HIC overall performance for variant X04 - OP = 72%	73
9.14	The torsional strength test	74
A.1	Determination of Upper Bumper Reference Line	88
A.2	Determination of Lower Bumper Reference Line	88
A.3	Determination of Corner of Bumper	88
A.4	Determination of wrap around distance	89
A.5	Determination of the Bonnet Side Reference Lines	89
A.6	The acceleration - time dependency for duration of impact 18 ms with RP=0.47 and MP=0.3	89
A.7	The acceleration - time dependency for duration of impact 18 ms with RP=0.6 and MP=0.15	90
A.8	Results for variant X04	90

List of Tables

5.1	Technical specification of impactors	17
6.1	Table with conversion of units for HIC calculation	21
6.2	HIC criteria for impact points according to figure 6.2	22
6.3	Internal energy	26
7.1	Summary of basic relations for idealized pulse shapes [20]	28
7.2	Comparison of analytical and numerical treatment of sinusoidal function	29
7.3	Sinusoidal function for different pulse duration T whilst preserving energy $E_n=138.5$ J	30
7.4	Sinusoidal function with 2 peaks for different pulse duration whilst preserving internal energy $E_n=138.5$ J	31
7.5	Rectangular function for different pulse durations	32
7.6	2 peak triangular function with variable parameter $k = 0.1$ for HIC value 650 and 1000	33
7.7	Triangular function with parameter $k = 0.1$	34
7.8	Triangular function with parameter $k = 0.1$ and variable parameter k_2 for trajectory MD=68.2mm	35
7.9	Results of trajectories for basic functions for HIC values 650 and 1000	36
7.10	Results of pulse duration and HIC values for basic functions within trajectory set to 68.2 mm	44
7.11	Results of pulse duration and trajectory for basic functions within HIC=1000	44
7.12	Results of pulse duration and trajectory for basic functions within HIC=650	44
8.1	Model of material - elastic-plastic behavior	52
8.2	Comparison of explicit and implicit characteristics	55
9.1	HIC value range for evaluation according to test protocol [26]	66
9.2	Modified HIC value range for evaluation	66
9.3	Overall performance for A35 variant	67
9.4	Variant X01	69
9.5	Overall performance for X01 variant	70
9.6	Variant 005	71
9.7	Overall performance for X02 variant	71
9.8	Variant 006	72
9.9	Overall performance for X03 variant	72
9.10	Overall performance for X04 variant	73
9.11	Overall rating for different variants	75

12. List of acronyms

ANSA pre-processor software for FEM

ASDH acute subdural haematoma

CAC Channel Amplitude Class

CFC Channel Frequency Class

DOF degrees of freedom

DSY file type - contains an animation of impact and geometry of model

EEVC European Enhanced Vehicle Safety Committee

EEVC EG17 EEVC Working Group 17

Euro NCAP European New Car Assessment Programme

FEM Finite Element Method

FMVSS Federal motor vehicle safety standards

FRICT value for Coulomb friction model

GSI Gadd Severity Index

HIC Head Injury Criterion

LINK link element

MADYMO MAtheMatical DYnamic MOdels software

Master active model entities in contact definition

MATLAB environment for numerical computation

META post-processor software for FEM

MTOCO multiple nodes to one node constrain

NHTSA National Highway Traffic Safety Administration

PAM-CRASH solver software for FEM

OP overall performance

PLINK point connection

PMHS post-mortem human surrogates

RIGID body element of infinite stiffness

SHELL shell element with defined thickness

Slave passive model entities in contact definition

SOLID volume element

Solver algorithm for solution by finite element method

SupP superficial part of bonnet

SUV sport utility vehicle

TIED special type of contact simulating glued joint

THP file type - contains all time history post processor entities

WAD wrap around distance

WSTC Wayne State Tolerance Curve

13. List of symbols

a	$[m \cdot s^{-2}]$	deceleration
A	$[g]$	acceleration in terms of g
A_p	$[g]$	magnitude of deceleration curve
b	$[m]$	distance between force and clamped boundary condition
BM	$[kg]$	mass of bonnet
c	$[m \cdot s^{-1}]$	velocity sound speed
c_T	$[\frac{Nm}{grad}]$	torsional strength
En	$[J]$	energy absorbed by bonnet
E	$[GPa]$	modulus of elasticity
F	$[N]$	force
\mathbf{F}	$[N]$	vector of loads
G	$[GPa]$	shear modulus
\mathbf{K}	$[N \cdot m^{-1}]$	stiffness matrix
L	$[m]$	characteristic length of element
m	$[-]$	slope
m_i	$[m \cdot s^{-2}]$	mass of impactor
MV	$[m \cdot s^{-1}]$	velocity
MP	$[-]$	local minimum between peaks
MD	$[mm]$	maximal allowable trajectory
RP	$[-]$	ratio of peaks
$s_{A,B}$	$[m]$	deflection at structural points A and B
t_1	$[ms]$	time instant for HIC criterion
t_2	$[ms]$	time instant for HIC criterion
T	$[ms]$	pulse duration
u, v, w	$[mm]$	displacements
\mathbf{U}	$[m]$	vector of displacements
v	$[m \cdot s^{-1}]$	velocity
v_0	$[m \cdot s^{-1}]$	initial velocity
Z_t	$[mm]$	maximal possible deflection of bonnet in Z direction
ε	$[-]$	strain
μ	$[-]$	Poisson's ratio
ρ	$[kg \cdot m^{-3}]$	density
σ	$[MPa]$	stress
σ_y	$[MPa]$	yield stress
$\varphi_{x,y,z}$	$[rad]$	rotation components
φ_{ist}	$[grad]$	angle of torsion

Appendix A

Figures

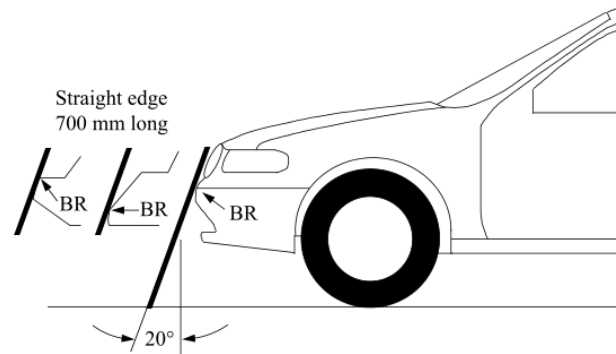


Figure A.1: Determination of Upper Bumper Reference Line

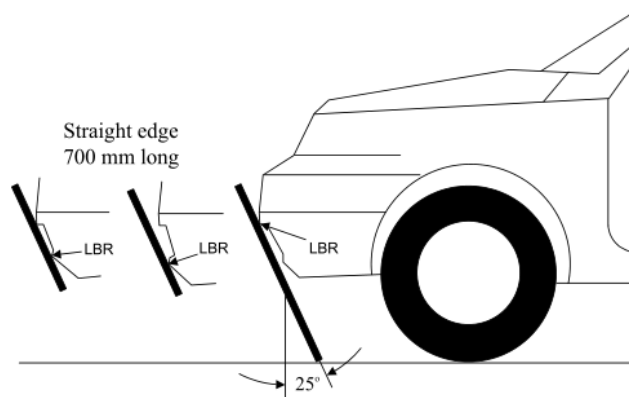


Figure A.2: Determination of Lower Bumper Reference Line

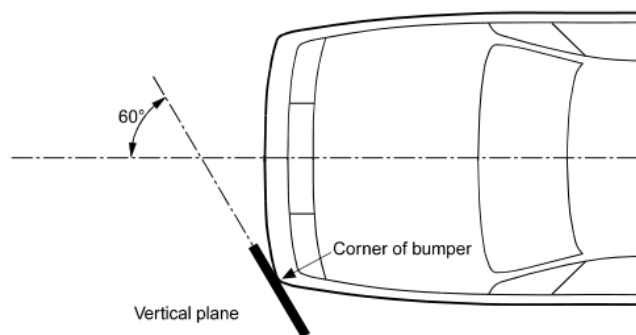


Figure A.3: Determination of Corner of Bumper

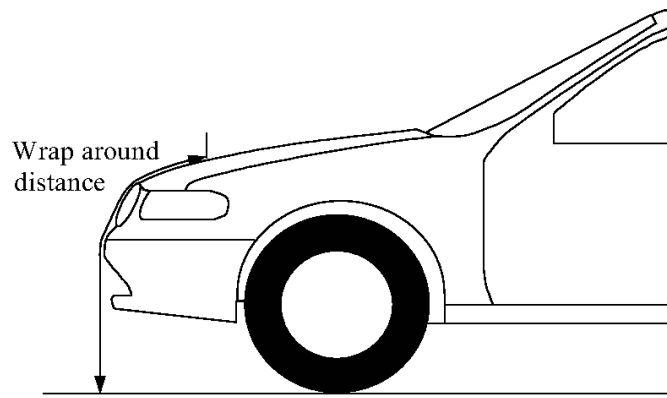


Figure A.4: Determination of wrap around distance

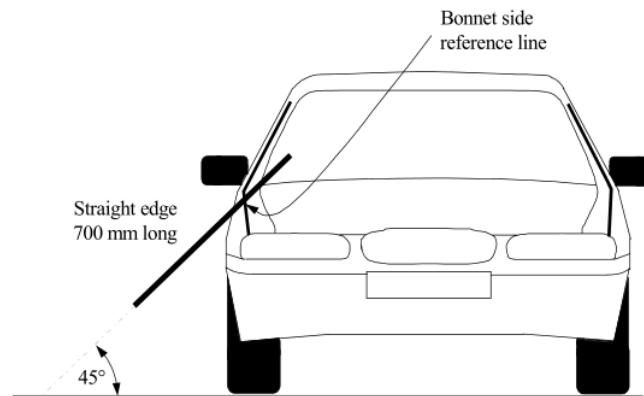


Figure A.5: Determination of the Bonnet Side Reference Lines

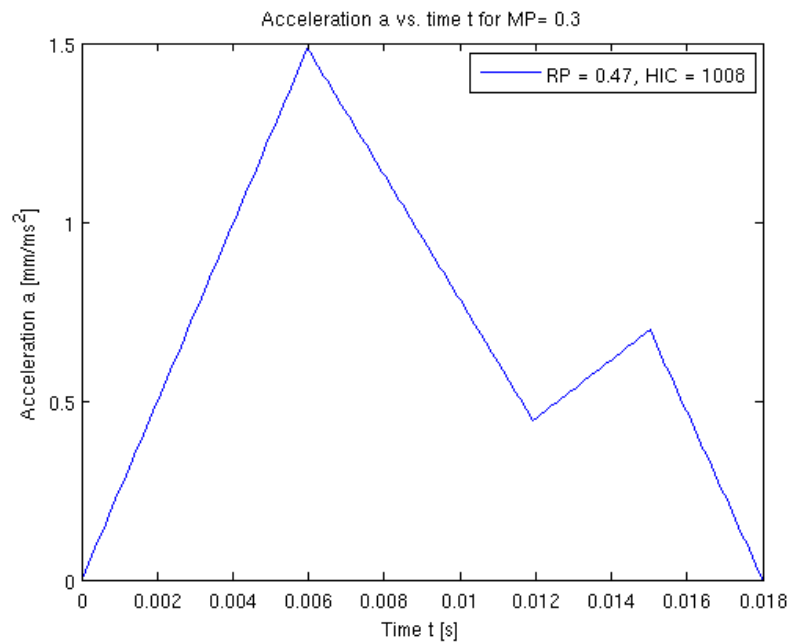


Figure A.6: The acceleration - time dependency for duration of impact 18 ms with RP=0.47 and MP=0.3

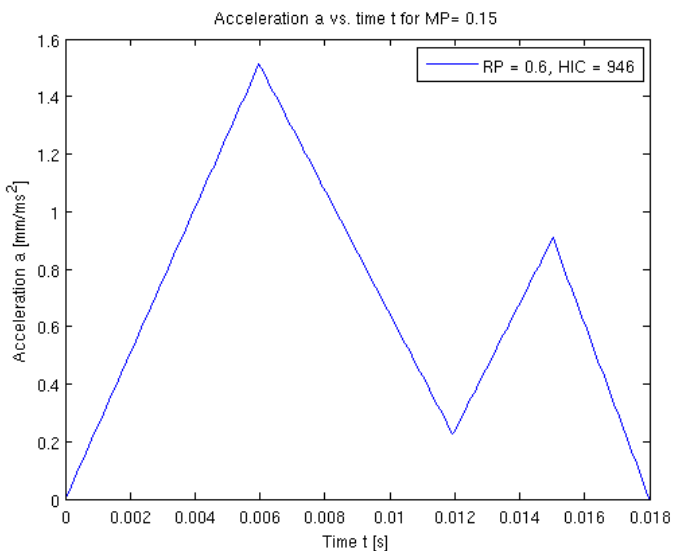
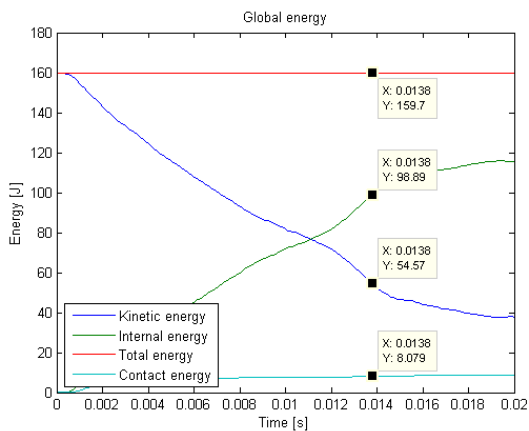
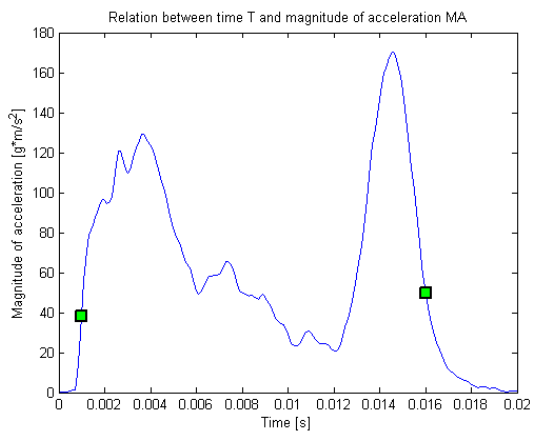
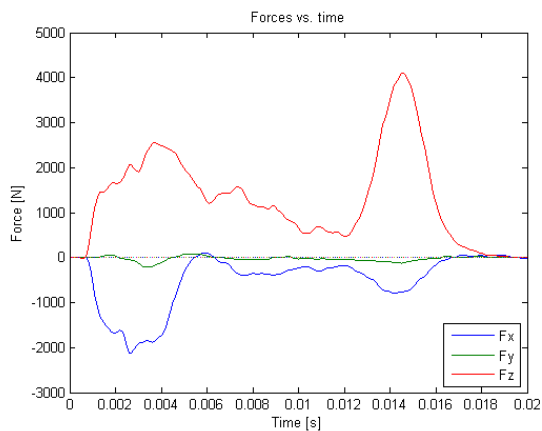


Figure A.7: The acceleration - time dependency for duration of impact 18 ms with RP=0.6 and MP=0.15



(a) Variant X04 - deceleration curve along pulse duration T

(b) Variant X04 - energy relations along pulse duration T



(c) Variant X04 - force curves along pulse duration T

Figure A.8: Results for variant X04

Appendix B

HIC analysis script *SK461_ALL.m*

```

clc;
close all;
clear;

spot=input('Which spot on bonnet would you like to investigate? ...
(use simple quotation marks) ');
label=['SK461_SPX_A12_Sc' spot '_ch101G_rt_A.crv'];

%% -----===== IMPORT PART =====-----

%Acceleration
[MA]=importdata(label,',' ,5);
[T]=importdata(label,',' ,5);
[XACC]=importdata(label,',' ,1457);
[YACC]=importdata(label,',' ,1663);
[ZACC]=importdata(label,',' ,1869);
[XRACC]=importdata(label,',' ,2075);
[YRACC]=importdata(label,',' ,2281);
[ZRACC]=importdata(label,',' ,2487);

%HIC
[HIC]=importdata(label,',' ,211);

%Displacement and angles
%GLOBAL COORDINATE SYSTEM
[XANG]=importdata(label,',' ,3311);
[YANG]=importdata(label,',' ,3517);
[ZANG]=importdata(label,',' ,3723);
[XD]=importdata(label,',' ,3929);
[YD]=importdata(label,',' ,4135);
[ZD]=importdata(label,',' ,4341);
%MAGNITUDE OF DISPLACEMENT
[MD]=importdata(label,',' ,4547);

%ENERGY
%GLOBAL
[KINen]=importdata(label,',' ,5372);
[INTen]=importdata(label,',' ,5578);
[TOTen]=importdata(label,',' ,5784);
[HOUen]=importdata(label,',' ,5990);
[CONen]=importdata(label,',' ,6402);

```

```

T=MA.data(:,1)/1000; %in seconds
MAMETA=MA.data(:,2)*1000;
MA=MA.data(:,2)*1000/9.81; %in multiples of 'g' constant
XACC=(XACC.data(:,2)*1000);
YACC=(YACC.data(:,2)*1000);
ZACC=(ZACC.data(:,2)*1000);
XRACC=(XRACC.data(:,2));
YRACC=(YRACC.data(:,2));
ZRACC=(ZRACC.data(:,2));
Dx=(XD.data(:,2)/1000); %in meter
Dy=(YD.data(:,2)/1000); %in meter
Dz=(ZD.data(:,2)/1000); %in meter
Dm=MD.data(:,2)/1000; %in meter

XANG=(XANG.data(:,2)); %v rad
YANG=(YANG.data(:,2)); %v rad
ZANG=(ZANG.data(:,2)); %v rad
KINen=KINen.data(:,2);
INTen=INTen.data(:,2);
TOTen=TOTen.data(:,2);
HOUen=HOUen.data(:,2);
CONen=CONen.data(:,2);

%% EVAULATION

m=2.5; %kg
I=0.0036; %kgm^2
Fx=m.*XACC; %force by Newton's law in X direction
Fy=m.*YACC; %force by Newton's law in Y direction
Fz=m.*ZACC; %force by Newton's law in Z direction
F=m.*MAMETA;
Mkx=I.*XRACC;
Mky=I.*YRACC;
Mkz=I.*ZRACC;

[hic,time,t1,t2]=HICcalc(T,MA);

format short g

hicmeta=HIC.data(2,2)
timemeta=(HIC.data(3,1)-HIC.data(1,1)) %in ms

hic
timems=time*1000 %in ms

```

```
%% POST-PROCESING...PLOTS
figure(1)
plot(T,Dx,T,Dy,T,Dz,T,0)
legend('Dx','Dy','Dz',3)
xlabel('Time [s]')
ylabel('Displacement [m]')
xlim([0 0.02])
title('Displacements vs. time')

figure(2)
plot(T,Fx,T,Fy,T,Fz,T,0)
legend('Fx','Fy','Fz',4)
xlabel('Time [s]')
ylabel('Force [N]')
xlim([0 0.02])
title('Forces vs. time')

figure(3)
p = plot(Dx,Fx,Dx,0);
title('Relation between force Fx and trajectory Dx')
xlabel('Trajectory Dx [m]')
ylabel('Force Fx [N]')
set(p,'Color','blue','LineWidth',2)

figure(4)
p = plot(Dy,Fy,Dy,0);
title('Relation between force Fy and trajectory Dy')
xlabel('Trajectory Dy [m]')
ylabel('Force Fy [N]')
set(p,'Color','green','LineWidth',2)

figure(5)
p = plot(Dz,Fz,Dz,0);
title('Relation between force Fz and trajectory Dz')
xlabel('Trajectory Dz [m]')
ylabel('Force Fz [N]')
set(p,'Color','red','LineWidth',2)

figure(6)
plot(T,XANG*180/pi,T,YANG*180/pi,T,ZANG*180/pi,T,0)
legend('angle x','angle y','angle z',3)
xlabel('Time [s]')
ylabel('Angles [deg]')
title('Angle change during impact')
```

```

xlim([0 0.02])

figure(7)
plot(T,Mkx,T,Mky,T,Mkz,T,0)
legend('Mkx','Mky','Mkz',3)
xlabel('Time [s]')
ylabel('Moment [Nm]')
title('Moment vs. time')

enx=trapz(Dx,Fx);
eny=trapz(Dy,Fy);
enz=trapz(Dz,Fz);

en=abs(enx+eny+enz);

enrx=trapz(XANG,Mkx);
enry=trapz(YANG,Mky);
enrz=trapz(ZANG,Mkz);
enr=enrx+enry+enrz;
%en1=trapz(s,F); %pocet presne podle METY

figure(8)
plot(T,MA)
xlabel('Time [s]')
ylabel('Magnitude of acceleration [g*m/s^2]')
title('Relation between time T and magnitude of acceleration MA')
legend(['HIC = ' num2str(round(hic))], 1)
xlim([0 0.02])
    k1 = find(T==t1);
    k2 = find(T==t2);
hold on
plot(t1,MA(k1),'--rs','LineWidth',2,...
     'MarkerEdgeColor','k',...
     'MarkerFaceColor','g',...
     'MarkerSize',10);
plot(t2,MA(k2),'--rs','LineWidth',2,...
     'MarkerEdgeColor','k',...
     'MarkerFaceColor','g',...
     'MarkerSize',10);

time=(t2-t1)*1000 ;

% figure(9)
% plot(T,Dm)
% xlabel('Time [s]')
% ylabel('Magnitude of displacement [g*m/s^2]')
% title('Relation between time T and magnitude of displacement Dm')

```

```
% xlim([0 0.02])

% figure(10)
% plot(Dm,MA)
% xlabel('Magnitude of displacement [g*m/s^2]')
% ylabel('Magnitude of acceleration [g*m/s^2]')
% title('Relation between magn. of displacement Dm and magn. of acc. MA')
% xlim([0 0.02])
%

    figure(11)
    plot(T,KINen,T,INTen,T,TOTen,T,CONen)
    legend('Kinetic energy','Internal energy','Total energy','Contact energy',3)
    xlabel('Time [s]')
    ylabel('Energy [J]')
    title('Global energy')
    xlim([0 0.02])
    ylim([0 180])

    totalenergy=KINen(end)+INTen(end)+CONen(end);

    energyINTCON=INTen(end)+CONen(end)

    energyINT=INTen(end)

en
```

Appendix C

HIC script "HICcalc.m"

```
1 function [hic,time,t1,t2]=HICcalc(T,MA)
2
3 v = cumtrapz(T,MA); % Velocity added from time t(1)
4 n = length(MA);
5 hic = -inf;
6 for it = 1:n-1
7     for jt = it+1:n
8         if (T(jt)-T(it))<0.015
9             h = (T(jt)-T(it))*((v(jt)-v(it))/(T(jt)-T(it)))^2.5;
10        if h > hic
11            hic = h;
12            t1=T(it);
13            t2=T(jt);
14        end
15        else
16            end
17        end
18    end
19    time=t2-t1;
20    end
```

Appendix D

Triangular parametric function "triangle_acctraj.m"

Due to long script, the file the *triangle_acctraj.m* is saved in CD.